EVALUATION OF ALTERNATIVES FOR SAFER AND MORE EFFICIENT REACTIONS: A STUDY OF THE *N*-OXIDATION OF ALKYLPYRIDINES

A Dissertation

by

LINA ROCIO SAENZ NOVAL

Submitted to the Office of Graduate Studies of
Texas A&M University
in partial fulfillment of the requirements for the degree of

DOCTOR OF PHILOSOPHY

December 2011

Major Subject: Chemical Engineering

Evaluation of Alternatives for Safer and More Efficient Reactions:

A Study of the *N*-oxidation of Alkylpyridines

EVALUATION OF ALTERNATIVES FOR SAFER AND MORE EFFICIENT REACTIONS: A STUDY OF THE *N*-OXIDATION OF ALKYLPYRIDINES

A Dissertation

by

LINA ROCIO SAENZ NOVAL

Submitted to the Office of Graduate Studies of
Texas A&M University
in partial fulfillment of the requirements for the degree of

DOCTOR OF PHILOSOPHY

Approved by:

Chair of Committee,	M. Sam Mannan
Committee Members,	Debjyoti Banerjee
	Carl Laird
	Victor Ugaz
Head of Department,	Charles Glover

December 2011

Major Subject: Chemical Engineering

ABSTRACT

Evaluation of Alternatives for Safer and More Efficient Reactions: A Study of the *N*-oxidation of Alkylpyridines. (December 2011)
Lina Rocio Saenz Noval, B.S., Universidad Industrial de Santander, Colombia
Chair of Advisory Committee: Dr. M. Sam Mannan

The catalytic *N*-oxidation of alkylpyridines, a reaction which uses hydrogen peroxide as the oxidizing agent and the water soluble phosphotungstic acid as the catalyst, is a reaction employed in the pharmaceutical industry. The safety concerns of this process revolve around the decomposition of hydrogen peroxide and the liquid-liquid phase separation of the reacting mixture. The decomposition of hydrogen peroxide is an undesired reaction parallel to the desired *N*-oxidation and is responsible for: 1) a high potential for runaway due to the condition sensitivity of the peroxide group, 2) a potential over-pressurization of the reaction vessel during a runaway due to the production of oxygen, and 3) the enrichment with oxygen of the flammable alkylpyridine environment. The presence of an organic phase and an aqueous phase occurs in a wide range of conditions and results in: 1) a dramatic reduction in the reaction selectivity, and consequently in the efficiency, due to the additional mass transfer constrains imposed by the phase separation, and 2) the safety of the process being seriously compromised because most of the catalyst remains in the aqueous phase, excessively promoting the decomposition of hydrogen peroxide over the *N*-oxidation.

With these concerns in mind, this research aimed to determine conditions for an inherently safer and more efficient *N*-oxidation reaction and focused on three key targets: i) the possibility of reducing the extend of the decomposition of hydrogen peroxide, thus leading to an inherently safer process, ii) the study of phase equilibrium so as to enable the identification of conditions that increase the efficiency of the *N*-oxidation and reduces the hazards, and iii) the evaluation of safety parameters that will

allow for the control of a potential runaway reaction. Two alkylpyridines were considered: 2-methylpyridine which represents the case of a homogeneous reacting mixture and 2,6-dimethylpyridine to study the two-liquid phase separation effects. The methodology employed calorimetric studies to assess the runaway behavior and to determine the conditions that favor the *N*-oxidation, and for the *N*-oxidation of 2,6-dimethylpyridine, thermodynamic studies were incorporated to evaluate the conditions for phase separation.

DEDICATION

To my mother, Nancy, without whom I would not be where I am today;
To my brother, Johanny, and my sister, Catalina; and
To all my friends and family

ACKNOWLEDGEMENTS

I would like to express my gratitude to Dr. Mannan for the opportunity to become part of the Mary Kay O'Connor Process Safety Center family. Thanks for his guidance and wisdom and for his leading role educating people to recognize the importance of safety in the industry. I am grateful for his kindness and understanding and for exposing me to different learning experiences and wonderful opportunities that have prepared me for the real world and enriched me personally and professionally.

I am deeply thankful for Dr. Maria Papadaki from the University of Ioannina, Greece for her continuous support. I would like to express my gratitude for all her teachings, not only in the reactive chemicals area, but also life. Thanks for meeting me in different parts of the world, and for always being there to correct my mistakes and encourage my work.

I would like to thank my committee members: Dr. Debjyoti Banerjee, Dr. Carl Laird, and Dr. Victor Ugaz for their participation and assistance during the doctorate program.

I am grateful with all the current and former members of the Mary Kay O'Connor Process Safety Center for sharing with me special moments during the years of graduate school. Thanks to Valerie and Donna for their patience and support, and a special thanks to Victor and Alba for their friendship.

I would like to thank Texas A&M University at Qatar for allowing performing some of this work at their facilities. Thanks to Dr. Simon Waldram for his advice and for sharing with me his experience in the reactive chemical area. Thanks to Dr. Subramanya Nayak for the unconditional support in the laboratory, and thanks to all the wonderful people I met there for helping me during my visit.

I would like to thank my mom, Nancy, for her encouragement and guidance, and for being my role-model for hard work. Thanks to all the members of my family who, even though they are not here with me, have supported me throughout my work.

Thanks to Keith and his family, Kenneth, Frieda, Kent and Krysta, for being my family in College Station and for the countless times that helped me and made me happy.

Thanks to all my friends for always putting a smile on my face during the development of this work, especially on those days when everything went wrong.

Finally, thanks God for the strength and knowledge to complete my studies, for guiding my steps, and for giving me the opportunity to meet all these wonderful people who, one way or another, contributed to the work presented here.

TABLE OF CONTENTS

Page

ABSTRACT iii
DEDICATION v
ACKNOWLEDGEMENTS vi
TABLE OF CONTENTS viii
LIST OF FIGURES x
LIST OF TABLES xiv
1. INTRODUCTION 1
1.1 The *N*-oxidation of Alkylpyridines 1
1.1.1 Alkylpyridines and Alkylpyridines N-oxides 2
1.1.2 Hydrogen Peroxide 3
1.1.3 Phosphotungstic Acid 4
1.2 Hazards in the *N*-oxidation of Alkylpyridines 5
1.3 Calorimetry as a Tool for Hazard Identification 6
1.4 Inherent Safety 9
2. RESEARCH METHODOLOGY AND METHODS 12
2.1 Previous Findings 12
2.1.1 Finding 1 12
2.1.2 Finding 2 13
2.1.3 Finding 3 13
2.1.4 Finding 4 14
2.1.5 Finding 5 14
2.2 Research Scope and Significance 15
2.3 Research Methodology 17
2.4 Materials and Methods 18
2.4.1 Automatic Pressure Tracking Adiabatic Calorimeter 19
2.4.2 Isothermal Calorimeter 22
2.4.3 Liquid-liquid Equilibrium Calculations 25
3. RUNAWAY STUDIES FOR THE 2-METHYLPYRIDINE *N*-OXIDATION 28
3.1 Study of 2-methylpyridine *N*-oxide Decomposition 30

Page

3.2 Study of the Decomposition of Hydrogen Peroxide 38
3.2.1 Hydrogen Peroxide Decomposition Runaway 43
3.2.2 Kinetics for the Non-catalytic H_2O_2 Decomposition 48
3.2.3 Kinetics for the Catalytic H_2O_2 Decomposition 52
3.3 Study of the Runaway for Hydrogen Peroxide, 2-methylpyridine *N*-oxide and Phosphotungstic Acid Mixtures 59
3.4 Summary 67

4. *N*-OXIDATION OF ALKYLPYRIDINES AT DIFFERENT CONDITIONS 69

4.1 2-methylpyridine *N*-oxidation 70
4.1.1 Effect of Catalyst and Temperature on the 2MP N-oxidation 71
4.1.2 Study of H_2O_2 Accumulation and Dosing Rate Effects 85
4.2 2,6-dimethylpyridine *N*-oxidation 90
4.3 Summary 94

5. PHASE EQUILIBRIUM IN THE *N*-OXIDATION OF ALKYLPYRIDINES 96

5.1 Experimental Liquid-Liquid Equilibrium for 26DMP/Water 96
5.2 Prediction of Liquid-Liquid Equilibrium 98
5.2.1 System: 26DMP/Water 98
5.2.2 System: 26DMP/Water/3MP 101
5.2.3 System Containing Hydrogen Peroxide 102
5.2.4 Systems Containing Acetic Acid 105
5.3 Summary 110

6. CONCLUSIONS AND FUTURE WORK 111

6.1 Conclusions 111
6.1.1 Conditions for a Safer and More Efficient N-oxidation Reaction 111
6.1.2 Additional Hazards in the *N*-oxidation of Alkylpyridines 114
6.2 Recommendations 116
6.2.1 Calorimetric Studies 116
6.2.2 Thermodynamic Studies 118

REFERENCES 120
APPENDIX A 126
VITA 129

LIST OF FIGURES

Page

Figure 1. Commonly employed alkylpyridines 2

Figure 2. Structure of the $[PW_{12}O_{40}]^{-3}$ anion 4

Figure 3. Reactor temperature profile during normal and upset operation leading to a runaway with secondary reactions 8

Figure 4. Relationship between temperature of desired and secondary reactions and the hazard of the process 10

Figure 5. Methodology for the study of the *N*-oxidation of Alkylpyridines. 17

Figure 6. Simplified diagram for the APTAC employed in the runaway studies 20

Figure 7. Typical temperature profiles for the a) Isothermal mode, and b) Heat-Wait-Search (HWS) mode in the APTAC 21

Figure 8. Isothermal calorimeter employed to study the *N*-oxidation reaction 23

Figure 9. Typical temperature and pressure profiles for the different steps in the experiments performed using the isothermal calorimeter 24

Figure 10. *N*-oxidation of 2MP and the potential secondary reactions during a runaway 29

Figure 11. Temperature and pressure profile for the decomposition of 2NOX studied using the APTAC in HWS mode 30

Figure 12. Temperature profiles for the isothermal decomposition of 2NOX at different temperatures and amounts of catalyst 32

Figure 13. Pressure increase during the isothermal decomposition of 2NOX a) at 230 ^{o}C and different amounts of catalyst, and b) at different temperatures with no catalyst 33

Figure 14. Pressure rate profiles for the isothermal decomposition of 2NOX a) at 230 ^{o}C and different amounts of catalyst, and b) at different temperatures and no catalyst 35

Figure 15. O_2 moles estimated from the mass loss at different temperatures and amounts of catalyst 36

Figure 16. Typical GC-MS spectrum for the product decomposition of 2NOX 37

Figure 17. Temperature and pressure profile for the decomposition of 17.5 % H_2O_2 without catalyst 39

Figure 18. a) Temperature and b) Pressure profiles for the decomposition of 17.5 % H_2O_2 with different amounts of catalyst 40

Figure 19. a) Temperature and b) Pressure profiles for the decomposition of 35 % H_2O_2 at different amounts of catalyst 42

Page

Figure 20. "Onset" temperature for the decomposition of 17.5 % and 35 % H_2O_2 44

Figure 21. Temperature at maximum rate, T_{max}, for the decomposition of 17.5 % and 35 % H_2O_2 45

Figure 22. Maximum heat rate, $(dT/dt)_{max}$, for the decomposition of 17.5 % and 35 % H_2O_2 45

Figure 23. Pressure rate at maximum rate $(dP/dt)_{max}$ for the decomposition of 17.5 % and 35 % H_2O_2 46

Figure 24. Adiabatic temperature increase for the decomposition of 17.5 % and 35 % H_2O_2 47

Figure 25. Prediction of non-catalytic H_2O_2 decomposition by a n^{th} order reaction rate 51

Figure 26. Prediction of a) the temperature and b) the heat rate for the catalytic decomposition of 17.5 % H_2O_2 54

Figure 27. Prediction of a) the temperature and b) the heat rate for the catalytic decomposition of 35 % H_2O_2 55

Figure 28. Relationship between the parameters A' and B' and the amount of catalyst Z_m for the decomposition of 17.5 % and 35 % H_2O_2 57

Figure 29. Relationship between the parameters A'', B'', and the catalyst-H_2O_2 ratio R' 58

Figure 30. a) Temperature, and b) Pressure profiles for the decomposition of 2NOX and 17.5 % H_2O_2 using different amounts of catalyst 61

Figure 31. a) Temperature and b) Pressure profiles for the decomposition of 2NOX and 35 % H_2O_2 at different amount of catalyst 62

Figure 32. Different cases for the mutual effect of the H_2O_2 and 2NOX decompositions 63

Figure 33. Comparison of the non-catalytic decompositions without and with 2NOX using a) 17.5 % H_2O_2 and b) 35 % H_2O_2 65

Figure 34. Comparison of the heat rate vs. temperature for the decomposition of 17.5 % H_2O_2 with and without 2NOX using 0.2 g of catalyst 66

Figure 35. Pressure increase during the dosing (and stir-out) period for the isothermal tests 72

Figure 36. Pressure increase during the baseline test 74

Figure 37. Pressure increase during the dosing (and stir-out) period for the isothermal *N*-oxidation of 2MP at different temperatures and amount of catalyst 75

Figure 38. Pressure rate during the dosing (and stir-out) period for the *N*-oxidation of 2MP at different temperatures and amounts of catalyst 76

Page

Figure 39. Reaction power and dosing power for the *N*-oxidation of 2MP at 110 ^{o}C and 3.5 g of catalyst 81

Figure 40. *N*-oxidation and decomposition power for the 2MP *N*-oxidation at 110 ^{o}C and 3.5 g of catalyst 83

Figure 41. Averaged power for the *N*-oxidation of 2MP at different temperatures and amounts of catalyst 84

Figure 42. Averaged H_2O_2 decomposition power for the *N*-oxidation at different temperatures and amounts of catalyst 84

Figure 43. Pressure increase for the two stages of dosing (and stir-out) during the *N*-oxidation of 2MP at 125 ^{o}C and 3.5 g of catalyst 86

Figure 44. Pressure increase for the two stages of dosing (and stir-out) for the study of H_2O_2 accumulation during the *N*-oxidation of 2MP at 110 ^{o}C and 3.5 g of catalyst....87

Figure 45. Pressure increase during the *N*-oxidation of 2MP at 110 ^{o}C and 3.5 g of catalyst using different dosing rates....89

Figure 46. Pressure increase for the four different dosing steps during the 26DMP *N*-oxidation at 110 ^{o}C and 7 g of catalyst....92

Figure 47. Pressure increase in the different dosing steps during the 26DMP *N*-oxidation at 120 ^{o}C and 7 g of catalyst....94

Figure 48. Experimental liquid-liquid phase diagram for 26DMP-water....97

Figure 49. Comparison between the experimental and the estimated LLE for 26DMP-water using ASPEN®....100

Figure 50. Comparison of experimental data with the prediction of the ternary diagram for 26DMP-3MP-Water at 79 ^{o}C using UNIFAC, UNIF-DMD, and UNIF-LBY methods....102

Figure 51. Predicted liquid-liquid phase diagram for the ternary system: 26DMP-Water-Hydrogen peroxide at 120 ^{o}C using the UNIFAC method and the UNIF-LBY method....104

Figure 52. Predicted liquid-liquid phase diagram for the ternary system 26DMP-3MP-H_2O_2 at 79 ^{o}C using UNIFAC and UNIF-LBY methods 105

Figure 53. Liquid-liquid phase diagram in terms of water wt. % for a mixture of 26DMP, water, and acetic acid at different initial concentrations 108

Figure 54. Predicted ternary liquid-liquid phase diagram for a mixture of 26DMP, water, and acetic acid at 120 ^{o}C 109

Figure 55. Predicted ternary phase diagram for 26DMP-water-acetic acid at different temperatures 109

Page

Figure 56. Reactor and jacket temperature before and after dosing for an experiment were water was dosed into a solution of 26DMP-water at 60 ^{o}C 118

Figure 57. Detection of the phase change of a solution of 26DMP-water (x_{26DMP} = 0.1) during the heating at 1 ^{o}C min^{-1}.....118

LIST OF TABLES

Page

Table 1. Properties of the reacting mixture affecting the safety of the *N*-oxidation of alkylpyridines....6

Table 2. Strategies for inherently safer process....9

Table 3. List of chemicals employed in the isothermal and in the adiabatic tests....19

Table 4. Amounts employed in the 2MP stability tests....29

Table 5. Experimental details for the study of the decomposition of 2NOX....31

Table 6. Experimental details for the study of the decomposition of hydrogen peroxide using the APTAC in HWS mode....38

Table 7. Parameters to assess the runaway behavior of the H_2O_2 decomposition....43

Table 8. Kinetic parameter for the non-catalytic decomposition of H_2O_2....51

Table 9. Kinetic parameters for the catalytic decomposition of H_2O_2....56

Table 10. Experimental details and "onset" temperatures for the runaway study of H_2O_2, 2NOX, and catalyst mixtures....59

Table 11. Experimental details for the study of the *N*-oxidation of 2MP using an isothermal calorimeter....71

Table 12. Pressure and conversion for the isothermal *N*-oxidation of 2MP at different temperatures and amounts of catalyst....77

Table 13. UA, baseline, and reaction heat estimated for the *N*-oxidation of 2MP at different temperatures and amounts of catalyst....80

Table 14. *N*-oxidation heat, decomposition heat, and heat of reaction for the *N*-oxidation at different temperatures and amounts of catalyst....82

Table 15. Dosing pressure, O_2 moles, and 2MP conversion for three isothermal tests studying different effects....90

Table 16. Experimental details for the isothermal *N*-oxidation of 26DMP....91

Table 17. Moles of oxygen produced in each dosing step during the *N*-oxidation of 26DMP at 110 ^{o}C and 7 g of catalyst....93

Table 18. Pressure increase and moles of oxygen for each dosing step during the *N*-oxidation of 26DMP at 120 ^{o}C and 7 g of catalyst....94

Table 19. Estimated UNIQUAC parameter for the LLE of 26DMP-water....99

Table 20. Estimated binary parameters for the systems 3MP-Water and 26DMP-3MP....101

Page

Table 21. UNIQUAC Binary parameters for the system 26DMP-H_2O_2 and H_2O_2-H_2O using the UNIFAC and UNIF-LBY methods.....103

Table 22. UNIQUAC Binary parameters for the system 26DMP-3MP and 3MP-H_2O_2 using the UNIFAC and UNIF-LBY methods.....104

Table 23. Estimated UNIQUAC binary parameters for the systems 26DMP-Acetic Acid and Acetic acid-water 106

Table 24. Initial concentrations for the generation of phase diagrams for a mixture of 26DMP, water, and acetic acid 107

Table 25. Summary of the conditions considered in this work to increase efficiency and safety of the *N*-oxidation reaction and the safety considerations associated with each condition 112

Table 26. Updated list of hazards related to the *N*-oxidation of alkylpyridines.....115

1. INTRODUCTION

The hazardous properties of the compounds and the hazardous situations that may emerge from abnormal circumstances determine the risks of chemical reactions in industrial processes. Within the alternatives to reduce these hazards and prevent a potential incident, the application of inherently safer approaches, e.g. change of the chemistry of the reaction, can address intrinsic process hazards and dramatically improve safety. However, the application of these alternatives can only be achieved through the detailed theoretical and/or experimental evaluation of kinetic and thermodynamic properties of the reaction mixture under all different conditions at which the reactor can operate.

In this research, alternatives to reduce the hazards of batch reactors without compromising the efficiency of the process are considered. The chemical reaction used to illustrate the methodology is the *N*-oxidation of alkylpyridines which is employed in the pharmaceutical industry. As will be demonstrated later, many of the hazards associated with this system are typical for numerous other batch reactions of the pharmaceutical, agrochemical and fine chemical industry.

1.1 The *N*-oxidation of Alkylpyridines

The *N*-oxidation of alkylpyridines is a reaction used in the pharmaceutical industry [1]. In the *N*-oxidation, (1), the alkylpyridine reacts with hydrogen peroxide (H_2O_2) to form alkylpyridine *N*-oxide and water (H_2O). The *N*-oxidation is catalyzed by phosphotungstic acid and it is generally performed in an open, isothermal semi-batch reactor equipped with an overhead condenser. The reaction is performed at atmospheric pressure and temperatures near the normal boiling point of the mixture (90-95 ^{o}C) [1, 2].

This dissertation follows the style of Journal of Hazardous Materials.

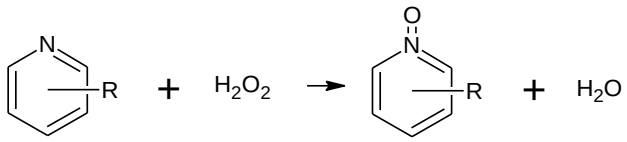

(1)

In the process, the alkylpyridine and catalyst are placed in the reactor and the mixture is heated to the desired temperature. An excess of hydrogen peroxide is dosed into the reactor, and shortly after the end of dosing, the excess of hydrogen peroxide is neutralized, and the mixture is taken for separation [1]. The reaction occurs in liquid phase because the catalyst, a white solid, is soluble in water. The *N*-oxidation is inevitably accompanied by the catalytic decomposition of hydrogen peroxide, which plays a key role in the safety and efficiency of this process.

1.1.1 Alkylpyridines and Alkylpyridines N-oxides

Alkylpyridines are compounds structurally similar to benzene derivatives, except for the presence of a nitrogen atom in the ring [3]. Alkylpyridines are used as solvents and as precursors of other substituted pyridines [3]. These compounds are also employed in the pharmaceutical industry to produce anti-ulcer drugs and anti-tuberculosis agents, and in the manufacture of herbicides, insecticides, fungicides and polymers. Specific uses include 2-methylpyridine in the production of the polymer 2-vinylpyridine for tires and 3-methylpyridine in the manufacture of vitamin B_3 (niacin) [3-5]. Some industrially common alkylpyridines are shown in Figure 1. 2-methylpyridine and 2,6-dimethylpyridine are the focus of this research.

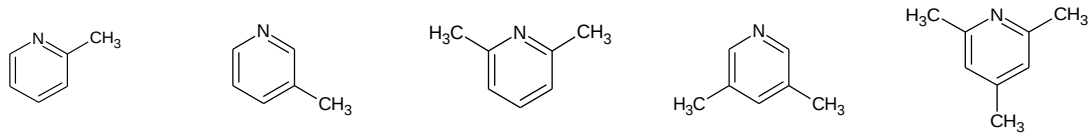

2-methylpyridine (2MP) | 3-methylpyridine (3MP) | **2,6-dimethylpyridine (26DMP)** | 3,5-dimethylpyridine (35DMP) | 2,4,6-trimethylpyridine (246TMP)

Figure 1. Commonly employed alkylpyridines. 2-methylpyridine and 2,6-dimethylpyridine are the focus of this study

For the alkylpyridines shown in Figure 1, the boiling points range from 130 ^{o}C to 173 ^{o}C. Additionally, these compounds are characterized for being flammable [3].

Alkylpyridine *N*-oxide, the product of the *N*-oxidation reaction, is employed in the synthesis of analgesic, anti-inflammatory, and antiulcer drugs like omeprazole [3, 4]. Many of these compounds are soluble in water and hygroscopic.

1.1.2 Hydrogen Peroxide

Hydrogen peroxide is considered an environmentally friendly oxidizer and is commonly used in the pulp and paper industry [6]. Hydrogen peroxide at different concentrations finds different applications in the chemical manufacture of organic and inorganic compounds, in the metal surface treatment, in the waste water treatment, and as a propellant [6, 7]. Due to the weakness of the peroxide bond (-O-O-), hydrogen peroxide decomposes very easily into water and oxygen, (2):

$$H_2O_2 \longrightarrow 1/2\,O_2 + H_2O \qquad (2)$$

The decomposition of hydrogen peroxide is exothermic and releases approximately 100 kJ per mol of H_2O_2 decomposed [6, 7]. At room temperature, H_2O_2 can decompose at a rate of 1% per year and the percentage increases as the temperature raises [8]. Hydrogen peroxide is very sensitive and its decomposition can be easily promoted by impurities and changes in the conditions of the system, e.g. pH [9]. Additionally, hydrogen peroxide is incompatible with many different materials, e.g. alcohols [10], and can also form explosive mixtures with organic compounds when the concentration exceeds 40 wt. % H_2O_2 [9]. Hydrogen peroxide is widely use in the industry, but because of its reactivity and its condition-sensitive decomposition, it has been the primary cause of numerous incidents [8, 10-13].

1.1.3 Phosphotungstic Acid

Phosphotungstic acid ($H_3[PW_{12}O_{40}].nH_2O$), Figure 2, belongs to the family of heteropolyacid catalysts. Heteropolyacids can be used as a homogeneous catalyst when in solution, or as a heterogeneous catalyst when supported on a substrate [14]. Because of their unique properties, several works have reported the growing potential in the use of these catalysts in the industry [15, 16]. Heteropolyacid catalysts are considered green catalyst because they are non-toxic, non-corrosive, non-volatile, and they have no smell [14, 16]. These catalysts have also high selectivities and activities, are stable in storage, and can be re-used [14].

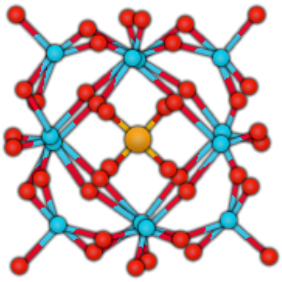

Figure 2. Structure of the $[PW_{12}O_{40}]^{-3}$ anion. Orange represents the phosphorus atom, blue represents the tungsten atoms, and red represents the oxygen atoms (Adapted from [17])

Phosphotungstic acid (PTA) is a white solid, and it is soluble in water and non-soluble in organic compounds like benzene [14, 18]. The solubility properties are associated with the capacity of the PTA molecules to interact with compounds containing oxygen atoms in the structure [18, 19]. This catalyst is characterized by its high Brønsted acidity and its thermal stability [14, 19].

In the *N*-oxidation, PTA provides high selectivity and offers the possibility of being separated for reuse while maintaining its activity. PTA is also employed in hydrations, esterifications, alkylations and polymerizations, among other reactions [14, 16, 19].

1.2 Hazards in the *N*-oxidation of Alkylpyridines

An *N*-oxidation reaction runaway could be developed if the reactor experiences an operational upset, e.g. a cooling failure. During the runaway reaction in an open reactor, the system behaves adiabatically and the heat released by the reaction increases the temperature of the mixture up to the boiling point (around 100 ^{o}C). From this point, the reaction heat is removed by evaporation, thus the temperature remains practically constant until the reactants are consumed or completely evaporated. However, an inadequately vented or closed reactor with an accumulation of hydrogen peroxide could experience an overpressure caused by the generation of vapors and gases. Additionally, the flammable vapors of the alkylpyridine combined with an oxygen-rich atmosphere caused by H_2O_2 decomposition could lead to a fire or an explosion if an ignition source, even of low energy, is present [9]. If the temperature increases significantly, secondary decompositions, e.g. product decomposition, could also start and worsen the consequences [20].

For high order alkylpyridines (26DMP, 35DMP, and 246TMP in Figure 1), two liquid phases can be distinguished during the reaction: an organic phase and an aqueous phase. As indicated earlier, the solubility of the catalyst in compounds lacking of oxygen atoms like alkylpyridines is poor; therefore, most of the catalyst remains in the aqueous phase promoting the decomposition of hydrogen peroxide. Similarly, the selectivity, thus the efficiency, of the *N*-oxidation reaction is reduced because part of the hydrogen peroxide is decomposed and because the reaction volume is not fully utilized (reaction takes place mostly at the interphase).

The key properties of the reacting compounds affecting the safety of the *N*-oxidation are summarized in Table 1.

Table 1. Properties of the reacting mixture affecting the safety of the *N*-oxidation of alkylpyridines

Hazards	
Alkylpyridines	▪ Flammable

Hydrogen peroxide	▪ Reactive and Unstable
	▪ Decomposes at "low" temperature
	▪ Decomposes vigorously with PTA
	Upon decomposition produces:
	▪ Heat
	▪ Oxygen
	  ▪ Oxygen enrichment
	  ▪ Over-pressurization

Hazardous conditions	
Phase separation	▪ Promotes H_2O_2 decomposition

The hazards are mainly associated with the flammability of the alkylpyridines and the reactivity and instability of hydrogen peroxide. The decomposition of hydrogen peroxide represents a hazard because it can occur at low temperature, e.g. 50 ^{o}C, especially under the presence of PTA, and releases oxygen and heat. The oxygen produced during the decomposition can over-pressurize the reaction vessel and can create a flammable atmosphere. The hazards associated with hydrogen peroxide are more significant during the *N*-oxidation of high order alkylpyridines because of the presence of two-liquid phases. As mentioned earlier, when a two-liquid phase mixture forms, the H_2O_2 decomposition is promoted in the aqueous phase. Additionally, the phase separation affects the efficiency of the *N*-oxidation because the reaction occurs mainly at the interphase and because not all the H_2O_2 is being used in the *N*-oxidation.

1.3 Calorimetry as a Tool for Hazard Identification

Incidents in the industry related to chemical reactivity occur mainly due to [21, 22]:

- Inadequate knowledge of the chemical and thermodynamic properties of the compounds and their mixtures;
- Inadequate identification and evaluation of hazards;
- Lack of understanding of the process;

- Inadequate process design;
- Inadequate procedures and training programs; and
- Lack of appropriate safety measures to prevent incidents.

Such incidents have occurred mainly in the chemical manufacturing and have involved different equipment of the process such as storage tanks, reaction vessels, and separation equipment [21].

In exothermic processes, situations such as poor temperature control, presence of contaminants, agitation failure, incorrect recipes, or inadequate operational procedures can create upset conditions that can cause an uncontrollable increase in temperature (heat generated is larger than heat removed) [20, 23]. Figure 3 shows the simplified temperature profile for an isothermal batch or semi-batch reaction under normal operation (bold line). The reaction mixture is heated to a desired temperature, $T_{desired}$, and maintain for a certain amount of time, at the end of which the products are cooled. Should a deviation occur during normal operation, the reaction starts behaving adiabatically increasing the temperature by ΔTad_1. In this case (Figure 3, dotted line), the maximum adiabatic temperature reaches the "onset" temperature for secondary decompositions, consequently leading to an additional increase in temperature (ΔTad_{sec}). The temperature increase is usually accompanied by gas and/or vapor evolution which increases the pressure of the system. If the reaction vessel is not designed to withstand these conditions, flammable or toxic materials may be released and may lead to fires or explosions [20].

From a safety point of view, it is very important to know the value of ($T_{desired}$ + ΔT_{ad}), called the maximum temperature attainable by the synthesis reaction (MTSR), because, together with the quantity ΔTad_{sec}, define the extent of potential damage. Finally, time lengths like the time to maximum rate (TMR) are of preponderant importance as they define the time available to avert damages.

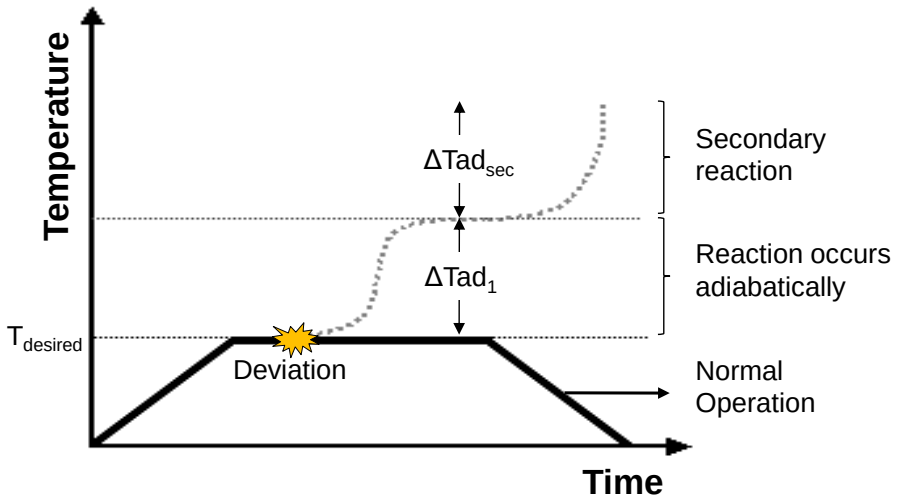

Figure 3. Reactor temperature profile during normal (bold line) and upset (dotted line) operation leading to a runaway with secondary reactions (Adapted from [23])

Qualitative and quantitative information on reaction behavior can be obtained by appropriately designed calorimetric experiments. Differential Scanning Calorimetry (DSC), heat-flow or power compensation reaction calorimetry, adiabatic and Dewar calorimetry are some typical tools employed. Calorimetry is used to characterize reactions, to assess reactivity hazards, and to identify the runaway behavior of a particular process [22]. For the characterization of the reaction, process variables, such as cooling requirements, concentrations, and dosing rates, can be determined. The kinetics and the critical limits of operability, e.g. maximum and minimum temperature and pressure, can be also defined [23, 24]. For a runaway, parameters for potential secondary reactions such as the adiabatic temperature increase and the pressure increase rate can be assessed [24]. The knowledge of all these parameters before the implementation of a full scale process, it is imperative for the prevention of undesired situations in case of a reaction runaway.

Screening methods using tools like the Differential Scanning Calorimeter (DSC) are useful to get a preliminary insight into the potential reactivity hazards related to a particular process and to determine whether additional testing is required [24]. More sophisticated tools, e.g. the Automatic Pressure Tracking Adiabatic Calorimeter

(APTAC), are employed to obtain detailed information on the consequences if a system undergoes a runaway. Compared with the aforementioned small scale methods, isothermal calorimeters employs larger samples to assess conditions more related to the normal process operation e.g. kinetics, degree of accumulation, and reaction enthalpy [24]. The selection of the experimental method for reactive hazard evaluation depends on the type of information required and the potential limitations of the equipment for the application. Some works have outlined the uses and pitfalls of different techniques in Calorimetry [20, 23, 24]. Other methodologies propose the use of computational calculations and experimental data to systematically identify reactive hazards [25].

1.4 Inherent Safety

Inherent safety was first proposed by Trevor Kletz with the concept *"What you don't have, can't leak"* [26]. This concept refers to the application of alternatives that eliminate or reduce (rather than control) the hazards in a process to the point where a safe condition can be maintained after an abnormality has occurred in the system.

An inherently safer process can be achieved by applying at least one of the strategies shown in Table 2. Moreover, the application requires a detailed study to determine the potential safety implications in other areas of the process [27]. A more comprehensive list of alternatives to consider for each strategy is provided by other authors [27-29].

Table 2. Strategies for inherently safer process

Strategy	Example
Minimize	Reduce inventory of hazardous materials
Substitute	Replace a toxic material by a less hazardous chemical Use alternative chemistry
Moderate	Operate at less severe conditions such as lower temperatures and pressures
Simplify	Reduce the complexity of the systems

In order to apply the inherent safety concept in the reactive chemicals field, it is important to understand the hazards associated with a particular process [27, 30]. Information from the literature as well as calorimetric studies are useful to fulfill such a purpose. Similarly, the identification of molecular groups in the structure of the compounds such as peroxides (-O-O-) and nitroso compounds (-C-N=O), can provide an idea of the reactivity [10, 23, 31]. Other tools such as the interaction matrix are helpful in the identification of additional hazards due to incompatibilities in case of inadvertent mixing or the presence of impurities in the system [30].

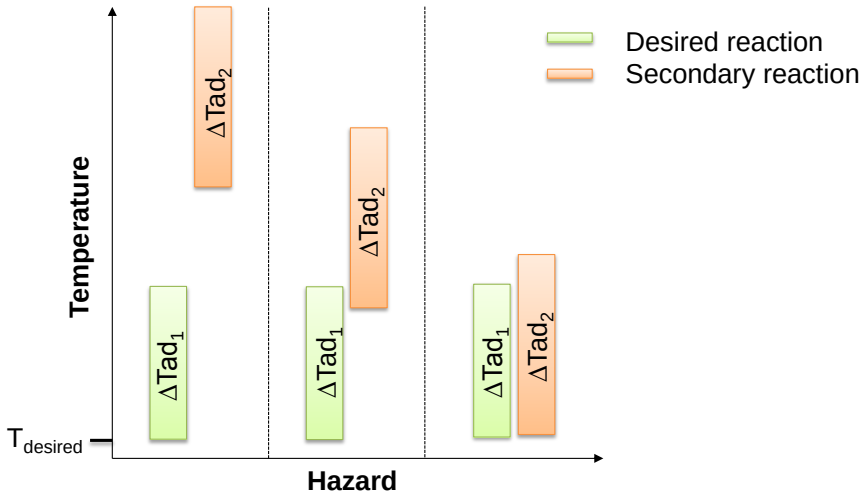

Figure 4. Relationship between temperature of desired and secondary reactions and the hazard of the process (Adapted from [24])

Empirical criteria can be used to determine whether a reaction is inherently safer or not. An example of such criteria is the difference between the maximum temperature of the reaction ($T_{desired}$ + ΔTad_1) and the temperature at which secondary decompositions start, Figure 4. If the difference is above 50 ^{o}C, the process is considered “safer”. As the difference between these two temperatures decreases, the reaction becomes more hazardous [24].This criterion can be applied as a preliminary evaluation of the hazards in simple reactions. For more complex systems like the *N*-oxidation of alkylpyridines, a

more thorough study is required due to the condition-dependency provided by the presence of hydrogen peroxide.

During the *N*-oxidation, the use of a semi-batch process where hydrogen peroxide is gradually dosed into the reactor is an example of one inherently safer alternative employed. This alternative reduces the possibility of H_2O_2 accumulation inside the reactor [24]. As such, if an abnormal situation occurs, the dosing can be stopped and the amount of hydrogen peroxide available to decompose is limited to the H_2O_2 accumulated in the reactor. This is practically zero at the initial stages of the reaction, but its concentration can be seriously destructive if a runaway occurs near the end of dosing.

2. RESEARCH METHODOLOGY AND METHODS

The present study addresses issues relevant with the efficiency and the inherent safety of the *N*-oxidation while advances further the research previously done in this area. Some of the key previous findings which are relevant in the present study are outlined in the next paragraphs. Moreover, through the course of the present work, using the *N*-oxidation of alkylpyridines as a model reaction, research and validation methodologies for complex batch systems employing reactive chemicals have been developed.

2.1 Previous Findings

The *N*-oxidation of alkylpyridines using hydrogen peroxide as the oxidizing agent and phosphotungstic acid as the catalyst has been previously studied at atmospheric pressure and temperatures between 85 and 100 ^{o}C using isothermal calorimeters [2, 32-39]. All collected evidence pointed out that the process would be more efficient and inherently safer if the reactor could operate in a single phase, at high alkylpyridine and low hydrogen peroxide concentrations, and at higher temperatures and/or higher catalyst concentrations. However, further research and validation are required to support sufficiently those findings.

2.1.1 Finding 1

A kinetic model for the *N*-oxidation of alkylpyridines and for the undesired decomposition of hydrogen peroxide has been proposed, and it has successfully described the *N*-oxidation of 2-methylpyridine and 3-methylpyridine in the range of temperatures between 85 ^{o}C and 100 ^{o}C. However, the error of the rate coefficients of the model was very high because at lower temperatures, H_2O_2 decomposition predominates and becomes essentially controlled by dosing, while, at the same time, it leaves little oxidant for the *N*-oxidation. At higher temperatures on the other hand, the *N*-oxidation becomes very fast so that insufficient data for kinetic studies can be collected. Additionally, for the *N*-oxidation of high order alkylpyridines such as 2,6-dimethylpyridine and 3,5-dimethylpyridine, the effects related with the presence of two-

liquid phases contributed to the presence of a variation between the modeled and the measured values [2, 36].

2.1.2 Finding 2

Temperature dramatically favors the synthesis reaction. Catalyst also enhances selectivity towards the *N*-oxidation. Therefore, it is plausible that they could be used to increase selectivity of H_2O_2 for *N*-oxidation to such an extent, so that decomposition of hydrogen peroxide is practically eliminated. Currently, the reaction is performed in an open vessel to allow escape of the produced oxygen. Thus, the normal boiling point of the reacting mixture (~100 ^{o}C) defines the maximum reaction temperature. However, the previous research indicates that this choice results in increased consumption and waste of hydrogen peroxide, in increased hazard if a runaway occurs near the end of dosing and in an increased number of separations as otherwise unnecessary chemicals are rapidly added into the reactor to neutralize the excess of H_2O_2. Based on these findings, a closed process that produces no oxygen is considered here as an alternative to an open process [36, 38]. *However, this argument has to be tested experimentally by performing the reaction in a closed system at higher temperatures and then identify the optimal process temperature and amount of catalyst. Moreover, before such an option is selected, the thermal stability of the product has to be studied so as to ensure that it does not decompose at those elevated temperatures. Additionally, in terms of safety, the effect of different conditions (e.g. temperature, catalyst concentration, hydrogen peroxide concentration) on the thermal decomposition of the product has to be studied employing adiabatic calorimetry.*

2.1.3 Finding 3

The presence of two-liquid phases during the *N*-oxidation of alkylpyridine with a reduced miscibility in water favors the decomposition of hydrogen peroxide over the *N*-oxidation. Moreover, the phase equilibrium changes as the reaction advances resulting in a homogenous mixture near reaction completion. As such, it is desirable to obtain conditions for homogeneous solution that improve the safety and the efficiency of this

process [36]. *However, limited information is available on the liquid-liquid equilibrium of mixtures containing alkylpyridines, and the thermodynamic data for alkylpyridine N-oxides is scarce.*

2.1.4 Finding 4

The catalytic decomposition of hydrogen peroxide is condition dependent; and the presence of alkylpyridines was found to have a detrimental effect on its decomposition rate. Similarly, the catalytic decomposition was determined to be approximately two orders of magnitude faster than the thermal H_2O_2 decomposition [2, 33, 36]. *However, the effect of different conditions, e.g. H_2O_2 concentration, on the consequences of the decomposition runaway has not been assessed yet.*

2.1.5 Finding 5

In addition to the proposed kinetic model for the *N*-oxidation which includes the undesired H_2O_2 decomposition (finding 1), a kinetic model for the catalytic decomposition of hydrogen peroxide alone was deduced from isothermal measurements. Both models can be employed to predict the reaction runaway for the decomposition by itself and during the *N*-oxidation [2, 35-37]. *However, no measurements in adiabatic mode have been performed to evaluate the runaway behavior of the H_2O_2 decomposition in the N-oxidation of alkylpyridines under different conditions. Moreover, no tests have been performed to see the role and the behavior of the produced N-oxide in such a runaway.*

In order to address the safety and efficiency concerns associated with this reaction and accurately represent the *N*-oxidation of alkylpyridines, it is important to continue further the work previously done. Because the possibility of increasing the selectivity of the *N*-oxidation as the temperature and amount of catalyst are increased is a finding relevant to the safety of the process, the aim of this research is to study the *N*-oxidation reaction over a more extended range of conditions. Additionally, this research deals with the

assessment of the *N*-oxidation during a runaway as well as the understanding of the role of the phase separation in the *N*-oxidation reaction.

2.2 Research Scope and Significance

The present research employs the *N*-oxidation of alkylpyridines as a model reaction, and aims to identify conditions for a more efficient and inherently safer process. One serious issue emerging from the application of the inherent safety methodologies is to ensure process safety *without jeopardizing process efficiency*. For instance, operation at lower temperatures can result in much longer processes, thus increasing the possibility of a fault to occur. Substitution of dangerous chemicals can result in the use of disproportionally large quantities of less harmful chemicals, etc.

Despite the safety concerns arising from the use of hydrogen peroxide, H_2O_2 is a highly effective oxidant leaving no residue at the end of the process, so no better alternatives can be found. Similarly, the catalyst, phosphotungstic acid, provides a unique selectivity for the *N*-oxidation, and it also represents a less expensive alternative due to the possibility of being reused. Consequently, the use of other catalysts and oxidizing agents to produce *N*-oxides [40-43], are not considered here. Instead, the present research focused on the investigation of the synergistic effects which can result in a threatening runaway and how to avert those by selecting the appropriate inherently safer operating conditions which, at the same time, favor the performance of the *N*-oxidation. In addition to the research exclusively serving the *N*-oxidation, the methodology followed here, the interpretation of the experimental results, and the deductions related with hydrogen peroxide and phosphotungstic acid can be easily adapted and serve other processes too.

The objectives of the present research can be summarized as follows:

- *Investigation of 2-methylpyridine N-oxide stability and decomposition paths using adiabatic calorimetry* to assess how operation at higher temperatures may affect product quality and reaction runaway. Additionally, products of decomposition and

synergistic effects arising from its coexistence with catalyst and hydrogen peroxide are examined.

- *Investigation of hydrogen peroxide decomposition paths using adiabatic calorimetry* to determine the effect of different factors on its runaway behavior. The study focuses on the effect that catalyst, H_2O_2 concentration, and 2-methylpyridine-*N*-oxide have on the pathways of its decomposition.

- *Study of 2-methylpyridine N-oxidation reaction over a more extended range of conditions* to validate model predictions indicating that selectivity towards the unwanted H_2O_2 decomposition can be practically zeroed at elevated temperatures.

- *Study of 2,6-dimethylpyridine N-oxidation*. 2,6-dimethylpyridine and higher order alkylpyridines have a reduced miscibility with water, which can further be affected by the presence of the catalyst and 2,6-dimethylpyridine *N*-oxide. As mentioned earlier, when reaction is taking place in two phases, both its efficiency and its safety suffer substantially because there is an excessive decomposition of hydrogen peroxide. Scarce water/alkylpyridine phase equilibrium data show homogeneous mixtures at all compositions at higher temperatures (See Section 5). This research focuses on studying the effect of the phase separation on the *N*-oxidation performed at elevated temperatures in a closed system. Additionally, thermodynamic studies are employed to identify conditions for a homogeneous mixture.

In a broad sense, the results from this research have direct relevance in the study of similar processes with comparable concerns, i.e. processes with phase separation and chemical reaction and processes that use hydrogen peroxide as the organic compound oxidant. Additionally, the methodology and results presented here can be used to evaluate the synergistic effects of chemicals during reaction runaway and use those in the design of improved and more efficient reactors. This research also provides the basis to understand better the *N*-oxidation of alkylpyridines under different conditions, which will allow implementing the appropriate control measures to avoid potential reaction runaways.

2.3 Research Methodology

In order to improve the efficiency and ensure a safe reaction, Moderate, one of the strategies from the inherent safety concept, was applied (See Subsection 1.4). As such, conditions that reduce the decomposition of hydrogen peroxide and favor the *N*-oxidation reaction were identified. Two members of the alkylpyridine family were employed in the present study: 2-methylpyridine (2MP) and 2,6-dimethylpyridine (26DMP). 2MP is the simplest alkylpyridine, and it forms a homogenous solution with water (consequently, phase separation is not a concern in this case). In contrast, 26DMP represents the case where two-liquid phases are present in the reacting mixture in most compositions at the typical conditions of its industrial production (1 atm, ~100 ^{o}C).

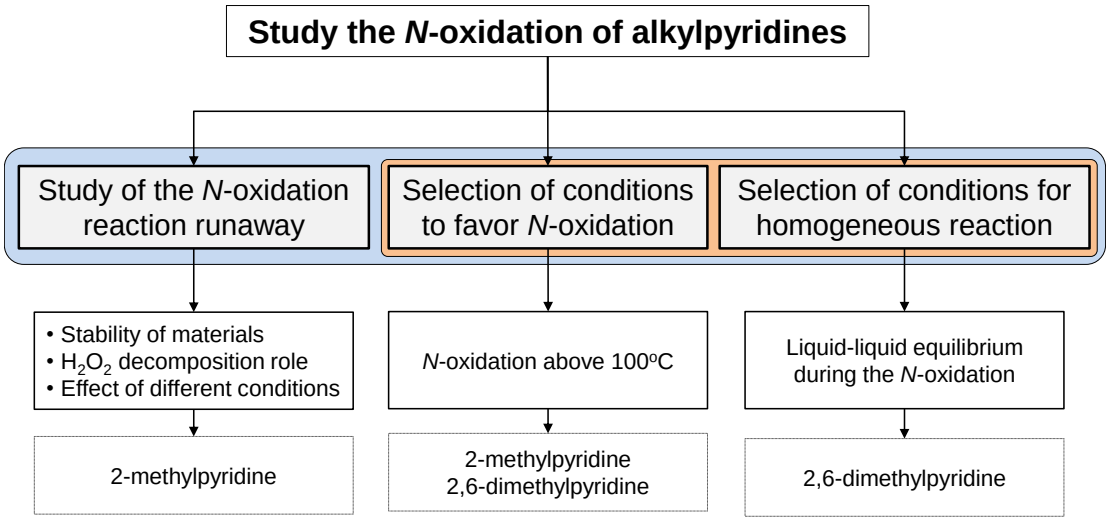

Figure 5. Methodology for the study of the *N*-oxidation of Alkylpyridines. The aspects in the blue box address the safety of the process. The aspects in the orange box address the efficiency of the process

The methodology used for this study is illustrated in Figure 5. Three aspects related to the *N*-oxidation are considered in this methodology: the study of alternatives to reduce the decomposition of hydrogen peroxide, the identification of conditions where homogeneous mixtures can form, and the study of the runaway behavior following

different scenarios. All three aspects are related to the safety of the process and are highlighted in blue (Figure 5). The first two aspects, the reduction of the H_2O_2 decomposition and the identification of conditions for a homogeneous mixture (in orange in Figure 5) can also increase the efficiency of the *N*-oxidation.

For the study of the runaway behavior, three key aspects were investigated: the stability of reactants and products in isolation and synergistically, the role of the decomposition of hydrogen peroxide during the runaway, and the effect of different reaction conditions on the runaway. These studies were performed using an Automatic Pressure Tracking Adiabatic Calorimeter (Subsection 2.4.1) and the results are shown in Section 3. 2-methylpyridine was selected to illustrate this part.

For the reduction of the decomposition of hydrogen peroxide, the *N*-oxidation of alkylpyridine was studied in an isothermal calorimeter (Subsection 2.4.2) at temperatures between 110 ^{o}C and 125 ^{o}C. 2-methylpyridine and 2,6-dimethylpyridine were considered to demonstrate the effect of homogeneous phase and phase separation on the *N*-oxidation, respectively. The results are shown in Section 4.

For the study of the liquid-liquid equilibrium, the Gibbs minimization method incorporated in ASPEN PLUS® (Section 2.4.3) was employed to generate the phase diagrams of different binary and ternary systems. The results are included in Section 5.

The final conclusions from this study and some recommendations for future work are presented in Section 6 and were developed based on three key aspects: feasibility, efficiency, and safety.

2.4 Materials and Methods

Two main calorimeters were employed in this research: an adiabatic calorimeter and an isothermal calorimeter. A description of these apparatus is given in the next subsections. Additionally, the thermodynamic methods employed for the study of liquid-

liquid equilibrium are included at the end. Table 3 lists the chemicals employed in the first two parts of this methodology, the isothermal and the adiabatic measurements.

Table 3. List of chemicals employed in the isothermal and in the adiabatic tests

Tests in the adiabatic calorimeter	Tests in the isothermal calorimeter
2-methylpyridine *N*-oxide **Aldrich P42207, ≥ 96 %**	2-methylpyridine **Fluka 80221**
2-methylpyridine **Fluka 80221**	2,6-dimethylpyridine **Aldrich 336106**
Hydrogen peroxide [a] **Sigma-Aldrich 516813, 50 wt. % in H_2O, stabilized**	Hydrogen peroxide **Alfa Aesar L14000, 35 wt. % in H_2O**
Phosphotungstic acid [b] **Sigma-Aldrich P4006**	

[a] Distilled water was added to obtain 35 wt. % and 17.5 wt. %
[b] Referred as the catalyst hereafter

2.4.1 Automatic Pressure Tracking Adiabatic Calorimeter

An Automatic Pressure Tracking Adiabatic Calorimeter (APTAC), Figure 6, was used to study the runaway behavior of the *N*-oxidation. This calorimeter can be operated in a batch process with small amounts of sample (below 30 g) at temperatures up to 500 ^{o}C and pressures up to 14 MPa (2000 psi) [44]. Only glass cells of approximate capacity of 100 ml were employed in the present study.

During the experiment, the sample cell is loaded with a certain amount of the test compound. The cell is then placed into the pressure vessel and the test is started. Nitrogen is introduced into the pressure vessel to compensate for changes of pressure inside the reaction cell. In this way, thin cells of minimal heat capacity, that reduce accumulation of heat and thus deviation from ideal adiabatic operation, can be employed. Heaters surround the pressure vessel to maintain a temperature close to the sample temperature, thus minimizing the exchange of heat between the cell and its surroundings and maintaining adiabatic conditions. Temperature, pressure, and rates of temperature and pressure change are measured throughout the experiment.

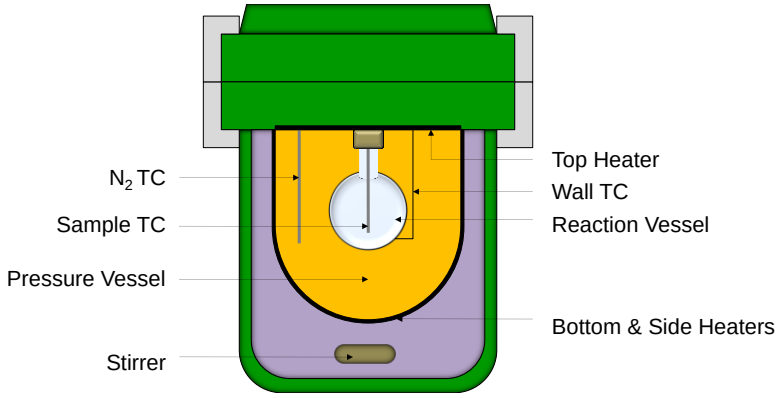

Figure 6. Simplified diagram for the APTAC employed in the runaway studies

The instrument can operate in a number of modes. In the present study, the APTAC was operated in Heat-Wait-Search mode (HWS) and isothermal mode. Typical curves obtained in each case are shown in Figure 7. During the isothermal mode, the temperature is maintained at a desired value for a predetermined length of time. However, the system switches over to adiabatic mode if a predefined threshold value of sample self-heating is exceeded. An additional requirement to switch-over to adiabatic mode when operating in isothermal mode is that an overall temperature rise of at least 1 ^{o}C is also measured [44].

In HWS mode, the sample is heated according to a temperature step rise program. During the “Heat” step, the sample temperature increases by a predefined value. Then, the system allows the temperature to stabilize for a predetermined length of time, “Wait”, to consequently seek an exotherm, “Search”. If no exotherm is detected, the next heating step is implemented. If an exotherm is traced, the system switches-over to adiabatic mode, and the temperature and pressure in the cell are tracked and recorded until completion. An exotherm is detected when the self-heating rate exceeds a predefined threshold value. The point at which the exotherm is detected is known as the "onset", and depends on the specified threshold values as well as the heating step. The increase in temperature caused by the exotherm is known as the adiabatic temperature increase (ΔTad), and, together with the pressure rise, are important parameters to assess the consequences of a runaway.

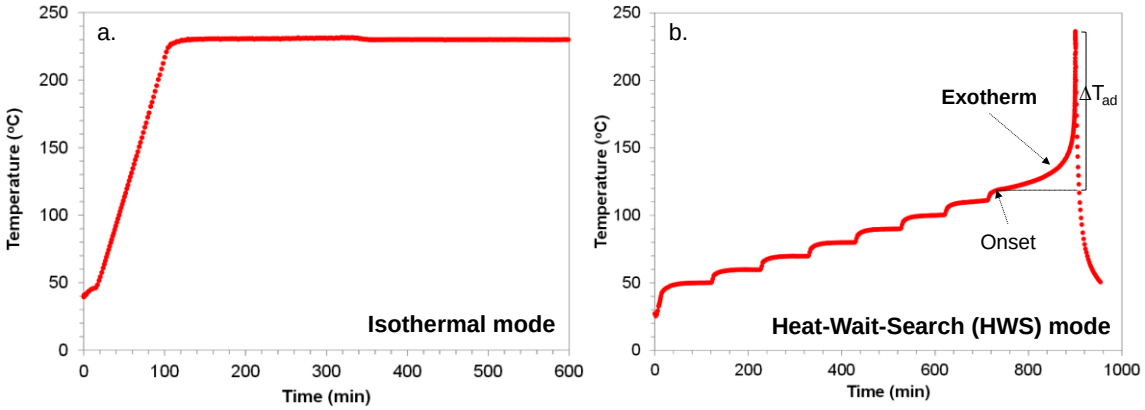

Figure 7. Typical temperature profiles for the **a)** Isothermal mode, and **b)** Heat-Wait-Search (HWS) mode in the APTAC

From the adiabatic measurements, the heat of reaction, i.e. the heat generated per mol reacted, (ΔH_{rxn}) can be estimated using equation (3):

$$\Delta H_{rxn} = \frac{m \cdot C_p \cdot \Delta T_{ad}}{n_{rxn}} \tag{3}$$

where

m	is the sample mass
C_p	is the heat capacity of the sample mass
ΔT_{ad}	is the adiabatic temperature increase
n_{rxn}	are the moles of material reacted

It is worth mentioning here that the operation of the cell approaches by it is not ideally adiabatic. To account for the deviation from adiabatic behavior due to the heating of the sample cell, a thermal inertia factor, ϕ, also called phi-factor, has been established [45]. This factor is defined by equation (4):

$$\phi = 1 + \frac{m_c \cdot C_{p,c}}{m_s \cdot C_{p,s}} \tag{4}$$

where

ϕ	is the thermal inertia or phi-factor

m is mass for the sample cell, *c*, and the sample, *s*

C_p is heat capacity for the sample cell, *c*, and the sample, *s*

In this work, the phi-factor was calculated using an average heat capacity for Pyrex of 0.85 J g^{-1} K^{-1} [46].

The adiabatic temperature increase is corrected by considering the phi-factor according to equation (5).

$$\Delta T_{ad} = \phi \cdot \Delta T_{ad}^{mes} \quad (5)$$

where

ΔT_{ad}^{mes} is the adiabatic temperature increase measured during the tests

To obtain an additional insight into the decomposition products, gas chromatography-mass spectrometry (GC-MS) was employed to analyze the final samples. For the analysis, samples of 1µL were run on a HP G1800C GCD system. This system consists of an HP 5890 gas-chromatograph, an electron ionization detector, and the HP G1701BA ChemStation software to identify the compounds. A cross-linked 5 % Ph Me silicone HP-5 GC column (30 m × 0.25 mm × 0.25 mm) with helium at 1 mL min^{-1} as the carrier gas were employed in the separation. The inlet and detector temperatures were held at 200 ^{o}C and 280 ^{o}C, respectively; while, a temperature ramp of 10 ^{o}C min^{-1} was used in the oven.

2.4.2 Isothermal Calorimeter

The *N*-oxidation of 2-methylpyridine and 2,6-dimethylpyridine were studied using an isothermal calorimeter, Figure 8.

The isothermal calorimeter employed was a HEL SIMULAR calorimeter. This calorimeter consists of a one-liter glass reactor that can withstand pressures of up to six bar. The jacketed reactor is equipped with a pressure transducer and a relief valve, both

of which are used to ensure the pressure inside the reactor does not exceed the maximum operating pressure. The temperature in the reactor vessel is measured using a platinum resistance thermometer and is maintained at the desired set temperature using a temperature control system. Additionally, the reactor contains an electrical heater for a fast temperature control and for calibrations. The addition of material into the reactor is achieved using a Prominent solenoid metering pump. To control the hardware, acquire data, set safety limits, and calibrate sensors, the calorimeter incorporates WinISO software.

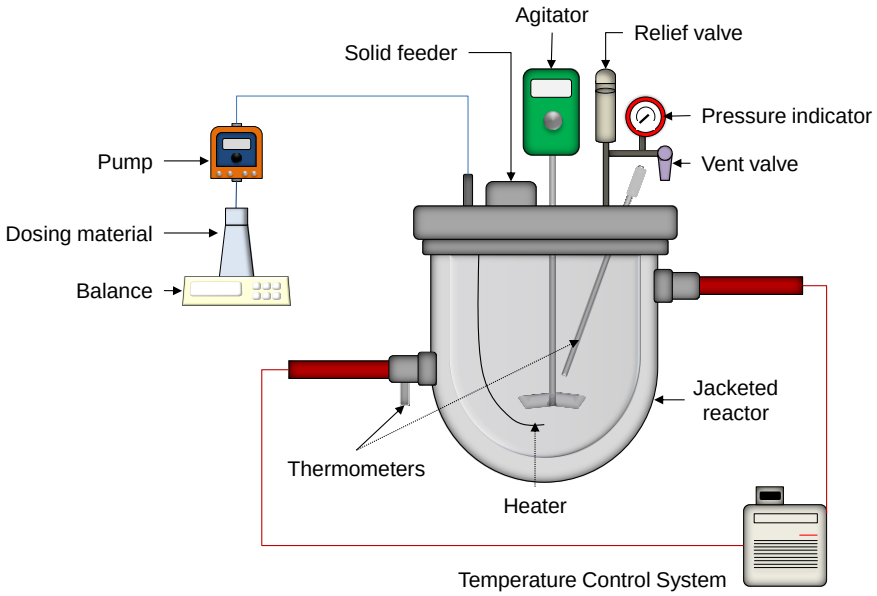

Figure 8. Isothermal calorimeter employed to study the *N*-oxidation reaction

The calorimeter has different operating modes where the temperature of the reactor can be held constant using the electric heater (power compensation mode) or the heat-transfer fluid (oil) circulating in the reactor jacket (heat flow mode). This study has employed the heat flow mode. Power compensation was used in some experiments, but as the temperature employed is above the boiling point of the reaction mixture, the power required to maintain a constant temperature caused boiling around the heater thus making the temperature unstable.

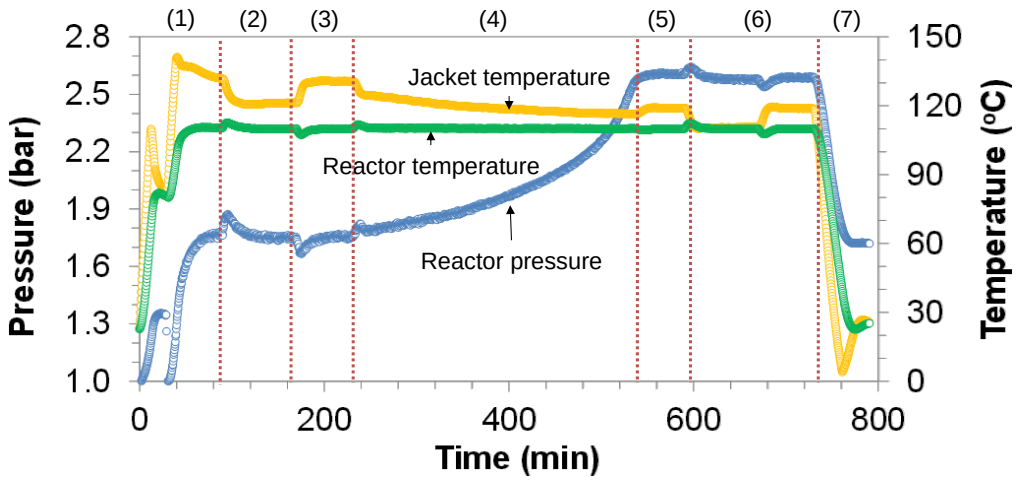

Figure 9. Typical temperature and pressure profiles for the different steps in the experiments performed using the isothermal calorimeter: (1) Heating, (2) Calibration, (3) Stabilization, (4) Dosing, (5) Stir-out, (6) Calibration, and (7) Cooling

Figure 9 illustrates the reactor and jacket temperatures and the pressure profile for the different steps in the experiment. In the process, the alkylpyridine/water mixture and the catalyst are added into the reactor and the system is heated to the desired temperature (step 1). Once the desired temperature is reached, a calibration is performed to determine the heat transfer coefficient (UA) that will be used later in the energy balance (Step 2). Subsequently, the temperature is allowed to stabilize (step 3) to then progressively dose the solution of hydrogen peroxide into the reactor for approximately five hours (step 4). The dosing is followed by a stir-out period (step 5) where accumulated hydrogen peroxide is allowed to react till completion. A second calibration (step 6) is then performed to determine the heat transfer coefficient (UA) after dosing (change in the heat transfer area). Finally, the mixture is cooled down to ambient temperature (step 7).

The following quantities are continuously measured during the experiment: reactor temperature, oil temperature at the entrance of the jacket, dosing temperature, mass and rate of addition of the hydrogen peroxide solution, stirrer speed, and power input from the heater. These quantities are used in the energy balance equation, equation (6), to determine the reaction power:

$$\dot{Q}_{rxn} = \dot{Q}_j - \dot{Q}_h + \dot{Q}_{dos} + Baseline \quad (6)$$

where

$\dot{Q}_{rxn}$	is the reaction power
$\dot{Q}_j$	is the power transferred to the jacket
$\dot{Q}_{dos}$	is the power spent to heat the dosed feed
$\dot{Q}_h$	is the power provided by the heater
Baseline	represents the constant power from stirring and all kinds of potential power losses

More details in the calculations of the reaction power are provided in Section 4.

2.4.3 Liquid-liquid Equilibrium Calculations

For the liquid-liquid equilibrium (LLE) calculations, there are two approaches: the fugacity or k-value method and the Gibbs minimization method. The equal fugacity method meets the mass balance and equal fugacity constraints, but the solutions do not always reach the minimum Gibbs free energy. The Gibbs minimization is appropriate for studying complex systems because this method guarantees the minimum, and therefore, stable solutions are provided [47-51].

In the Gibbs minimization method, as its name indicates, the Gibbs free energy of the system is minimized, equation (7). The minimization is subject to two constraints: the mass balance and the equal fugacity requirements for each component in the mixture:

$$\frac{\Delta_{mix}G}{RT} = \frac{\bar{G}_i(T,P,x) - G_i(T,P)}{RT} = \sum_{i=1}^{c}\sum_{j=1}^{p} n_{ij} \cdot ln\left(\frac{\hat{f}_{ij}}{f_{ij}^{o}}\right) \quad (7)$$

where

$\Delta_{mix}G$	is the Gibbs energy of mixing
$\bar{G}_i$	is the partial molar Gibbs energy
G_i	is the Gibbs energy of pure-component i

n_{ij} is the moles of component i in the phase j

$\hat{f}_{ij}$ is the fugacity of component i in the mixture

f_{ij}^{o} is the fugacity of the pure component i

T is temperature

P is pressure

x is the mole fraction

R is the gas constant

c is the total number of components

p is the total number of phases

For liquid-liquid equilibrium, equation (7) becomes:

$$\frac{\Delta_{mix}G}{RT} = \sum_{i=1}^{c}\sum_{j=1}^{p} n_{ij} \cdot ln\left(x_{ij}\gamma_{ij}\right) \tag{8}$$

where

γ is the activity coefficient of component i in phase j.

For the estimation of the activity coefficients used in equation (8), the universal quasi-chemical (UNIQUAC) method was employed [52-54]. In this method, the activity coefficients are represented by:

$$ln(\gamma_i) = ln\left(\frac{\Phi_i}{x_i}\right) + \frac{z}{2} \cdot q_i \cdot ln\left(\frac{\theta_i}{\Phi_i}\right) + \mathrm{l}_i - \frac{\Phi_i}{\mathrm{x}_i}\sum_k \mathrm{x}_k \mathrm{l}_k - \mathrm{q}_i \cdot ln\left(\sum_k \theta_k' \cdot \tau_{ki}\right) + q_i' - q_i' \cdot \sum_k \frac{\theta_k' \cdot \tau_{ik}}{\sum_h \theta_h' \cdot \tau_{hk}} \tag{9}$$

l_i is defined by equation (10), the segment fraction, Φ_i, is defined by equation (11), and the area fractions, θ_i and $\theta_i^{'}$, are defined by equations (12) and (13).

$$l_i = \frac{z}{2}(r_i - q_i) - (r_i - 1) \tag{10}$$

$$\Phi_i = \frac{r_i x_i}{\sum_k r_k x_k} \tag{11}$$

$$\theta_i = \frac{q_i x_i}{\sum_k q_k x_k} \tag{12}$$

$$\theta_i' = \frac{q_i' x_i}{\sum_k q_k' x_k} \tag{13}$$

where

r	is the molecular volume parameter
q	is the molecular area parameter
q'	is the molecular interaction area parameter
z	is the coordination number (z = 10)
τ_{ki}	is the UNIQUAC binary parameter

r and q are parameters that depend on the molecular structure of the components. τ_{ki} represent the binary parameters and is related to the interaction energy, Δu_{ki}, by:

$$\tau_{ki} = exp\left[\frac{-\Delta u_{ki}}{RT}\right] = exp\left[\frac{-(u_{ki} - u_{ii})}{RT}\right] \tag{14}$$

The liquid-liquid equilibrium (LLE) of different binary and ternary systems in the *N*-oxidation reaction were generated using ASPEN Properties® to estimate the parameters employed in the property model and ASPEN Plus® to determine the phase split. The property method selected for this study was UNIQUAC because it is appropriate to simulate the (LLE) of non-ideal systems. For the phase split, the Gibbs minimization method in the liquid-liquid decanter was employed. More details of the calculations are given in Section 5.

3. RUNAWAY STUDIES FOR THE 2-METHYLPYRIDINE *N*-OXIDATION*

This section includes the adiabatic measurements performed in order to investigate the stability and the decomposition paths of 2-methylpyridine, 2-methylpyridine *N*-oxide and hydrogen peroxide. The decomposition products and the synergistic effects arising from their coexistence as wells as with the catalyst are also shown. Different concentrations of catalyst and hydrogen peroxide were tested to determine the effect of these conditions on the runaway behavior. For the decomposition of hydrogen peroxide, additional studies to develop the kinetics of the decomposition are included. All the measurements shown in this section were performed using the adiabatic calorimeter described in Subsection 2.4.1.

The *N*-oxidation of 2MP can be represented schematically in Figure 10, where in addition to the main reaction, potential secondary reactions related to reactant and products are included. In a potential reaction runaway, all three side decomposition reactions need to be taken into account. Thus, their thermal effects and their rates need to be investigated both in isolation as well as in the presence of the remaining reactants and products.

As already discussed in Section 1, hydrogen peroxide decomposes to form water and oxygen. This decomposition can be thermal or catalytic, the latter being two orders of magnitude faster than the former [36]. The catalytic decomposition of hydrogen peroxide under different conditions as well as its effect on secondary decompositions is shown in Subsections 3.2 and 3.3.

* Part of this section is reprinted with permission from "2-methylpyridine *N*-oxidation runaway studies" by L. Saenz, V. H. C. Vazquez, L. Liu, W. J. Rogers, M. S. Mannan, and M. Papadaki, 2009. Journal of Loss Prevention in the Process Industries, 22, 839-843, Copyright [2009] by Elsevier and from "Thermal decomposition of 2-methylpyridine *N*-oxide: Effect of temperature and influence of phosphotungstic acid as the catalyst" by L. R. Saenz, V. H. Carreto-Vazquez, M. Papadaki, and M. S. Mannan, 2011. Catalyst Communications, 12, 1370-1373, Copyright [2011] by Elsevier.

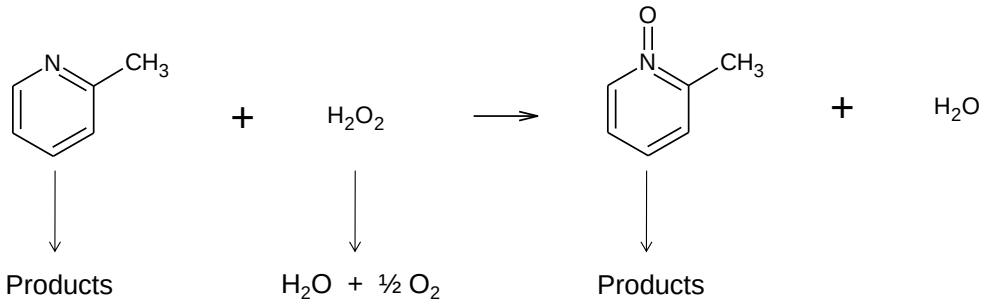

Figure 10. *N*-oxidation of 2MP and the potential secondary reactions during a runaway

To determine the potential for other secondary reactions, the stability of 2-methylpyridine (2MP) and 2-methylpyridine *N*-oxide (2NOX) were tested. For 2MP, the stability was studied between 50 ^{o}C and 350 ^{o}C using different amounts of 2MP and adding different quantities of catalyst; however, no exotherm was detected for any of these measurements, from which it is concluded that 2MP is stable up to 350 ^{o}C. The conditions for the measurements to test the 2MP stability are shown in Table 4.

Table 4. Amounts employed in the 2MP stability tests. All the measurements were performed using APTAC in HWS from 50 ^{o}C to 350 ^{o}C

2MP (g)	Catalyst (g)	Water (g)
6.6	0.00	0.0
1.6	0.09	14.4
1.6	0.30	14.2
3.2	0.09	12.8

The stability of 2NOX was tested in the APTAC using HWS mode with heating steps of 10 ^{o}C. For a preliminary test employing 2.29 g of 2NOX, 14.04 g of water, and 0.10 g of catalyst, a small exotherm was detected at 238 ^{o}C (the exotherm is highlighted by the dotted line in Figure 11). During this test, a pressure increase was traced before the equipment switched over to adiabatic mode indicating initiation of the 2NOX decomposition at a lower temperature than the identified "onset" which is common in calorimetric measurements, especially when fast heating and short wait times are

employed. Further tests were performed to identify the temperature at which the exponential rise of the decomposition rate becomes fast enough for the application of interest. The results are presented in Subsection 3.1.

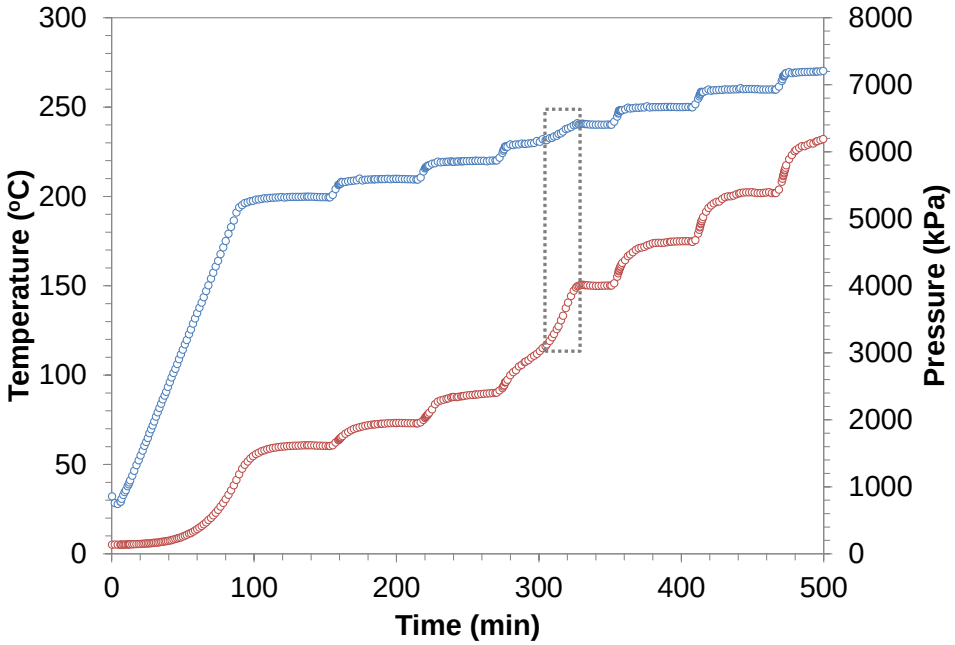

Figure 11. Temperature (blue) and pressure (red) profile for the decomposition of 2NOX studied using the APTAC in HWS mode (2.29 g of 2NOX, 14.04 g of water, and 0.10 g of catalyst)

In conclusion, two secondary reactions related to the stability of reactants and products could be seen during the runaway: the H_2O_2 decomposition and the 2NOX decomposition. These two reactions are the object of study in the next two sections: 2NOX decomposition in Subsection 3.1 and H_2O_2 decomposition in Subsection 3.2. The role of the decomposition of hydrogen peroxide on the decomposition of 2NOX, and vice versa, is studied in Subsection 3.3.

3.1 Study of 2-methylpyridine *N*-oxide Decomposition

In order to determine the effect of temperature on the rate of 2NOX decomposition, different measurements were performed using the APTAC in isothermal mode. The

details for each measurement and the quantities of reactants employed in the experiments are shown in Table 5. The amount of 2NOX was 6.89 g for all but one test. The mass of catalyst changed in each experiment from 0.0 g to 0.5 g; while the amount of water was adjusted to maintain a total liquid mass of approximately 16.44 g. The measurements were conducted at temperatures between 192 ^{o}C and 250 ^{o}C.

Table 5. Experimental details for the study of the decomposition of 2NOX

Temperature (^{o}C)	Catalyst (g)	2NOX (g)	Water (g)	ΔMass* (g)	O_2 moles from Δmass	O_2 moles in 2NOX
192	0.30	6.89	9.24	0.75	0.0234	0.0316
192	0.50	6.89	9.05	1.02	0.0319	0.0316
200	0.00	6.89	9.55	0.25	0.0078	0.0316
200	0.10	6.89	9.45	0.92	0.0288	0.0316
200	0.30	6.89	9.25	0.98	0.0306	0.0316
210	0.00	6.89	9.55	1.04	0.0325	0.0316
210	0.10	6.89	9.45	1.02	0.0319	0.0316
210	0.21	6.88	9.35	0.80	0.0250	0.0315
210	0.30	6.89	9.25	1.27	0.0397	0.0316
220	0.00	6.89	9.55	1.02	0.0319	0.0316
220	0.10	6.89	9.45	1.02	0.0319	0.0316
220	0.20	6.89	9.35	**	**	0.0316
230	0.00	6.89	9.55	0.86	0.0269	0.0316
230	0.10	6.89	9.44	1.19	0.0372	0.0316
249	0.00	6.89	9.56	0.88	0.0275	0.0316

*$\Delta Mass = Mass_{initial} - Mass_{final}$
** Not measured

Figure 12 shows the temperature profile for the decomposition of 2NOX at different temperatures and amounts of catalyst. As mentioned in Subsection 2.4, if certain threshold values are reached during isothermal operation of APTAC, the equipment switches to adiabatic mode. This did not happen for any of the tests shown in Figure 12, but since the APTAC is not equipped with a cooling system, a slight temperature

increase was observed in all the temperature profiles. This increase in temperature provides an indication of when the reaction is significant at that temperature and amount of catalyst.

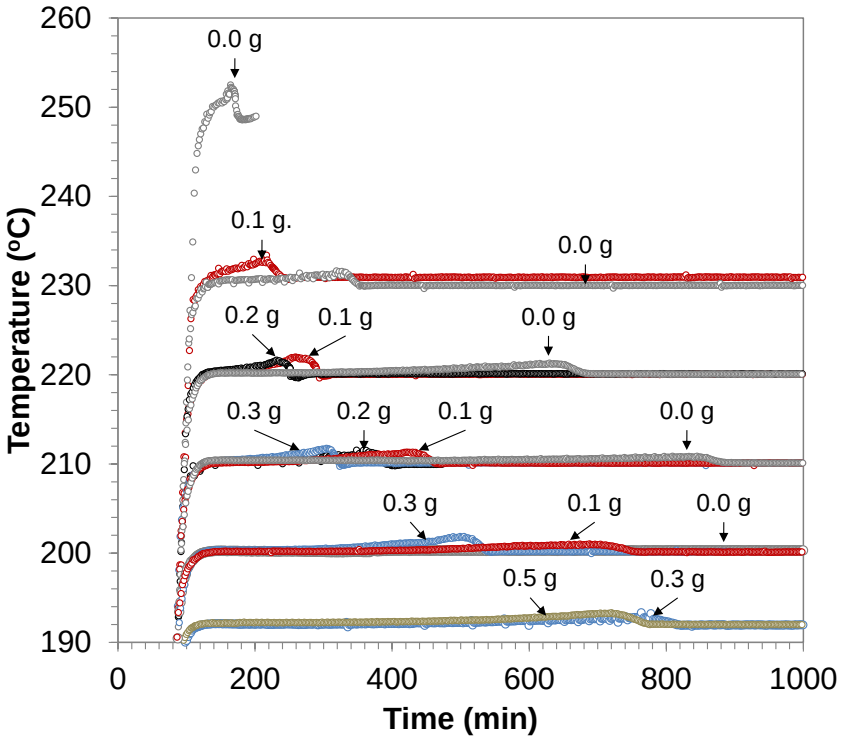

Figure 12. Temperature profiles for the isothermal decomposition of 2NOX at different temperatures and amounts of catalyst (Adapted from [55] and [56])

Figure 12 shows that temperature and catalyst promote the decomposition of 2NOX. When using 0.0 g of catalyst (grey line), the decomposition occurs slowly at 200 ^{o}C and it cannot be detected within the first 1000 min. When the temperature increases to 210 ^{o}C, the reaction is detectable at around 800 min. This time is reduced as the temperature increases, and at 249 ^{o}C, the increase of temperature is measured as soon as the isothermal temperature is reached. A similar behavior can be seen when using 0.1 g, 0.2 g, and 0.3 g of catalyst. At a temperature of 192 ^{o}C, the decomposition was measurable within the first 1000 min only when considerable amounts of catalyst were employed.

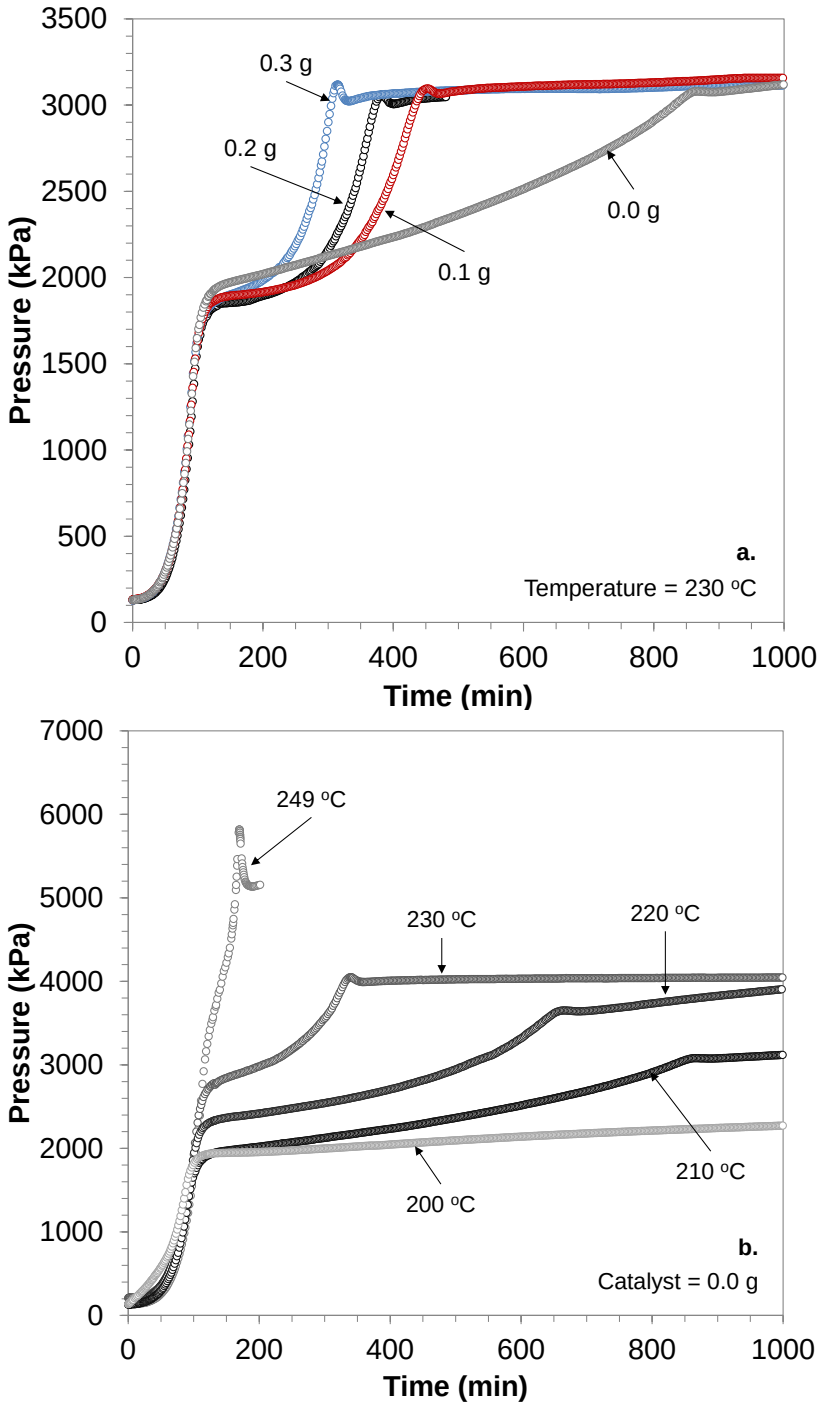

Figure 13. Pressure increase during the isothermal decomposition of 2NOX **a)** at 230 ^{o}C and different amounts of catalyst, and **b)** at different temperatures with no catalyst

The pressure increase during different isothermal measurements is shown in Figure 13. For the measurement at 230 ^{o}C and different amounts of catalyst, Figure 13a, the pressure increase was almost the same in all cases and approximately equal to 1200 kPa, indicating that a similar quantity of gases was produced in all measurements at that temperature. Figure 13a also shows that a rapid pressure increase occurred when 0.3 g of catalyst were employed. This rate decreased as the amount of catalyst was reduced. The pressure profile for the non-catalytic decomposition of 2NOX at different temperatures is shown in Figure 13b. The pressure for the measurement at 200 ^{o}C increased gradually by approximately 310 kPa; while at 249 ^{o}C, the pressure rapidly increased reaching almost 6000 kPa in less than 200 min. When comparing the slopes in the pressure profiles from Figure 13, it can be seen that the pressure rate increased with temperature and catalyst. Additionally, Figure 13 shows that, after the first steep rise in pressure, a much slower pressure rise is observed potentially indicating secondary decompositions (those have not been investigated in the present study).

Figure 14 shows the pressure rate for different isothermal tests for the decomposition of 2NOX. The first peak shown in Figure 14a and Figure 14b corresponds to the pressure increase during the heating step caused by the vapor pressure of the reaction mixture. The second peak corresponds to the decomposition of 2NOX. In Figure 14a, the pressure rate for the measurements at 230 ^{o}C increases as the amount of catalyst is increased and it can be clearly observed from the slope of the second peak. For 0.0 g, the maximum pressure rate was reached 700 min after the heating step. However, with 0.3 g of catalyst, the time to maximum pressure rate was reduced to 150 min after the isothermal temperature was reached. For the 2NOX decomposition without catalyst, Figure 14b, the pressure rate increased with temperature. At 200 ^{o}C, the pressure rate remained nearly flat the first 1000 min of reaction; while at 249 ^{o}C, the pressure rate increased abruptly after the heating step. This rapid pressure increase indicates that even when no catalyst is present, the decomposition of 2NOX can have dramatic consequences.

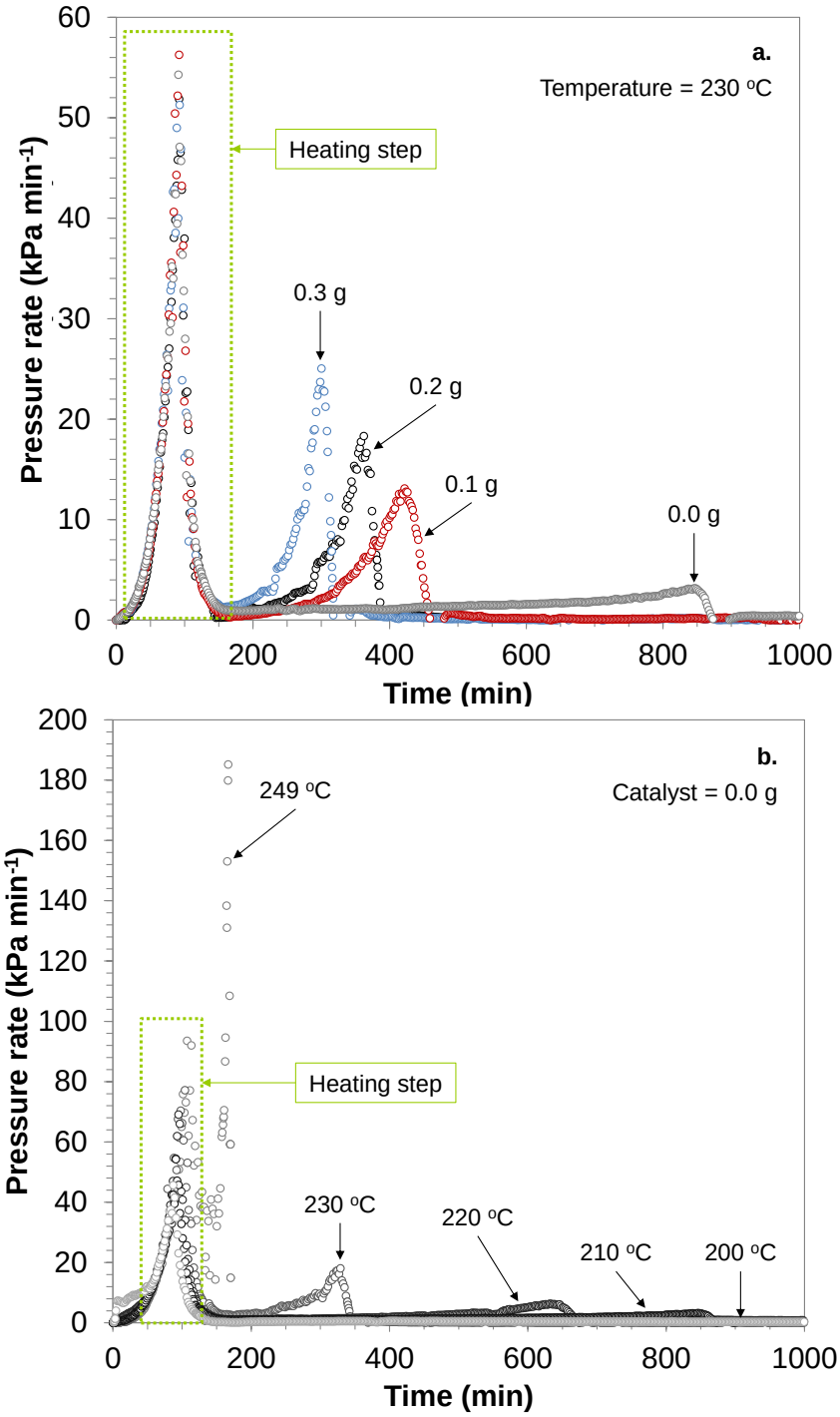

Figure 14. Pressure rate profiles for the isothermal decomposition of 2NOX **a)** at 230 ^{o}C and different amounts of catalyst, and **b)** at different temperatures and no catalyst

The pressure increase is a measure of the quantity of non-condensable gases produced. For that reason, the mass loss of the samples was employed as a rough guide in the identification of the type of gases generated during the decomposition. Table 5 shows the mass loss for each of the measurements which is defined as the difference between the mass at the beginning and at the end of each measurement. Given that the test cell was vented at ambient temperature prior to weighing, it can be assumed that the mass difference is equal to the non-condensable gases produced during decomposition. Considering that the most likely path of 2NOX decomposition involves the loss of oxygen, it was examined whether the mass loss corresponds to oxygen loss from 2NOX. The moles of oxygen estimated from the mass loss are shown in Table 5. Finally, the moles of oxygen contained in the mass of 2NOX employed in the experiments were calculated (also shown in Table 5) and their value was compared with the value calculated from the sample mass loss. The comparison of these values is shown in Figure 15.

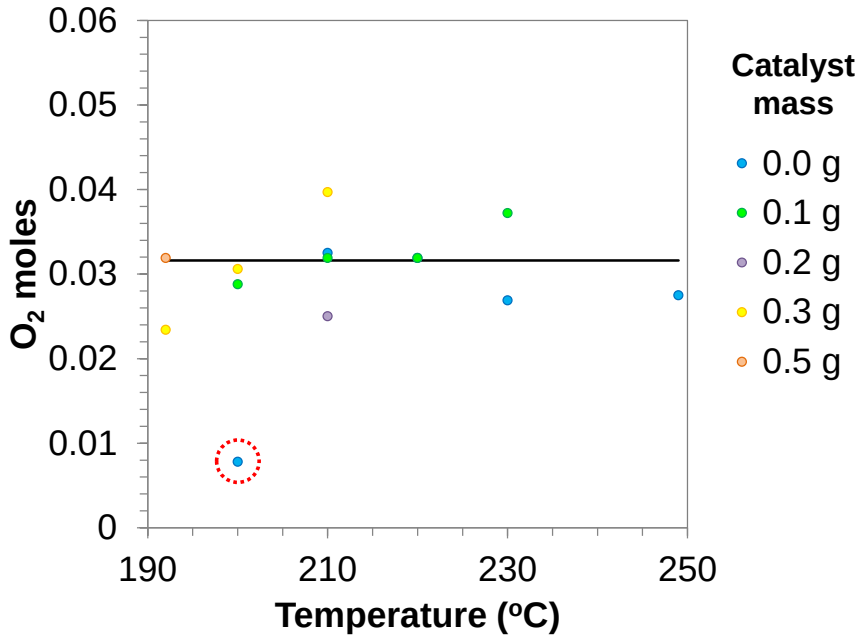

Figure 15. O_2 moles estimated from the mass loss (markers) at different temperatures and amounts of catalyst. The moles of O_2 contained in 2NOX are shown with a solid line

As Figure 15 shows, the O_2 moles from the mass loss (dots) and from the 2NOX (black line) are is good agreement with each other indicating that all or most of the production of non-condensable gases is due to the detachment of the oxygen atom from the molecules of 2NOX. The values under the moles of 2NOX corresponds to lower amounts of catalyst and/or lower temperature, thus slower reactions, most likely indicating incomplete reaction at that temperature and amount of catalyst. Additionally, time also plays an important role since the isothermal time was different for each experiment. O_2 moles over the solid black line probably indicate that further decomposition with additional production of gases took place during the decomposition. The value enclosed by the dotted red circle in Figure 15 (and highlighted in red in Table 5) indicates that the lowest value of mass loss, obtained at 200 ^{o}C and 0.0 g of catalyst, is most likely due to a slow decomposition with no significant production of gases.

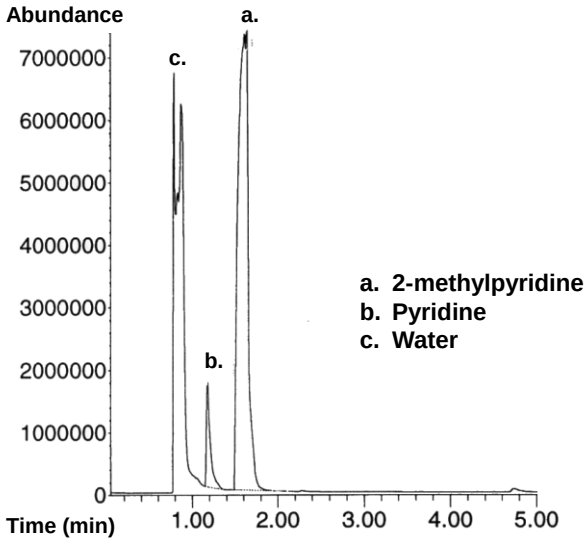

Figure 16. Typical GC-MS spectrum for the product decomposition of 2NOX (Taken from [56])

GC-MS analyses were performed to identify the decomposition products present in the final sample (Subsection 2.4). For most of the measurements, three main peaks were identified. A typical measurement is shown in Figure 16. The first peak corresponds to water which is employed as the solvent; while, the second peak and third peak

correspond to pyridine and 2-methylpyridine, respectively. For incomplete reactions, an additional peak with a retention time around 11 min was identified, which represented the presence of 2NOX. Other small peaks corresponding to compounds such as acetic acid, ammonia, 1-(2-pyridinyl)-ethanone, 1,2-di-(2-pyridyl)-ethane, and trans-1,2-di-(2-pyridyl) ethylene were also identified. However, the pathways of the formation of these compounds during the decomposition has not been studied further [56].

The results obtained from GC-MS confirmed the detachment of the oxygen atom from 2-methylpyridine *N*-oxide to form 2-methylpyridine and oxygen. The next step in the decomposition appears to be pyridine formation with additional production of gases. However, this reaction has not been investigated further. But it is interesting to notice, that although 2MP was not found to decompose up to 350 ^{o}C, it appears to be possible to decompose to give pyridine when 2NOX is present.

3.2 Study of the Decomposition of Hydrogen Peroxide

The decomposition of hydrogen peroxide was studied using the APTAC in HWS mode with a heating step of 10 ^{o}C. The details of the measurements are shown in Table 6. The measurements were performed to evaluate the effect of the catalyst and H_2O_2 concentration on the rate of decomposition and to obtain global data (temperature and pressure rise, temperature and pressure rate of increase, etc.) of its runaway behavior.

Table 6. Experimental details for the study of the decomposition of hydrogen peroxide using the APTAC in HWS mode

Mass of 17.5 % H_2O_2 (g)	Mass of 35 % H_2O_2 (g)	Mass of catalyst (g)	Sample volume (mL)
14.4 (Repeated twice)	-	0.00	13.6
14.4	-	0.09	13.6
14.4	-	0.20	13.6
14.4	-	0.40	13.6
-	14.4	0.00	12.8
-	14.4	0.09	12.8
-	14.4	0.20	12.8
-	14.4	0.40	12.8

Figure 17 shows the temperature and pressure as a function of time of two identical measurements employing 17.5 % H_2O_2 without catalyst. Other measurements using the same concentration of hydrogen peroxide and different mass of catalyst are shown in Figure 18. As can be seen in Figure 17, the "onset" temperature of the non-catalytic decomposition of H_2O_2 is approximately 150 ^oC. The two identical otherwise measurements gave a difference in their "onset" of approximately 10 ^oC, i.e. equal to the heating step. As mentioned earlier, this is a typical shortfall of adiabatic calorimetry where the accuracy of the measured "onset" temperature depends strongly on the heating step and the wait time. The absolute error of the "onset" temperature is at least equal to the heating step value as the "onset" can coincide with the initiation of the heating step. The measured pressure profiles show that the reaction occurred at a similar rate and had similar duration.

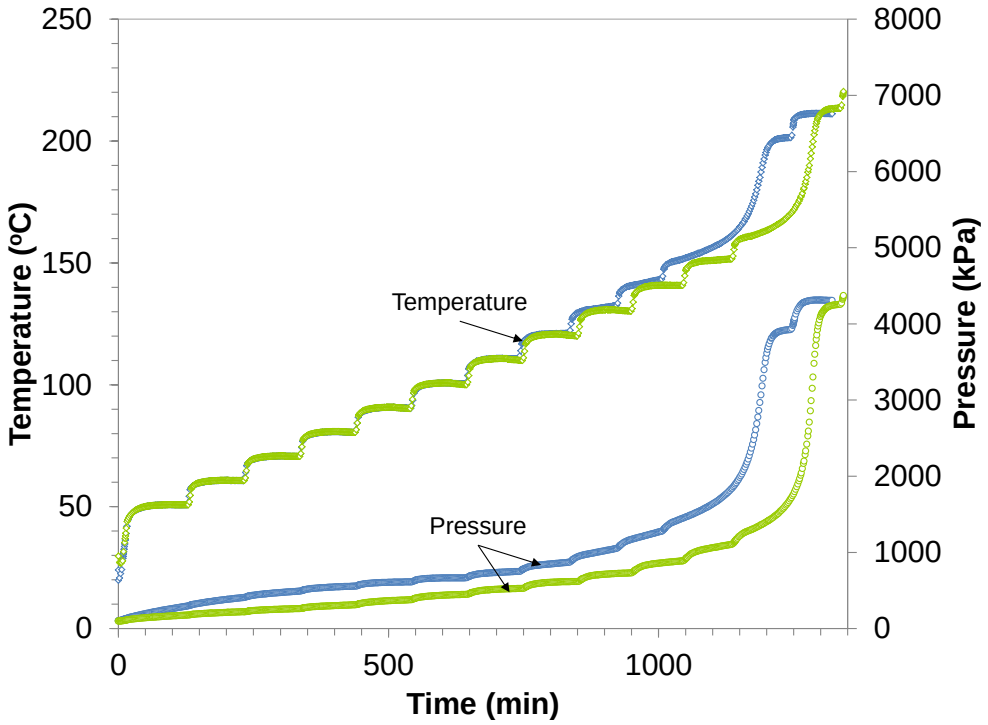

Figure 17. Temperature and pressure profile for the decomposition of 17.5 % H_2O_2 without catalyst

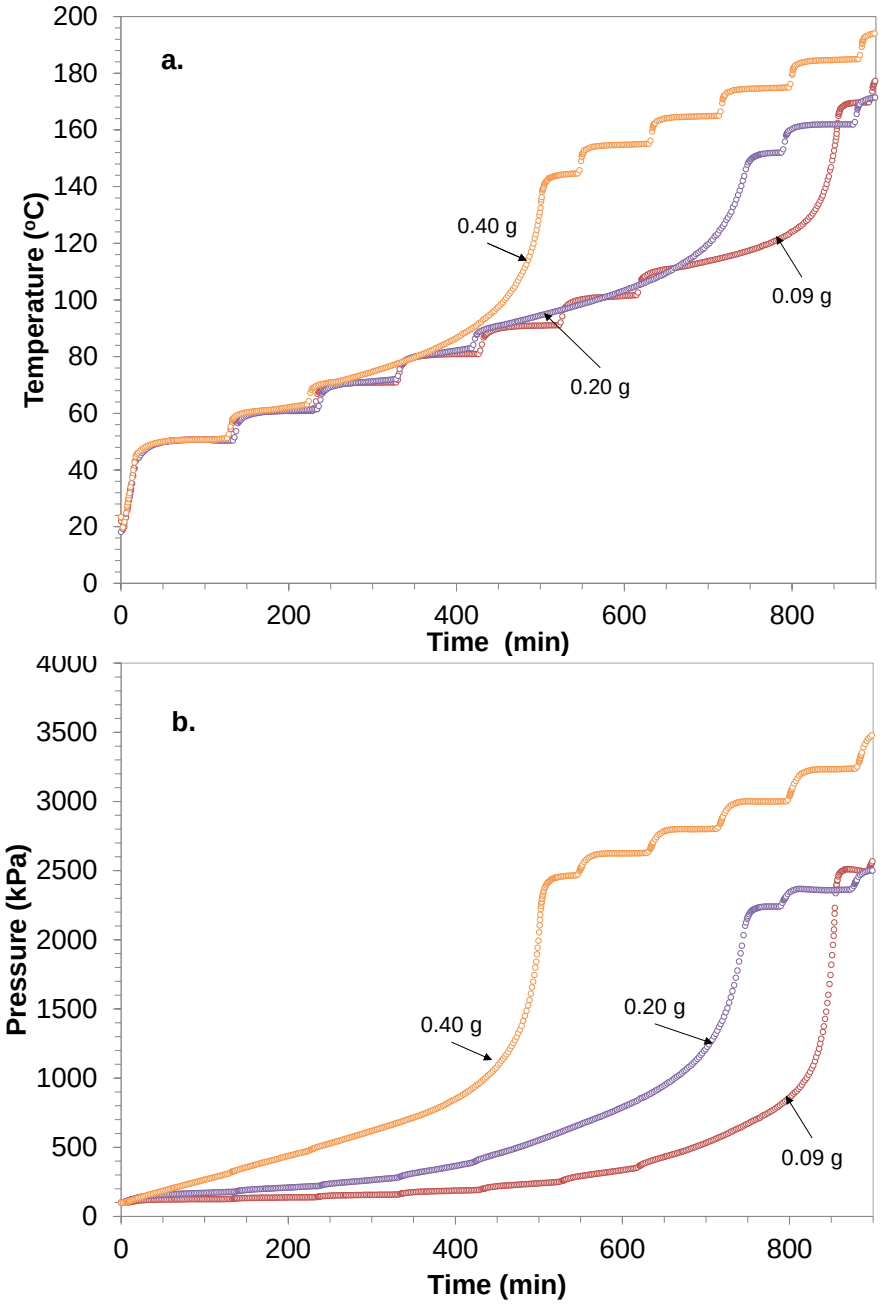

Figure 18. a) Temperature and **b)** Pressure profiles for the decomposition of 17.5 % H_2O_2 with different amounts of catalyst

Figure 18a shows the temperature profiles for the catalytic decomposition of 17.5 % H_2O_2. This figure shows that as the amount of catalyst increases, the "onset" of the decomposition decreases. Figure 18b shows the pressure profiles associated with the catalytic decomposition of 17.5 % H_2O_2. A similar pressure increase is measured in all cases indicating a similar production of gases as the amount of H_2O_2 employed in the measurements was the same. For all cases presented in Figure 18b, the pressure increased very rapidly by approximately 2000 kPa demonstrating that control of a potential runaway is not practically feasible and inherent safety measures are the only ones which can effectively avert potential consequences.

The temperature and pressure profiles for the decomposition of 35 % hydrogen peroxide at different amounts of catalyst are shown in Figure 19. As in the decomposition of 17.5 % H_2O_2, Figure 19a shows that the "onset" temperature for 35 % H_2O_2 decreases when increasing the amount of catalyst. However, the temperature increase for a more concentrated H_2O_2 occurred so fast that the shutdown conditions of the equipment were quickly reached. For the measurement with 0.2 g of catalyst, the system was initially pressurized, thus initial vaporization of the mixture was adverted which allowed for a complete detection of the exotherm. The pressure increase for the measurements is shown in Figure 19b. The pressure reached in this case is approximately twice the pressure reached when 17.5 % H_2O_2 was used, as expected since the amount of H_2O_2 used here was doubled. Similarly to 17.5 %, the rate of pressure rise is a serious concern; but in this case it is more threatening as the rate with this concentration is much higher.

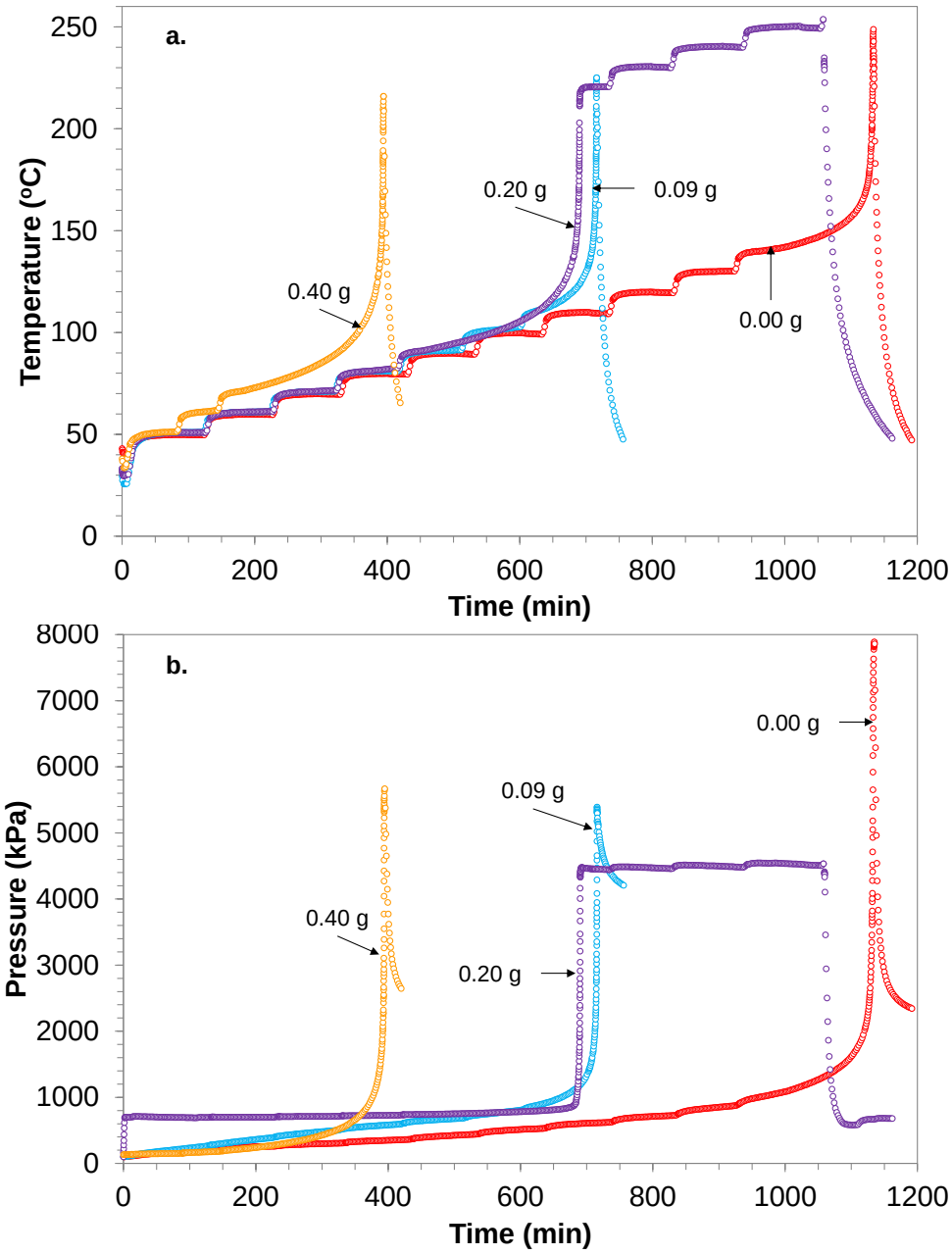

Figure 19. a) Temperature and **b)** Pressure profiles for the decomposition of 35 % H_2O_2 at different amounts of catalyst

3.2.1 Hydrogen Peroxide Decomposition Runaway

Adiabatic calorimetry experiments can be used for the evaluation of a number of quantities like "onset" temperature, adiabatic temperature rise, maximum temperature reached by the runaway, etc. Such values are used with empirical criteria in order to quantify the safety of the process. During the adiabatic period, the heat rate starts increasing as a consequence of the reaction. This increase causes a further acceleration of the reaction, which simultaneously sustains the rise in the heat rate. However, there is a point where the consumption of reactants is such that the temperature rise rate, which is equivalent to the heat generation and thus the reaction rate, starts decreasing, while the temperature still increases. This point is considered the point at maximum rate and it is equal to the maximum value of the first time derivative of temperature.

For the measurements shown in Figure 18 and Figure 19, Table 7 summarizes the parameters employed to evaluate the runaway behavior of the decomposition of 17.5 % and 35 % H_2O_2.

Table 7. Parameters to assess the runaway behavior of the H_2O_2 decomposition

Catalyst (g)	T_o (^oC)	T_f (^oC)	ΔT_{ad} (^oC)	T_{max} (^oC)	$(dT/dt)_{max}$ (^oC min^{-1})	$(dP/dt)_{max}$ (kPa min^{-1})	Φ	$(CpM)_s$ (J K^{-1})	H_2O_2 N^{ad*} (mol)
17.5 wt. %									
0.00	155.22	201.36	46.149	189.15	1.01	58.27	1.79	58.97	0.049
0.00	165.97	213.51	47.536	199.78	1.40	92.52	1.84	59.64	0.052
0.09	113.82	169.69	55.873	162.44	3.01	140.29	1.87	57.47	0.060
0.20	94.77	151.95	57.179	146.08	1.05	38.88	1.87	56.93	0.061
0.40	75.47	144.57	69.106	136.23	2.80	96.62	1.88	56.65	0.073
35 wt. %									
0.00	142.61	248.70	106.083	231.18	38.29	3,223.58	1.84	56.27	0.110
0.09	120.90	224.94	104.034	210.92	163.62	7,154.84	1.91	54.67	0.109
0.20	94.64	220.57	125.922	199.44	111.40	6,489.74	1.92	54.15	0.131
0.40	72.82	215.82	142.994	193.97	206.74	11,669.59	1.89	53.78	0.145

*H_2O_2 N^{ad} = Initial H_2O_2 moles – H_2O_2 moles reacted before adiabatic period

where

T_o	is the "onset" temperature
T_{max}	is the temperature at maximum rate
$(dT/dt)_{max}$	is the temperature rate at maximum rate
$(dP/dt)_{max}$	is the pressure rate at maximum rate
ΔT_{ab}	is the measured adiabatic temperature increase
ϕ	is the thermal inertia or the phi-factor, calculated using equation (4)
M_sCp_s	is the product of the heat capacity and the mass of the sample
N_{ad}	are the moles of H_2O_2 decomposed during the adiabatic period

For each test shown in Table 6, the enthalpy of reaction was calculated using equation (3). However, the calculation of the heat of reaction resulted in values up to 40 % smaller than the typical value reported in the literature (100 kJ mol^{-1}). As such, it was concluded that H_2O_2 was slowly decomposing at a non-measurable rate before the adiabatic period started, thus a small amount of H_2O_2 was already consumed. The remaining moles, N_{ad}, were calculated as the n_{rxn} in equation (3) setting ΔH_{rxn} equal to 100 kJ mol^{-1} and with the ΔT_{ad} measured in the experiments (See equation (5)).

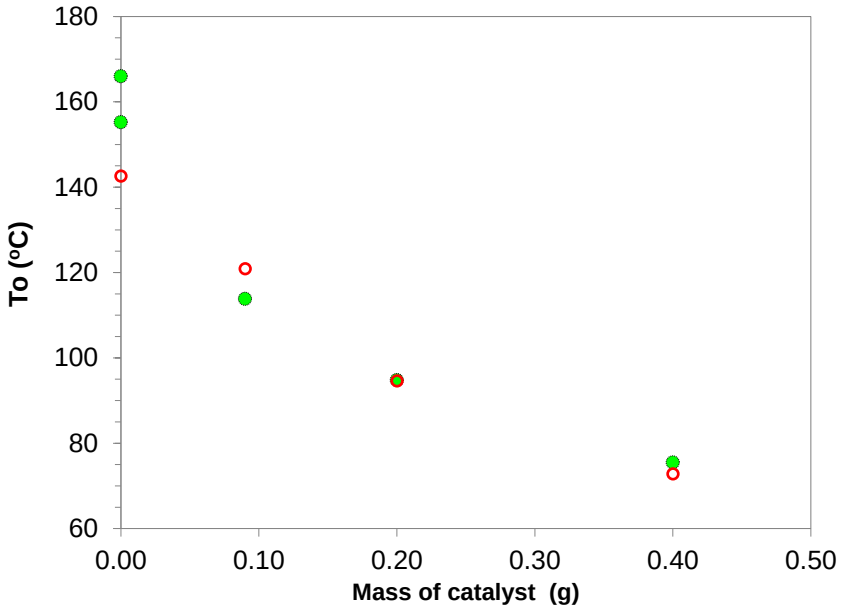

Figure 20. "Onset" temperature for the decomposition of 17.5 % (green dots) and 35 % H_2O_2 (red dots)

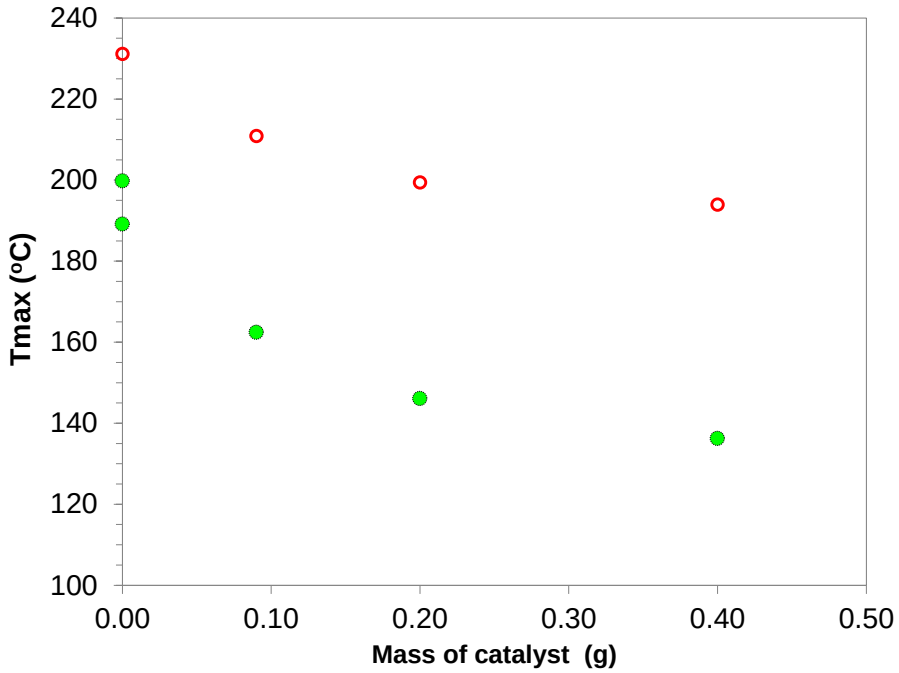

Figure 21. Temperature at maximum rate, T_{max}, for the decomposition of 17.5 % (green dots) and 35 % H_2O_2 (red dots)

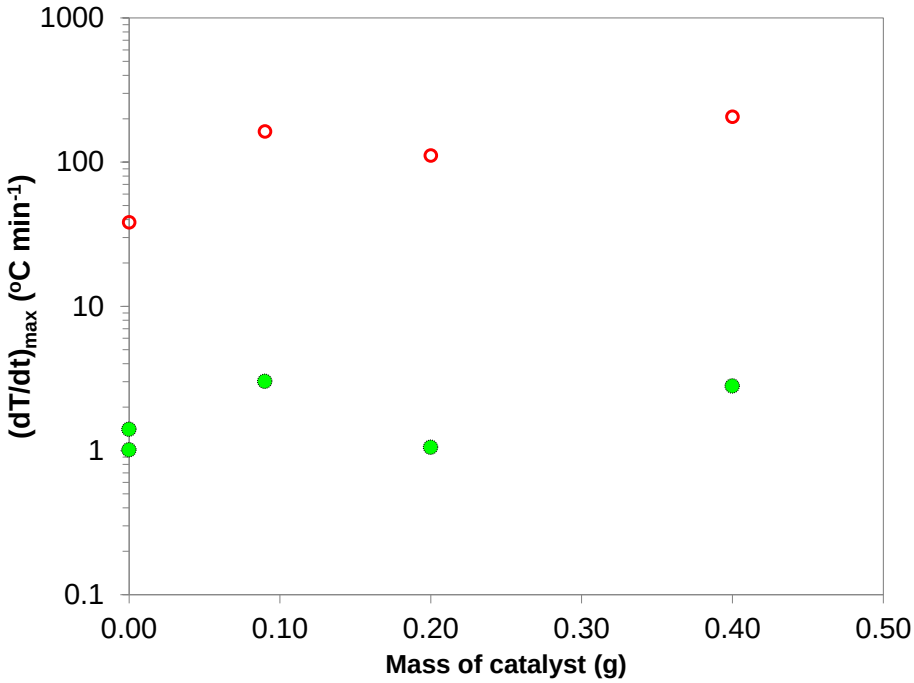

Figure 22. Maximum heat rate, $(dT/dt)_{max}$, for the decomposition of 17.5 % (green dots) and 35 % H_2O_2 (red dots)

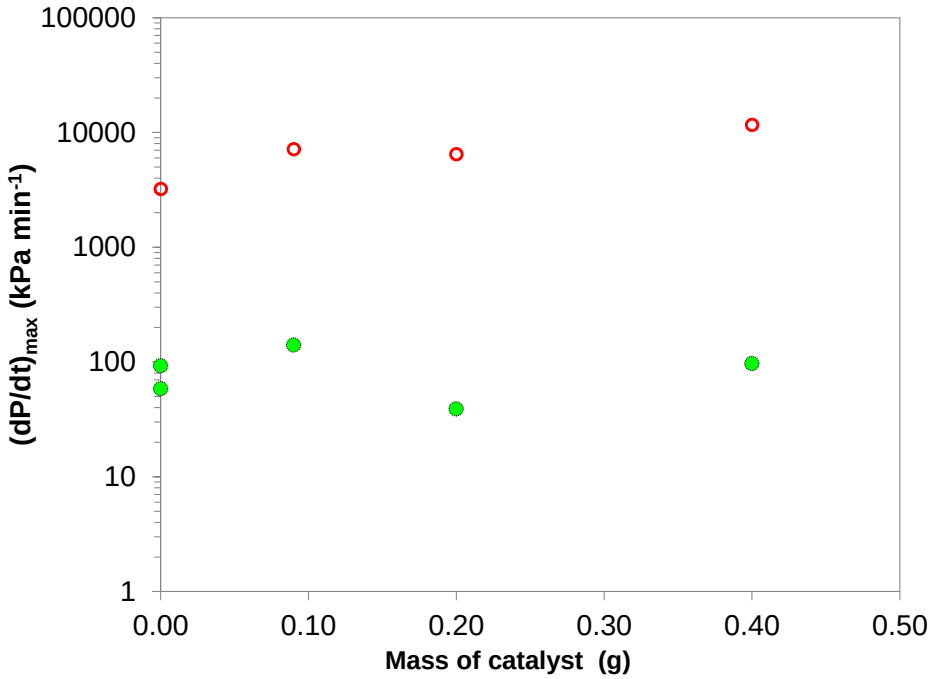

Figure 23. Pressure rate at maximum rate $(dP/dt)_{max}$ for the decomposition of 17.5 % (green dots) and 35 % H_2O_2 (red dots)

Figure 20 through Figure 23 show the "onset" temperature and the parameters at maximum rate for the measurements in Table 7. It can be seen that the "onset" temperature (Figure 20) and the temperature at maximum rate (Figure 21) for both 17.5 % and 35 % H_2O_2 decreases as the amount of catalyst increases. For the "onset" temperature, the most significant effect on the "onset" is determined by the catalyst rather than by the concentration of H_2O_2. The reaction "onset" is an empirical quantity which gives information about the rate of the reaction to be then compared with a specific application. In terms of science, there is no reaction "onset" since there is not a starting temperature for a reaction. The reaction is always there and its rate only can be different as temperature changes. Thus, the "onset", which is extensively used in runaway reaction studies is a measure of how fast the reaction advances and when its rate becomes measurable. Therefore, what is shown in Figure 20 is that the higher the catalyst concentration, the faster the reaction. Moreover, considering the experimental error, this figure suggests that compared to the effect of the catalyst, no H_2O_2 autocatalytic effects can be seen as both the 17.5 % and the 35 % H_2O_2 curves essentially coincide. For the temperature at maximum rate, T_{max}, in Figure 21, it can be

seen that as the mass of catalyst increases, the maximum rate is reached at a lower temperature, as low as 130 ^{o}C for the highest mass of catalyst and H_2O_2 concentration employed in this work. The change in $(dT/dt)_{max}$ and $(dP/dt)_{max}$ with catalyst, Figure 22 and Figure 23, does not show any clear trend; however, when considering the average, it can be said that these parameters remain almost constant for both concentrations, but the rates for 35 % H_2O_2 are two orders of magnitude larger than those for 17.5 %.

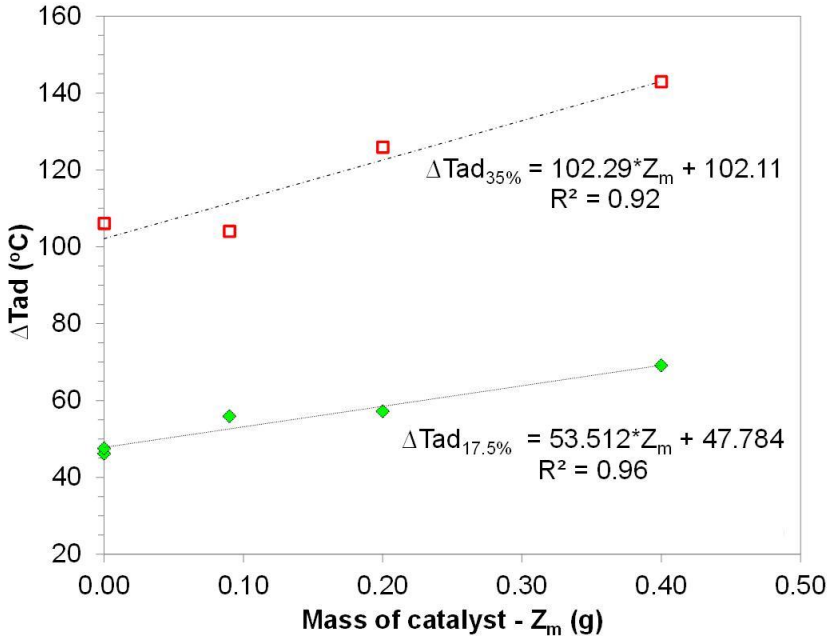

Figure 24. Adiabatic temperature increase for the decomposition of 17.5 % (green dots) and 35 % H_2O_2 (red dots)

The adiabatic temperature increase, ΔT_{ab}, should be the same in all cases where the same amount of H_2O_2 has been used, if the process were really adiabatic and if the thermal mass of the system had a constant value throughout the process. Moreover, its value for the measurements employing 17.5 % H_2O_2 should be twice the value found in the measurements employing 35 % H_2O_2 as the reactant mass was doubled in this case. However, ΔT_{ab} in Figure 24 shows a linear increase with catalyst for both concentrations. Thus the values shown here are apparent values, which also demonstrate the limitations of the employed experimental technique. These limitations

in experimental techniques are often misinterpreted and the apparent increase in adiabatic temperature is used for the calculation of the enthalpy of the reaction without any further consideration. The heat of reaction calculated from those values will be different for each measurement and it will appear to change with conditions.

In Figure 24, the linear regressions of the apparent ΔT_{ab} gave a correlation coefficient (R^2) higher than 0.9. The slope in the linear regressions indicates that the apparent ΔT_{ad}, thus the reaction rate, increases faster for the decomposition of 35 % than for 17.5 % H_2O_2.

3.2.2 Kinetics for the Non-catalytic H_2O_2 Decomposition

Among the numerous studies of the decomposition of hydrogen peroxide [57-63], different authors have proposed an *n*th-order model to describe the kinetics of this reaction. Chen et al. reported reaction orders between 1.29 and 2.84 when studied the thermal decomposition of hydrogen peroxide at concentrations ranging from 10 to 45 % H_2O_2 in water [60]. The kinetics of the decomposition under the catalytic action of iron (III) nitrate was studied by Phong and Aires, and it was modeled using the *n*th order reaction where orders that ranged from 0.64 to 0.95 were determined [61]. The catalytic action of potassium dichromate on the decomposition of H_2O_2 was studied by Frikha et al. This work developed a thermal stability criterion for its runway based on a model where the reaction rate in respect to H_2O_2 is zeroth order at high concentrations of hydrogen peroxide and second order for low concentrations [62]. Hiroki and LaVerne studied the effect of different types of ceramic oxides on decomposition and described the decomposition as a first-order reaction [63].

Following such previous works, an *n*th-order rate equation was chosen to represent the decomposition of hydrogen peroxide in the absence of catalyst. As such, the rate of consumption of hydrogen peroxide can be expressed as:

$$\frac{dC_{H_2O_2}}{dt} = -r = -k \cdot C_{H_2O_2}^{n} \qquad (15)$$

where

$C_{H_2O_2}$ is the concentration of hydrogen peroxide at time t

r is the reaction rate

k is the rate constant

n is the reaction order

The rate constant, k, is assumed to follow the Arrhenius equation according to expression (16).

$$k = A \cdot exp\left(-\frac{E}{RT}\right) \tag{16}$$

where

A is the frequency factor

E is the activation energy of the reaction

R is the gas constant

T is temperature

For the model, the following assumptions were made:

- Adiabatic behavior;
- Complete decomposition of the H_2O_2 moles indicated in Table 7; and
- Constant thermal mass of the system throughout the reaction.

Based on these assumptions, the concentration of hydrogen peroxide during the adiabatic decomposition was calculated using equation (17).

$$C_{H_2O_2} = \frac{T_f - T}{T_f - T_o} \cdot C^o_{H_2O_2} \tag{17}$$

where

$C^o_{H_2O_2}$ is the initial concentration of hydrogen peroxide

T is the temperature at time t

T_o is the "onset" temperature

T_f is the temperature at the end of the adiabatic period

If the derivative of equation (17) is replaced in equation (15), the following expression is obtained:

$$\frac{dT}{dt} = r \cdot \frac{T_f - T_o}{C^0_{H_2O_2}} \tag{18}$$

The temperature of reaction can then be calculated employing equation (18) and a predefined time step.

The parameters A, E, and n from equations (15) and (16) were estimated by minimizing the difference between the temperature, and thus the heat rate calculated from equation (18) and the temperature and heat rate from the experimental measurements. The method employed for the minimization was the Generalized Reduced Gradient (GRG) method included in the Excel Solver tool. The parameters for the three non-catalytic measurements are shown in Table 8. The comparison between the model and the experimental results is shown in Figure 25.

As shown in Table 8, the parameters obtained for the experiments with 17.5 % H_2O_2 agree with each other within the margin of experimental error. For 35 %, the values for E/R and ln(A) were smaller compared with 17.5 %; while the order of the reaction had a slightly increase. For all cases, the prediction of the temperature and the heat rate (dotted line in Figure 25) shows a good agreement with the experimental data.

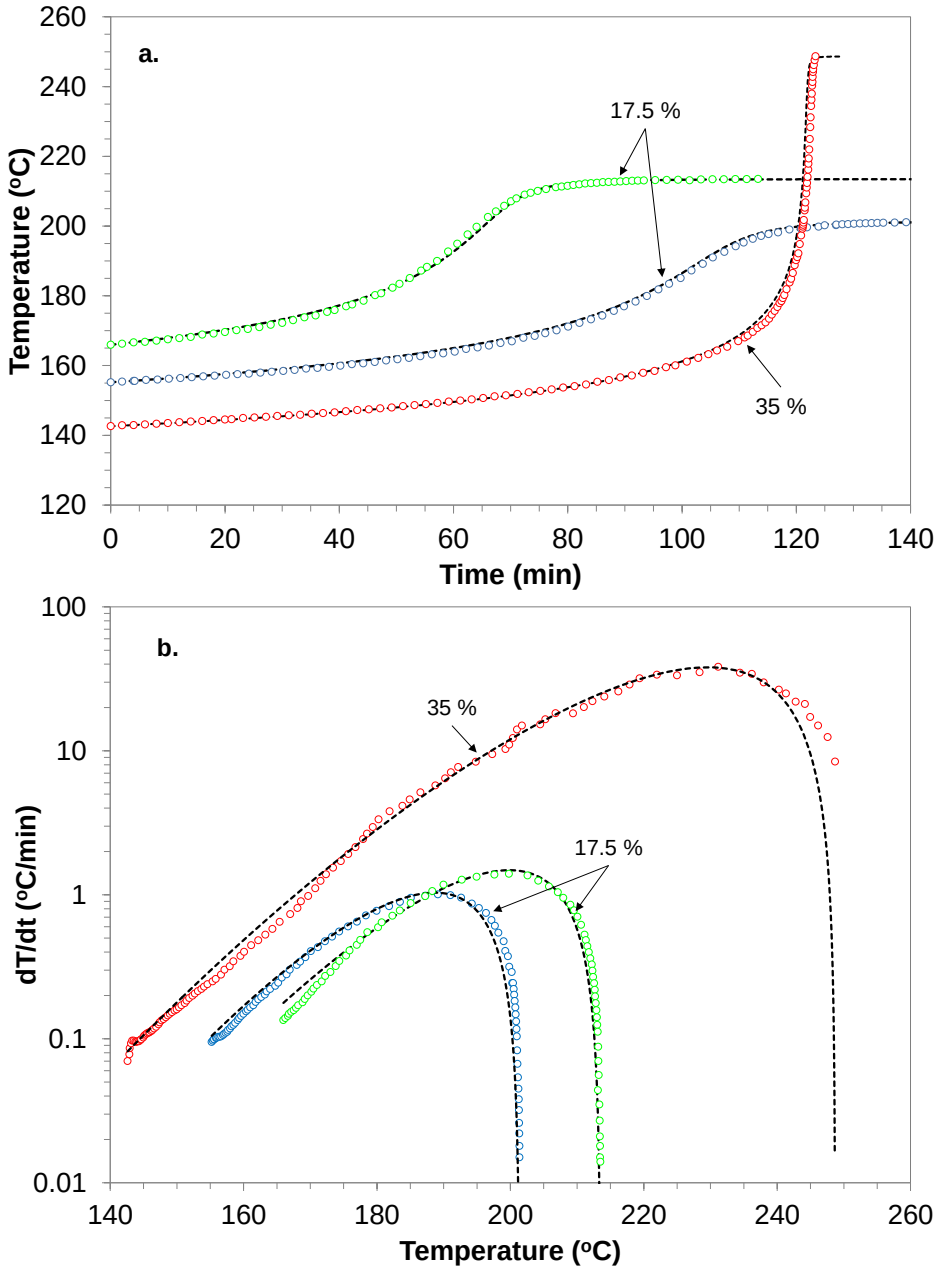

Figure 25. Prediction of non-catalytic H_2O_2 decomposition by a n^{th} order reaction rate

Table 8. Kinetic parameter for the non-catalytic decomposition of H_2O_2

	E/R	ln(A)	n
17.5 %-1	24,773.36	51.16	1.474
17.5 %-2	24,406.96	49.35	1.493
35.0 %-1	21,408.03	43.05	1.618

3.2.3 Kinetics for the Catalytic H_2O_2 Decomposition

Papadaki [35] proposed a kinetic model for the decomposition of hydrogen peroxide catalyzed by phosphotungstic acid. The model consists of two parts and it is shown in equation (19).

$$r = r_1 + r_2 = \frac{\left(k_1 \cdot Z_{0,ap}^2\right) \cdot K_b^2 \cdot \left(C_{H_2O_2}\right)^2}{\left(1 + K_b \cdot C_{H_2O_2}\right)^2 \cdot V^2} + \frac{\left(k_2 \cdot Z_{0,ap}\right) \cdot K_b \cdot \left(C_{H_2O_2}\right)^2}{\left(1 + K_b \cdot C_{H_2O_2}\right) \cdot V} \quad (19)$$

where

k_1 is the rate constant for reaction 1, r_1

k_2 is the rate constant for reaction 2, r_2

$Z_{o,ap}$ is the apparent concentration of catalyst

K_b is the effective equilibrium constant between H_2O_2 and the catalyst

V is the reaction volume

For all the measurements presented here where the concentration of catalyst is high, the contribution of the second reaction rate, r_2, is insignificant compared to the first one. As such, the reaction rate for the catalytic decomposition of hydrogen peroxide is adequately well represented by equation (20).

$$r = r_1 = \frac{\left(k_1 \cdot Z_{0,ap}^2\right) \cdot K_b^2 \cdot \left(C_{H_2O_2}\right)^2}{\left(1 + K_b \cdot C_{H_2O_2}\right)^2 \cdot V^2} \quad (20)$$

To extend the applicability of the previous model [35], the kinetic parameters were estimated for the measurements shown in Table 6. Similarly to [35], the quantities k_1 and Z_o were grouped to form a single reaction rate constant represented by equation (21). For K_b, the value of 40 L mol^{-1} previously proposed [35] was employed in this study. Sensitivity analysis showed that the representation of the experimental data presented here is very insensitive to this value. Consequently, the present experiments cannot serve for its accurate evaluation.

$$\left(k_1 \cdot Z_{0,ap}^2\right) = exp\left(A - \frac{B}{T}\right) \quad (21)$$

where

A is an apparent frequency factor

B is the activation energy for $\left(k_1 \cdot Z_{0,ap}^2\right)$

An approach similar to the non-catalytic case was used to estimate the heat rate. The heat rate was calculated using equation (22).

$$\left(\frac{dT}{dt}\right)_{cal} = 2 \cdot \frac{T_f - T_o}{C_{H_2O_2}^0} \cdot \frac{\left(k_1 \cdot Z_{0,ap}^2\right) \cdot K_b^2 \cdot \left(C_{H_2O_2}\right)^2}{\left(1 + K_b \cdot C_{H_2O_2}\right)^2 \cdot V^2} \quad (22)$$

The parameters A and B from equation (21) were estimated for all the catalytic measurements using the Generalized Reduced Gradient (GRG) method included in the Solver tool from Excel. As in the non-catalytic case, the differences between the experimental and the calculated temperature and heat rates were minimized. The comparison between the experimental and the predicted values for the decomposition of 17.5 % and 35 % hydrogen peroxide are shown in Figure 26 and Figure 27, respectively. The estimated parameters are shown in Table 9. This table also includes five additional estimated parameters: B' which is the product of the parameter B and the amount of catalyst (Z_m), A' which is the product of A and the square of the amount of catalyst (Z_m), R' which is the ratio of the amount of catalyst and the amount of hydrogen peroxide, B" which is the product of B and R', and A" which is the product of A and the square of R'.

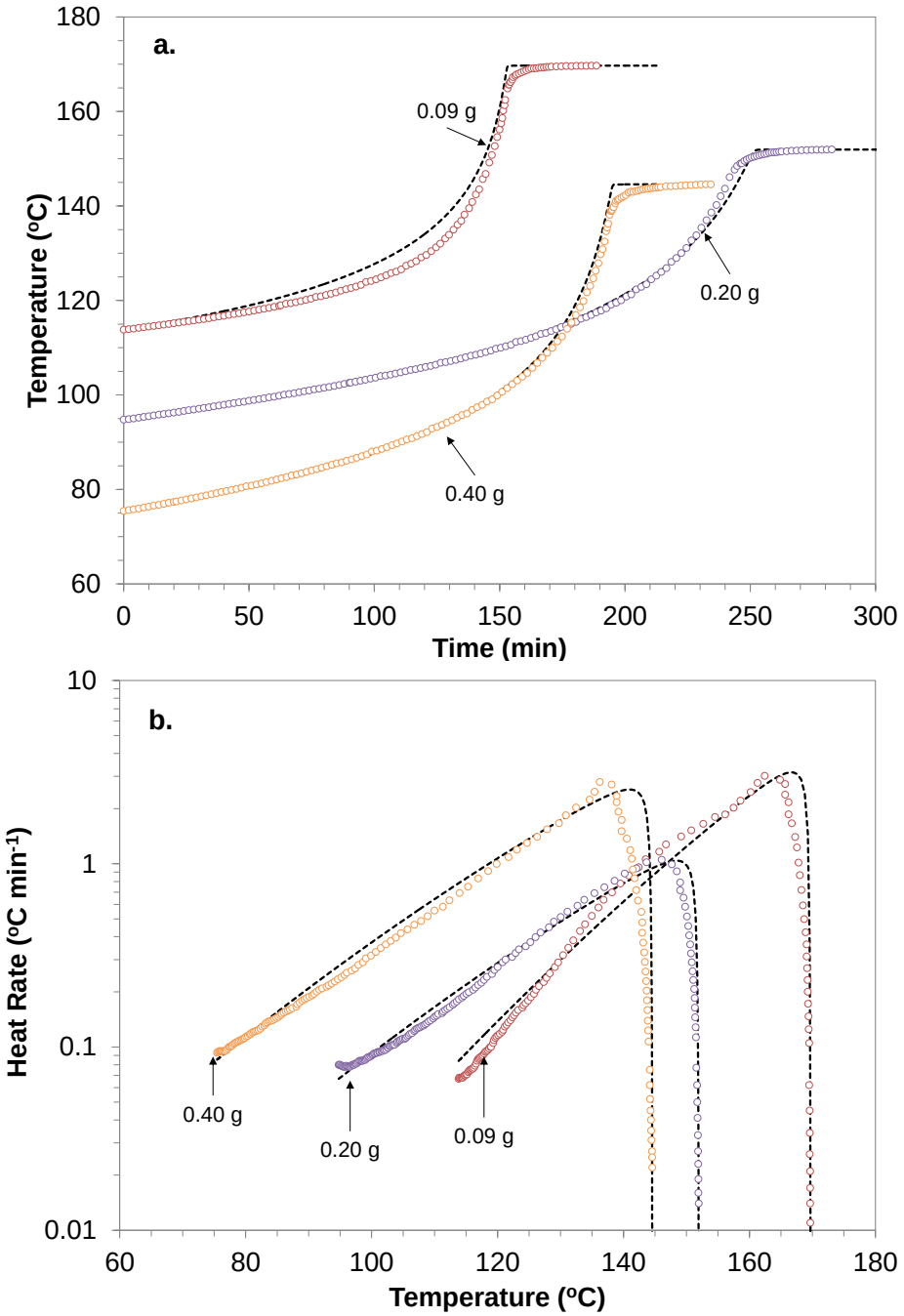

Figure 26. Prediction of **a)** the temperature and **b)** the heat rate for the catalytic decomposition of 17.5 % H_2O_2

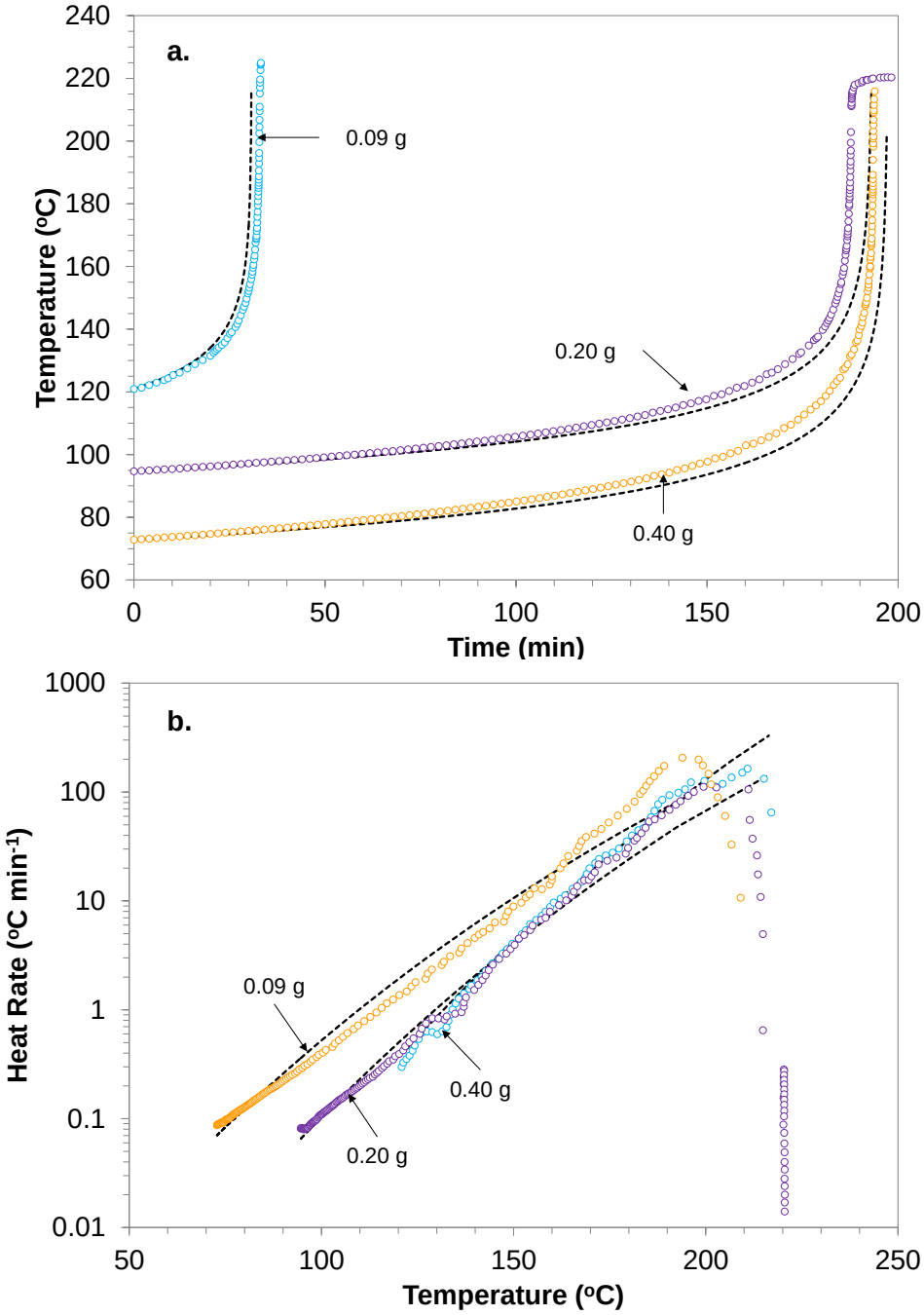

Figure 27. Prediction of **a)** the temperature and **b)** the heat rate for the catalytic decomposition of 35 % H_2O_2

Table 9. Kinetic parameters for the catalytic decomposition of H_2O_2

H_2O_2 (%)	Z_m	$k_1(Z_o)^2$ (L·mol·s^{-1})		Z_m·B	Z_m^2·A	Cat (g)/H_2O_2(g)	B·R'	A·(R')^2
	Cat (g)	A	B	B'	A'	R'	B"	A"
17.5	0.09	17.36	12274.77	1104.73	0.14	0.04	438.38	0.022
17.5	0.20	7.40	8386.25	1677.25	0.30	0.08	665.58	0.047
17.5	0.40	6.61	7827.65	3131.06	1.06	0.16	1242.48	0.166
35.0	0.09	21.89	13713.28	1234.20	0.18	0.02	244.88	0.007
35.0	0.20	15.90	11551.25	2310.25	0.64	0.04	458.38	0.025
35.0	0.40	11.37	9521.00	3808.40	1.82	0.08	755.63	0.072

As can be seen in Table 9, the values of A and B from different measurements are different. Therefore, they are not useful for a rate equation. However, if those quantities are multiplied by the square of the moles of catalyst and by the moles of catalyst respectively, the resulting constants, A' and B', give a good linear relation as a function of the mass of catalyst. Those two quantities, A' and B', where subsequently divided by the square of the mass of hydrogen peroxide and the mass of hydrogen peroxide, respectively, and a single straight line was derived. Thus a unified equation was determined and can be used for any concentration of H_2O_2.

Figure 28 shows the relationship between the parameters A' and B' and the amount of catalyst Z_m. For both parameters and both concentrations of H_2O_2, linear regressions were determined with regression coefficients (R^2) above 0.96. The equations included in Figure 28 allow for the prediction of the kinetic parameters for the catalytic decomposition of 17.5 % and 35 % H_2O_2 based on the amount of catalyst.

Figure 29 shows the relationship between the parameters A", B", and the ratio between the amount of catalyst and the amount of hydrogen peroxide, R'. Since the amount of H_2O_2 is included in the parameter R', a single straight line was established for each parameter. The linear relationships included in Figure 29 provide a general expression for the calculation of the kinetic parameters of the catalytic decomposition of H_2O_2 for different amounts of catalyst and different concentrations of hydrogen peroxide.

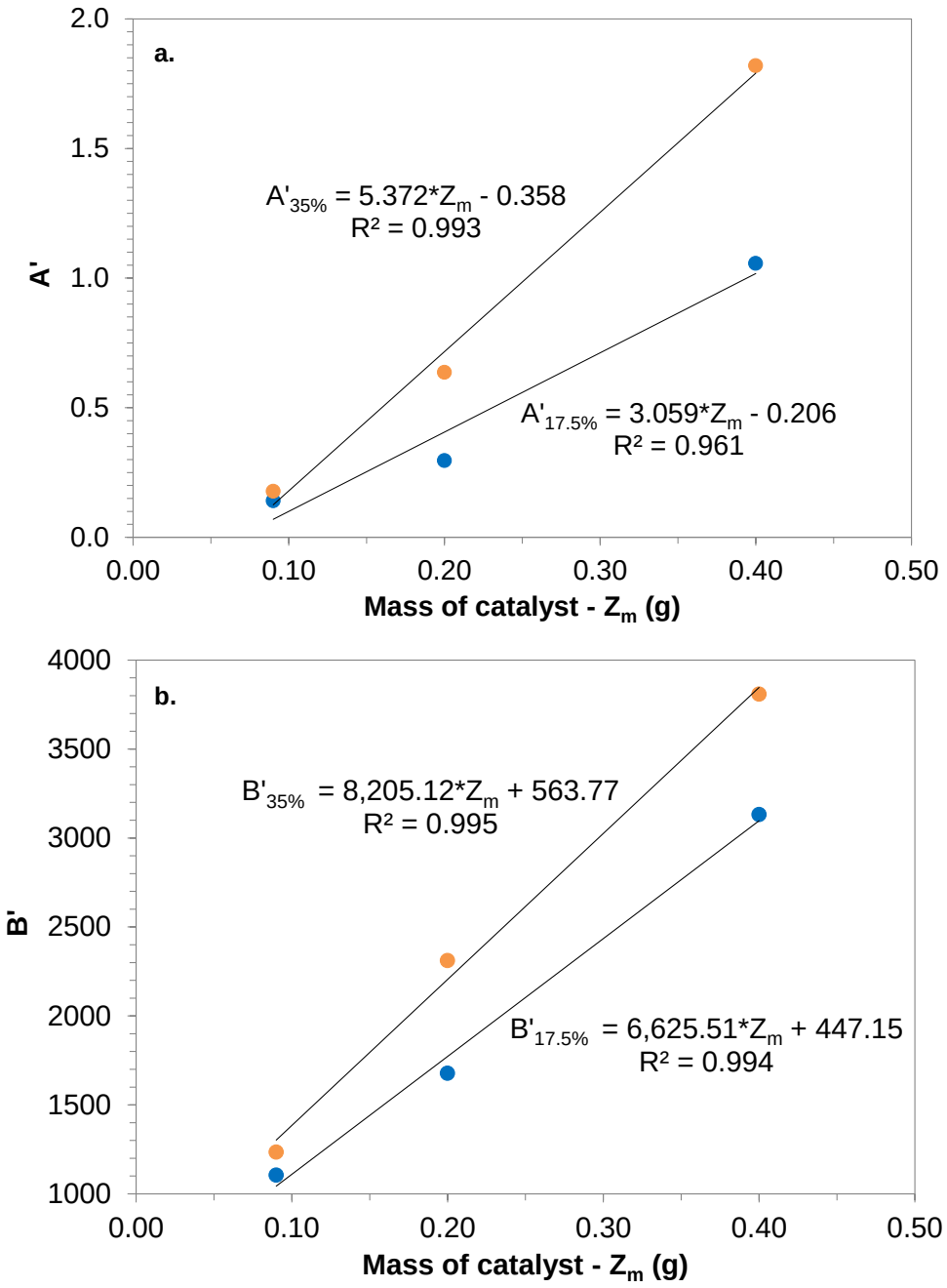

Figure 28. Relationship between the parameters A' and B' and the amount of catalyst Z_m for the decomposition of 17.5 % (orange dots) and 35 % (blue dots) H_2O_2

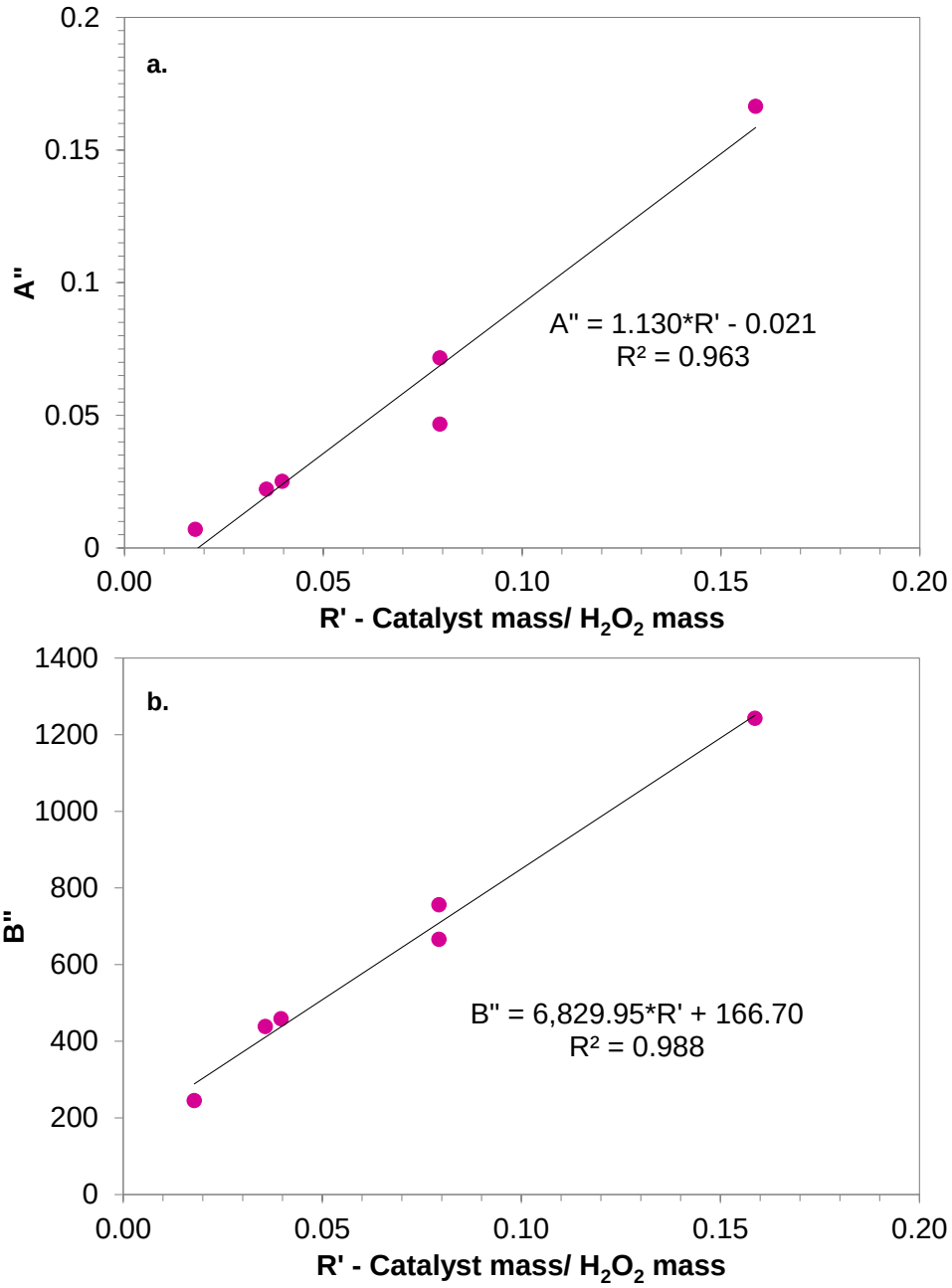

Figure 29. Relationship between the parameters A", B", and the catalyst-H_2O_2 ratio R'

3.3 Study of the Runaway for Hydrogen Peroxide, 2-methylpyridine *N*-oxide and Phosphotungstic Acid Mixtures

The decomposition of hydrogen peroxide and the decomposition of 2-methylpyridine *N*-oxide (2NOX) studied in isolation were presented in the previous two sections. This section includes the synergistic effects observed in adiabatic measurements that were performed using mixtures of 2-methylpyridine *N*-oxide, hydrogen peroxide and catalyst. Moreover, these measurements come to investigate the pressure and temperature profiles that could result if a runaway occurs at the end of the reaction where the mixture is mostly composed by the product, 2-methylpyridine *N*-oxide, water and the accumulated hydrogen peroxide.

The measurements were performed in the APTAC using the HWS mode with a heating step of 10 ^{o}C and a wait length of 30 min. The details of the measurements are shown in Table 10. This table also includes the "onset" temperatures (T_o) and the phi-factors (ϕ) for each of the experiments.

Table 10. Experimental details and "onset" temperatures for the runaway study of H_2O_2, 2NOX, and catalyst mixtures

2NOX (g)	Catalyst (g)	17.5 % H_2O_2 (g)	35 % H_2O_2 (g)	To_1 (^{o}C)	To_2 (^{o}C)	ϕ
1.60	0.00	14.40	-	124.06	-	1.61
1.60	0.09	14.40	-	85.20	-	1.65
1.60	0.20	14.40	-	82.79	207.07	1.64/1.58
1.60	0.00	-	14.40	114.50	-	1.64
1.60	0.09	-	14.40	86.95	-	1.63
1.60	0.20	-	14.40	73.60	-	1.64
1.60	0.40	-	14.40	73.84	-	1.67

The phi-factor was estimated using equation (4) included in Subsection 2.4. The heat capacity of 2NOX was not found in the literature. Moreover, the composition of the reacting mixture is variable with different unknown products. Therefore, it was resolved

to assume that the heat capacity of the sample was equal to water and it was estimated as the average of its value at the "onset" temperature and at the maximum temperature.

Figure 30 shows the temperature and pressure profiles for the decompositions of 2NOX and 17.5 % H_2O_2 using different amounts of catalyst. As mentioned in the previous sections, the "onset" for the decomposition of 17.5 % H_2O_2 was determined to be in the range between 75 ^oC and 160 ^oC depending on how much catalyst was present. For 2NOX, the "onset" was determined to be practically higher than 200 ^oC for either its catalytic or non-catalytic decomposition. Therefore, if no synergistic effects were to exist, H_2O_2 decomposition should start first, and depending on the conditions and its quantity, it could cause a subsequent decomposition of 2NOX.

As can be seen in Figure 30, for the non-catalytic case (in blue), a single exotherm was measured at approximately 124 ^oC, and finished at approximately 250 ^oC. The total pressure increase produced by this strong exotherm was approximately 4000 kPa. For the measurement employing 0.09 g of catalyst (in green), the exotherm was measured at around 85 ^oC and rapidly increased the temperature to approximately 200 ^oC. The temperature increase was enough to trigger the decomposition of 2NOX at a different rate and produced an additional temperature increase of 80 ^oC. The first decomposition stage produced a pressure increase of approximately 3000 kPa followed by an additional increase of approximately 4500 kPa caused by the second stage decomposition. Such a rapid generation of gas during the decompositions can have dramatic effects on the integrity of the reaction vessel. The last case in Figure 30 represents the measurement employing 0.2 g of catalyst (in purple) and follows again two stages of decomposition. The "onset" of the first stage, presumably due to the H_2O_2 decomposition, was approximately 83 ^oC. In this case, the hydrogen peroxide was consumed before the second decomposition was triggered, and the exotherm ended at approximately 170 ^oC. After a few HWS steps, the second exotherm was measured at around 207 ^oC and ended approximately 70 ^oC higher. Both exotherms caused significant pressure rises.

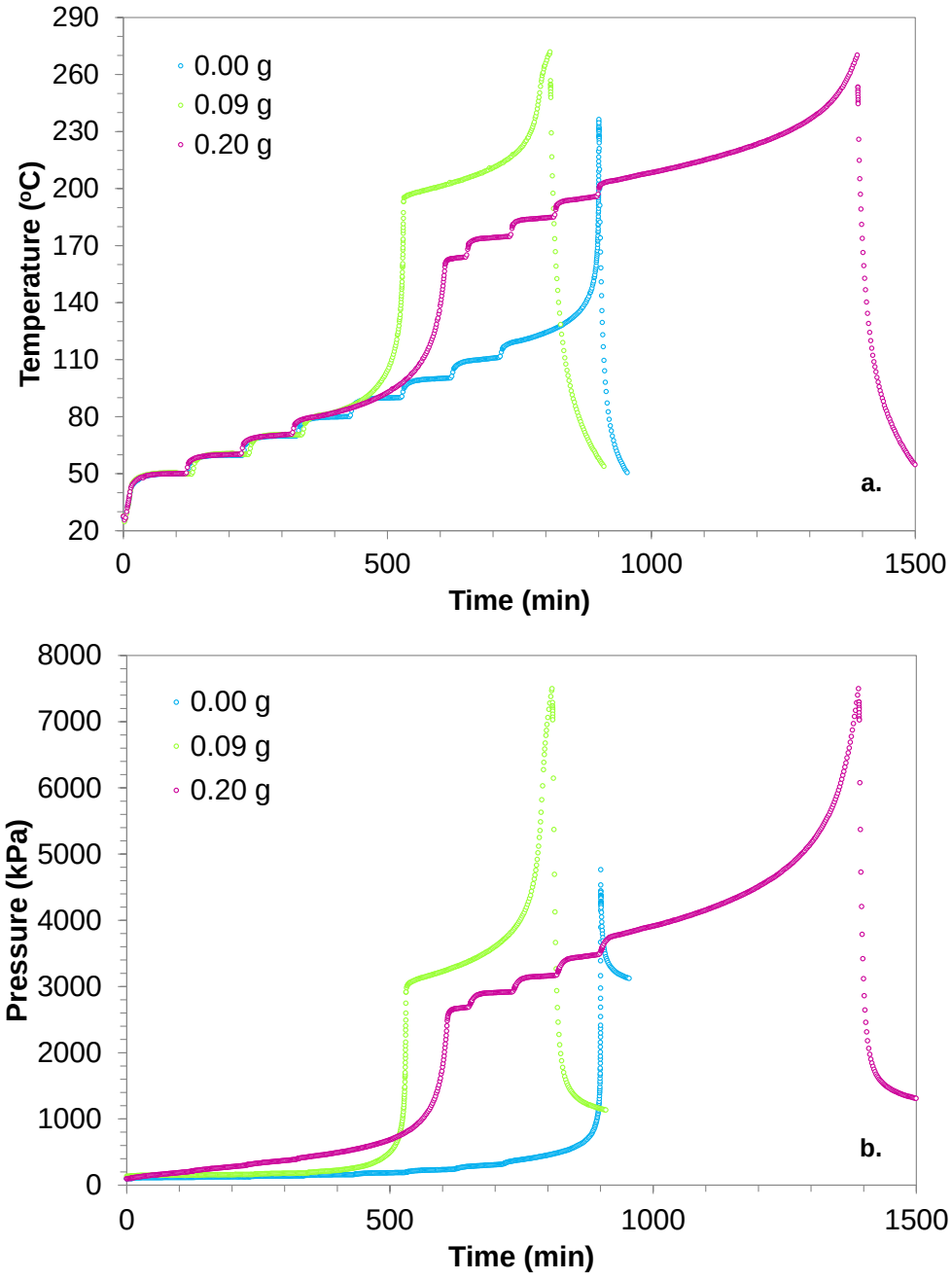

Figure 30. **a)** Temperature, and **b)** Pressure profiles for the decomposition of 2NOX and 17.5 % H_2O_2 using different amounts of catalyst

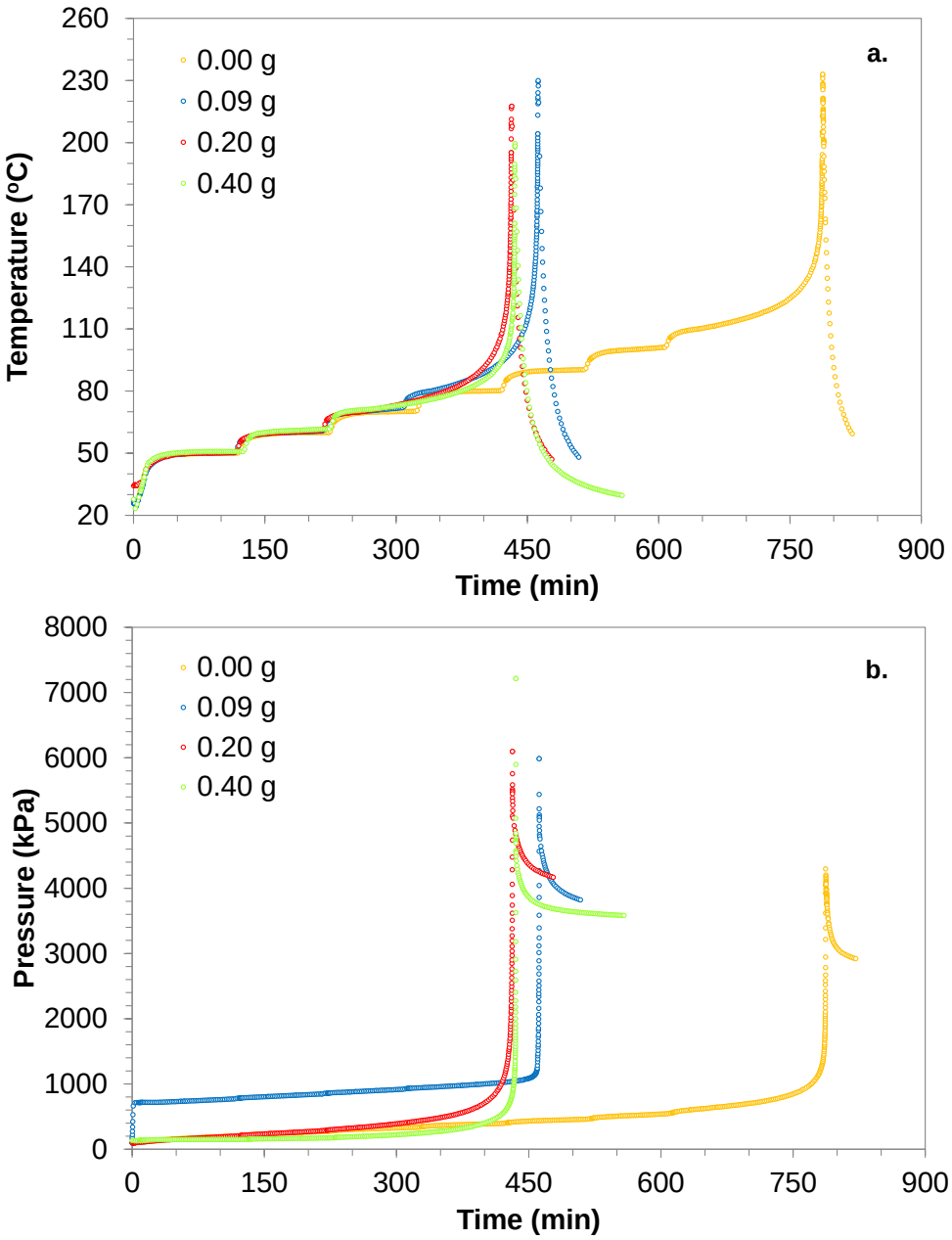

Figure 31. a) Temperature and **b)** Pressure profiles for the decomposition of 2NOX and 35 % H_2O_2 at different amount of catalyst

The temperature and pressure profiles for the decomposition of 2NOX and the decomposition of 35 % H_2O_2 employing different amounts of catalyst are shown in Figure 31. The temperature profile, Figure 31a, shows that for all cases, a fast, single stage decomposition was measured. Additionally, as shown in Table 10, the "onset" that represents the combined decompositions decreases with catalyst. Figure 31b shows the pressure profile for these measurements. As previously noted, significant pressure increases are developed due to the production of non-condensable gases from both decompositions. For the measurement were 0.09 g of catalyst were employed, the systems was pressurized before the HWS stepwise procedure was started.

From the temperature and pressure profiles shown in Figure 30 and Figure 31, three different cases were identified for the runaway of the H_2O_2 and 2NOX decompositions. These cases are represented in Figure 32.

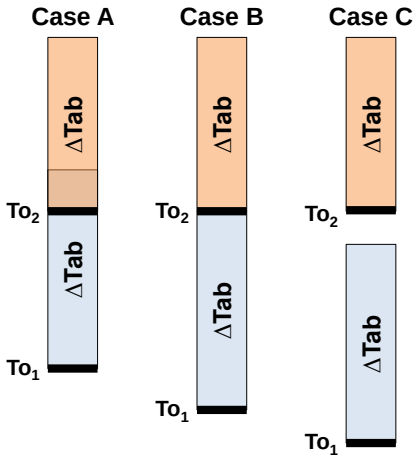

Figure 32. Different cases for the mutual effect of the H_2O_2 and 2NOX decompositions

Depending on the conditions, e.g. mass of catalyst, the "onset" temperature of the first decomposition (To_1) decreases changing the behavior of the runaway. In Figure 32, Case A represents the case where the adiabatic temperature increase caused by the first decomposition reaches a temperature above the "onset" of the second

decomposition (To_2). In this case, a single exotherm represents both decompositions. For Case B, the adiabatic temperature increase from the first decomposition nearly reaches the "onset" for the second decomposition. In this case, the second decomposition is triggered at a different rate, and both decompositions can be distinguished. The resulting consequences will depend on the combination of both decompositions. For Case C, the "onset" temperature for the first decomposition is so low that the adiabatic temperature increase does not reach the "onset" for the second decomposition. If appropriate measures are taken to control the temperature before the second decomposition starts, the consequences can be lessened.

For the measurements presented in this section, a complete decomposition of 2NOX was not obtained because the exotherm rapidly reached the shutdown conditions of the equipment, especially for the measurements representing Case A where a single exotherm was measured. The incomplete decomposition of 2NOX was confirmed by the presence of the 2NOX peak in the GC-MS analyses of the end products of each measurement. Under different conditions and without the shutdown restrictions, the 2NOX would proceed until completion resulting in a higher temperature and pressure increase than the ones shown here.

A comparison between the non-catalytic decomposition of H_2O_2 in isolation and under the presence of 2NOX is shown in Figure 33. For the decomposition of H_2O_2 alone, the detected exotherm for 17.5 % ends as soon as the H_2O_2 is consumed in the mixture; while for 35 %, the exotherm is strong with a steep temperature increase. For the decomposition of H_2O_2 under the presence of 2NOX, a single exotherm was measured for 17.5 % and 35 % H_2O_2. In this case, despite the increase in the H_2O_2 concentration, a similar temperature increase was measured in both cases because the exotherm rapidly reached the shutdown conditions of the equipment. When comparing the "onset" for the measurements with and without *N*-oxide, Table 10 with Table 7, it can be seen that the presence of 2NOX, in general, decreases the H_2O_2 decomposition "onset" by approximately 30 ^{o}C. This can be also seen in Figure 33.

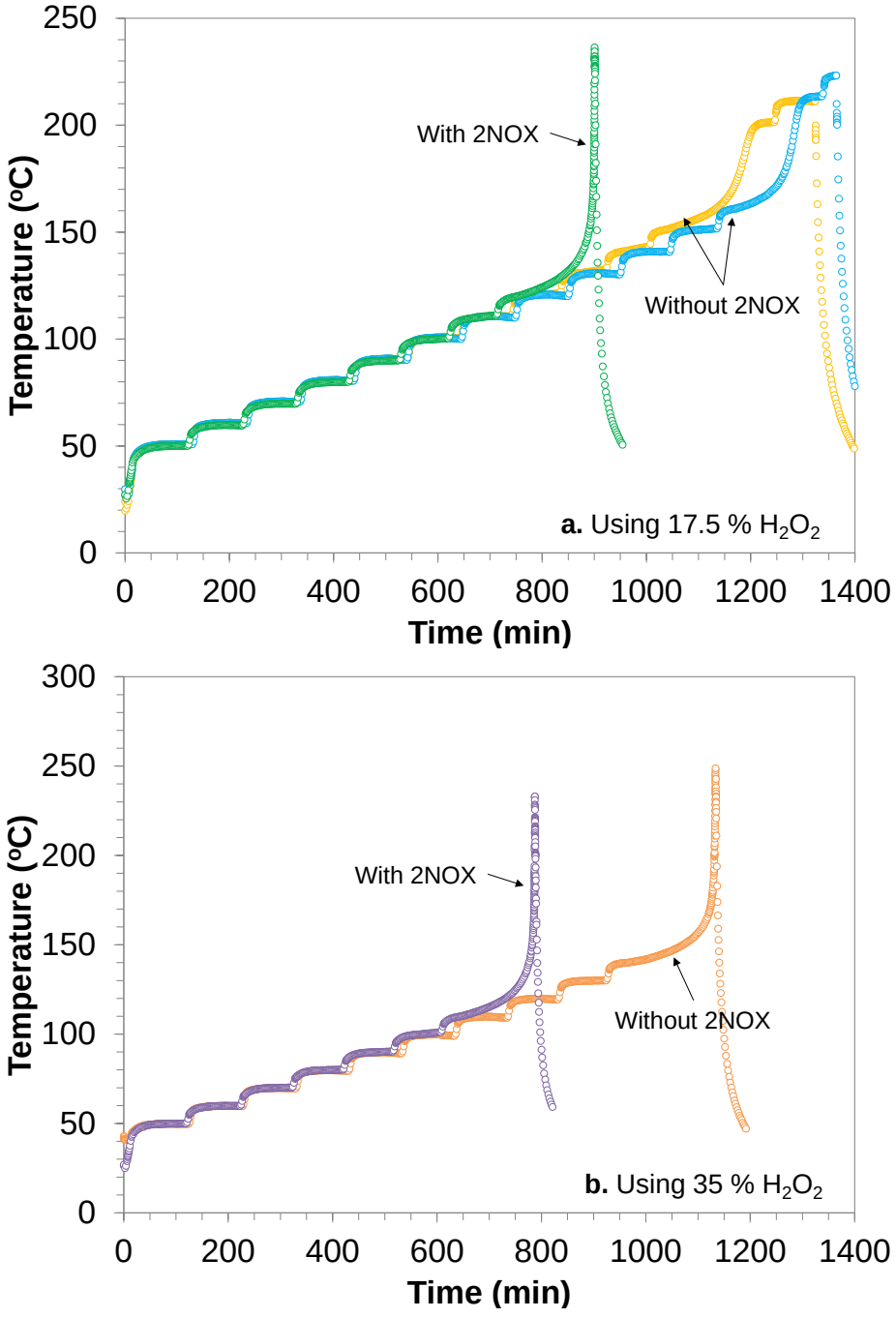

Figure 33. Comparison of the non-catalytic decompositions without and with 2NOX using **a)** 17.5 % H_2O_2 and **b)** 35 % H_2O_2

The heat rate vs. temperature profile for the decomposition of 17.5 % H_2O_2 using 0.2 g of catalyst and 1.6 g of 2NOX is shown in Figure 34. The rate of this measurement has been plotted because, as Figure 30 and Figure 31 show, this was the only measurement were the H_2O_2 decomposition in the presence of 2NOX was clearly distinguished. This heat rate profile was compared with the profile for the measurement presented in Subsection 3.2 of the decomposition of hydrogen peroxide with the same H_2O_2 concentration and the same amount of catalyst (17.5 % H_2O_2 and 0.2 g), but without 2NOX. The comparison is presented in Figure 34 and shows that the increase in the heat rate with temperature is similar for both cases demonstrating that under these conditions, the presence of *N*-oxide did not affect the rate of H_2O_2 decomposition; However, the presence of *N*-oxide reduced the "onset" for the its decomposition. For the other cases presented in Figure 30 and Figure 31, it is presumed that, as the "onset" for the first decomposition increases, the contribution of the 2NOX becomes more significant. Thus, the effect of second decomposition on the first decomposition increases from Case C to Case A in Figure 32.

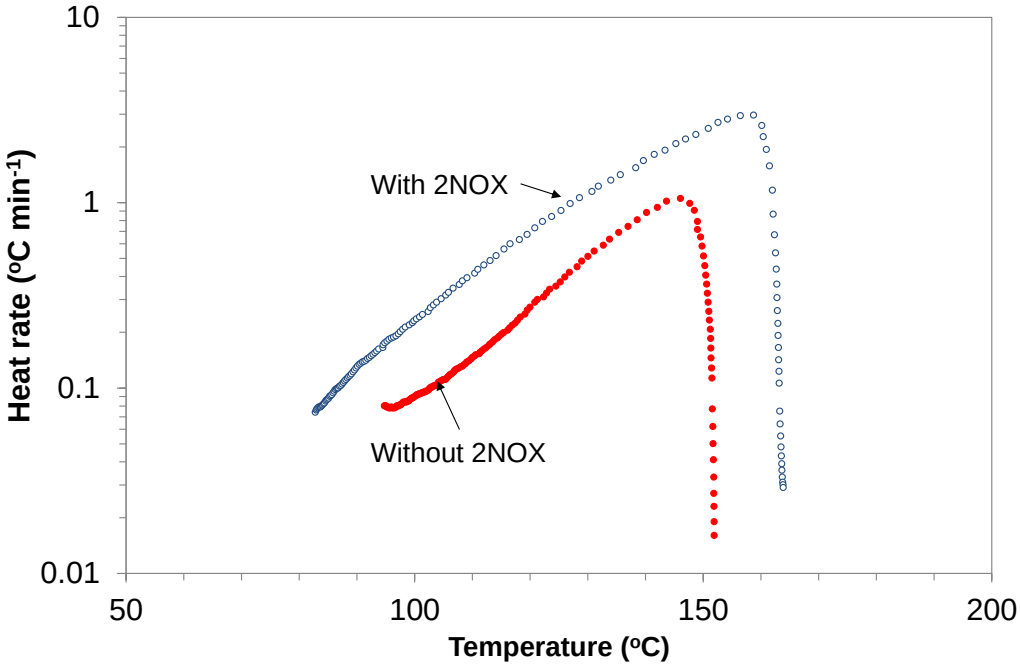

Figure 34. Comparison of the heat rate vs. temperature for the decomposition of 17.5 % H_2O_2 with and without 2NOX using 0.2 g of catalyst

In conclusion, the decomposition of hydrogen peroxide rapidly promotes the decomposition of 2-methylpyridine *N*-oxide. Similarly, the hydrogen peroxide decomposition is affected by the presence of 2-methylpyridine *N*-oxide. For both H_2O_2 concentrations, the decomposition "onset" decreases with catalyst. For 35 % H_2O_2, the two decompositions cannot be distinguished; while two stages of decomposition can be observed for 17.5 % depending on the amount of catalyst employed. The "onsets" measured in a mixture of hydrogen peroxide, 2-methylpyridine *N*-oxide and catalyst were lower than those obtained for pure materials.

3.4 Summary

A potential runaway of the *N*-oxidation of 2-methylpyridine synthesis reaction can develop through the course of two decompositions: The decomposition of unreacted hydrogen peroxide and the decomposition of 2-methylpyridine *N*-oxide. The decomposition of hydrogen peroxide, the decomposition of 2-methylpyridine *N*-oxide and the decomposition of mixtures of those two compounds were studied without catalyst and with different concentrations of catalyst. The following points summarize the findings from Section 3:

- 2-methylpyridine with or without catalyst, appears to be stable up to 350 ^{o}C, the upper limit of temperature employed in this work.

- 2-methylpyridine *N*-oxide decomposes significantly at temperatures above 200 ^{o}C.

- The decomposition of 2-methylpyridine *N*-oxide is enhanced by catalyst and temperature and produces mainly 2-methylpyridine and pyridine as well as non-condensable gases.

- The measurement of the "onset" for the decomposition of hydrogen peroxide decreases with catalyst. This indicates that at low catalyst concentrations the reaction is much slower and it becomes detectable after some H_2O_2 has already decomposed.

- Two kinetic models that represent very successfully the catalytic and non-catalytic decomposition of H_2O_2, at different H_2O_2 and catalyst concentrations were developed.

- The presence of 2-methylpyridine *N*-oxide affects the decomposition of H_2O_2, and vice versa: When those two compounds are together, the decomposition of both occurs at substantially lower temperatures.

4. *N*-OXIDATION OF ALKYLPYRIDINES AT DIFFERENT CONDITIONS

As mentioned in Section 2, previous studies performed in the limited range of 85 to 100 ^{o}C showed that as the temperature and the amount of catalyst increased, the extent of the decomposition of hydrogen peroxide during the *N*-oxidation of alkylpyridines was reduced [36, 38]. Thus, this finding provided a clear indication that changing the conditions of the process could turn the *N*-oxidation into a more competitive process, practically consuming the hydrogen peroxide before it decomposes.

Previous studies have also proposed a complex kinetic model for the synthesis of the *N*-oxide and the simultaneous decomposition of H_2O_2 [2, 36]. The experimental measurements of 2-methylpyridine and 3-methylpyridine, performed in the range of temperatures mentioned above, were in excellent agreement with the modeled values, while the model appeared promising for the other alkylpyridines in homogeneous reactors. According to this model, the *N*-oxidation rate is first order in respect to the concentration of both hydrogen peroxide and alkylpyridine. The rate of decomposition of hydrogen peroxide on the other hand, is second order in respect to H_2O_2 concentration. As the synthesis reaction progresses, the *N*-oxidation rate decreases because of the dropping concentration of alkylpyridine. As the *N*-oxidation becomes slower, hydrogen peroxide can accumulate and its decomposition rate, being proportional to the square of its concentration, becomes more significant at the end of the reaction. During normal operation, the gradual addition of hydrogen peroxide controls the rate of its decomposition by maintaining the H_2O_2 concentration inside the reactor low. However, an abnormal situation like a dosing pump malfunction, where the pump delivers oxidant at a higher rate than the requested safe value, or for a longer period of time, or both, can produce H_2O_2 accumulation and lead to its decomposition runaway.

For the *N*-oxidation of 2-methylpyridine, two key aspects have been investigated and are presented in this section: the conditions at which the need for H_2O_2 excess can be reduced and the effect of operation at higher temperatures and catalyst concentrations. For the *N*-oxidation of 2,6-dimethylpyridine, an additional aspect was considered which corresponds to the effect of the presence of two-liquid phases during the reaction.

For the study at higher temperatures, the reaction has to be performed in a closed glass reactor, and such reactors can usually withstand up to 5-6 bar. Metals reactors could not be used in this study, as metals are well known catalysts of H_2O_2 decomposition. Based on the maximum operating pressure of the reactor, the vapor pressure of the system sets the upper temperature limit of operation and this was near 125 ^oC. An additional restriction is set by the decomposition "onset" of the product. As mentioned in Section 3, 2-methylpyridine *N*-oxide can decompose at high temperature and its decomposition "onset" drops in the presence of H_2O_2 and catalyst. According to the restrictions mentioned above, the *N*-oxidation was studied at temperatures between 110 ^oC and 125 ^oC.

4.1 2-methylpyridine *N*-oxidation

The *N*-oxidation of 2-methylpyridine (2MP) at temperatures above 100 ^oC was studied using the isothermal calorimeter described in Subsection 2.4. The details of the experimental tests are shown in Table 11. All the properties for the calculations (vapor pressures, densities and heat capacities) have been obtained from DIPPR Project 801 [64]. A stoichiometric amount of H_2O_2 was employed in all cases but the fifth.

The first two measurements in Table 11 were conducted to determine the reproducibility of the data, which was determined to be very good. The third measurement employed a higher amount of catalyst; while the fourth was performed at a higher temperature with the normal amount of catalyst. The temperature was increased to 125 ^oC in the fifth measurement; however, the dosing was performed in two steps because the pressure reached the maximum safe limit imposed at the beginning of the experiment to prevent the rupture of the vessel (P_{max} = 600 kPa). The last two tests in Table 11 were performed to study the effect of accumulation and dosing rate, respectively.

Table 11. Experimental details for the study of the *N*-oxidation of 2MP using an isothermal calorimeter. The heater power used during the calibrations was 37.7 W and the base power used during the measurements was 14.8 W. The agitator speed was 200 rpm for all measurements

T (^oC)	2MP (g)	Water (g)	Catalyst (g)	H_2O_2* (g)	Dosing rate (g min^{-1})	T_{amb} (^oC)
110	150	100	3.5	156.5	0.52	22.8
110	150	100	3.5	156.5	0.52	23
110	150	100	5.0	156.5	0.52	23.5
120	150	100	3.5	156.5	0.52	23.3
125	150	100	3.5	59.8 75.0	0.52	23.5
110	150	100	3.5	62.4 93.4	0.52	22.9
110	150	100	3.5	15.2 14.9 20.1 24.9 40.0 41.3	0.26 0.52 0.78 1.04 1.30 0.78	23.6

*H_2O_2 represents the amount of H_2O_2 solution (35 wt. % in H_2O)

4.1.1 Effect of Catalyst and Temperature on the 2MP N-oxidation

This subsection focuses on the results obtained for the first four measurements shown in Table 11. The pressure increase during the dosing and stir-out periods was employed to determine the amount of hydrogen peroxide decomposed during the isothermal *N*-oxidation of 2MP of every measurement. The pressure increase is defined as the pressure difference between any point in the dosing period and the initial pressure (pressure just before the dosing started).

As the reactor is a closed system, the pressure increase, shown schematically in Figure 35, is caused by vapors and non-condensable gases existing prior to the reaction, which are heated during the process, or formed during it at the process temperature. Those are further compressed due to the reduction of the available headspace of the reactor, due to the addition of reactant.

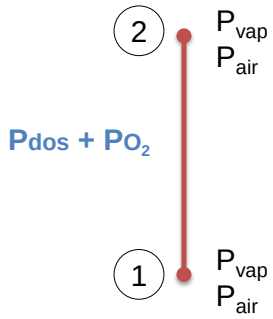

Figure 35. Pressure increase during the dosing (and stir-out) period for the isothermal tests

In Figure 35, point 1, P_1, represents the equilibrium pressure before dosing, and point 2, P_2, represent the pressure after the end dosing, when a steady state has been reached during the stir-out period. The pressure increase from point 1 to point 2 is given by equation (23):

$$P_2 - P_1 = \left(P_{vap_2} + \Delta P_{air_2} + P_{O_2}\right) - \left(P_{vap_1} + \Delta P_{air_1}\right) \quad (23)$$

where

P_{vap} is the vapor pressure of the mixture

P_{air} is the pressure caused by the air initially contained in the vessel headspace

P_{O_2} is the pressure that the produced oxygen exerts

Due to the lack of sufficient information in the literature, it is assumed that the vapor pressure for the reaction mixture is equal to the vapor pressure of water, and because the temperature is maintained constant, the vapor pressure terms can be eliminated from equation (23). When considering the vapor pressure of 2MP at the beginning of the mixture and assuming a vapor pressure for 2NOX similar to that for water, the value for P_{vap_2}-P_{vap_1} is estimated to be approximately 19 kPa at 110 ^{o}C, 27 kPa at 120 ^{o}C, and 32 kPa at 125 ^{o}C.

The change in air pressure in point 1, ΔP_{air_1}, is caused by the change in temperature from 80 ^{o}C, T_1, which was the temperature at which the reactor was sealed with the air pressure equal to atmospheric, P_{atm} = 100 kPa; to the temperature of reaction, T_2. This change in air pressure is calculated assuming ideal gas behavior using equation (24).

$$\Delta P_{air_1} = \frac{P_{atm} \cdot T_2}{T_1} - P_{atm} \tag{24}$$

The change in the air pressure in point 2, ΔP_{air_2}, is caused by the reduction of the vapor space due to dosing and again, it can be calculated assuming ideal gas behaviors as:

$$\Delta P_{air_2} = \frac{P_{air_1} \cdot V_i}{V_f} - P_{air_1} \tag{25}$$

where

V_i is the initial volume of the reactor headspace, before dosing

V_f is the final volume of the reactor headspace, after dosing

P_{air_1} is the pressure of the headspace at point 1

To ensure that the pressure calculations agree with the data obtained experimentally, a “baseline” test was conducted with only water and employing the same amounts of initial mixture and dosing material. Because no reaction took place in this baseline test, the P_{O_2} term in equation (23) is equal to zero and the equation becomes:

$$\Delta P_{air_2} - \Delta P_{air_1} = P_{dos} \tag{26}$$

The change in air pressure, ΔP_{air}, in points 1 and 2 were calculated using equations (24) and (25), respectively. Additionally, the initial and final pressures were calculated by adding the vapor pressure to the change in air pressure. The pressure increase during the baseline test as well as the experimental, P_{exp}, and calculated, P_{cal}, pressures are included in Figure 36. This figure shows that the calculated pressure values agree with the experimental data (within the experimental range of error), and therefore, equations

(26) and (23) were applied to estimate the dosing pressure and the O_2 pressure for all the other isothermal measurements, respectively.

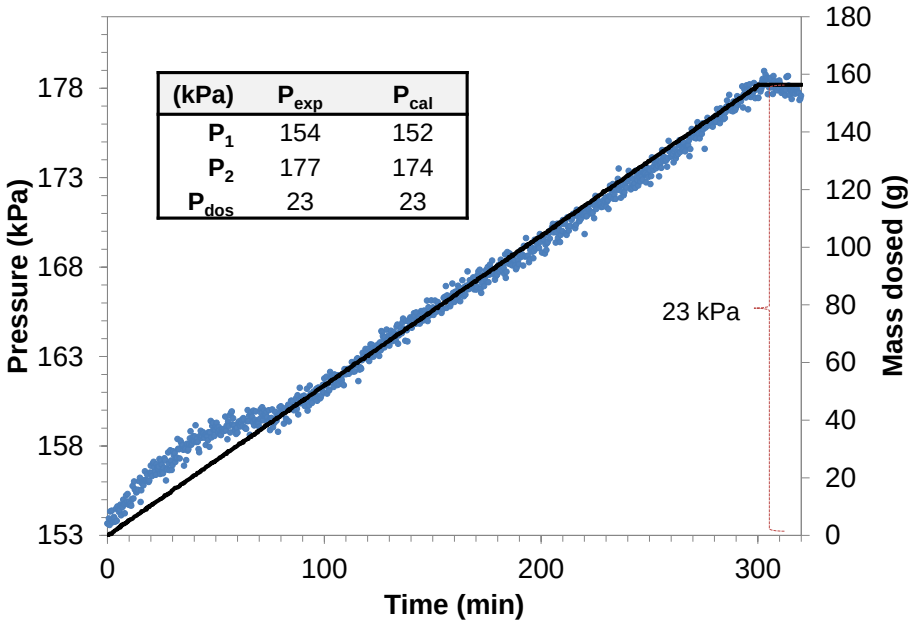

Figure 36. Pressure increase during the baseline test (blue dots). The experimental and calculated pressure values are included in the table. The black line represents the mass of water dosed

Figure 37 shows the pressure increase for the isothermal *N*-oxidation of 2MP for the first four tests in Table 11. As mentioned earlier, the pressure increase in a particular point is given by the total pressure at that point minus the constant initial pressure (pressure just before the dosing). In the first 20 min of the dosing period, there is an upset in the reactor temperature, and therefore in its pressure, caused by the start of addition of cold H_2O_2 which is immediately followed by the sudden energy release from the reaction. Beyond this slight initial temperature increase, the temperature remains constant for the rest of the dosing period. The pressure increase for the two measurements at 110 ^oC and 3.5 g was identical showing an excellent reproducibility of the data.

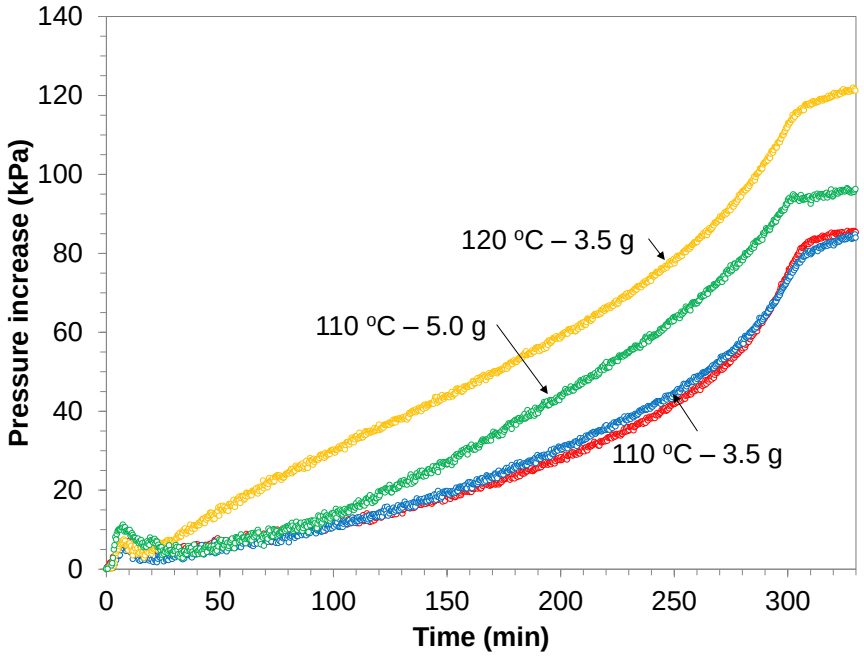

Figure 37. Pressure increase during the dosing (and stir-out) period for the isothermal *N*-oxidation of 2MP at different temperatures and amount of catalyst

The results shown in Figure 37 indicate that the pressure increase becomes larger as the amount of catalyst and temperature increase. However, this difference is only visual as the error associated with the measurement is larger than the visualized differences. Similarly, as is later shown in Table 12, the 1 % difference for the conversion of 2MP is also associated with the measurement error. Unfortunately calorimetric measurements suffer of many sources of error and the results presented here cannot form an exception. The main sources of error in the present measurements are listed below:

- As explained earlier, in the lack of other data, the mixture properties and most importantly its vapor pressure were assumed to be those of water. That cannot be true, especially during the beginning of the measurement, as 2MP has different properties from those of water. This difference inevitably introduces an error in the pressure calculation which ultimately affects the accuracy of the estimation of the oxygen moles. The effect of this error is higher at higher temperatures.

- During the measurements, the dosing tube was not submerged in the solution, and therefore, the dosed H_2O_2 had to travel approximately 8 cm through the vapor space. This could have caused some of the solution to vaporize or decompose. As mentioned earlier, the decomposition of H_2O_2 is suppressed during the *N*-oxidation because, as the temperature increases, the *N*-oxidation becomes more competitive than the H_2O_2 decomposition, and therefore, the dosed H_2O_2 is consumed by the *N*-oxidation before it decomposes. However, as shown in Subsection 3.2, in absence of 2MP to react and at temperatures above 100 ^{o}C, hydrogen peroxide is above the decomposition "onset". Thus, possible decomposition of H_2O_2 during the trajectory from the dosing tube to the reaction mixture cannot be ruled out.

Figure 38 shows the ten-minute mean average rate of pressure increase for the first four isothermal measurements in Table 11. As seen in Figure 38, the pressure rates are comparable for all the measurements indicating similar reaction rates for all measurements.

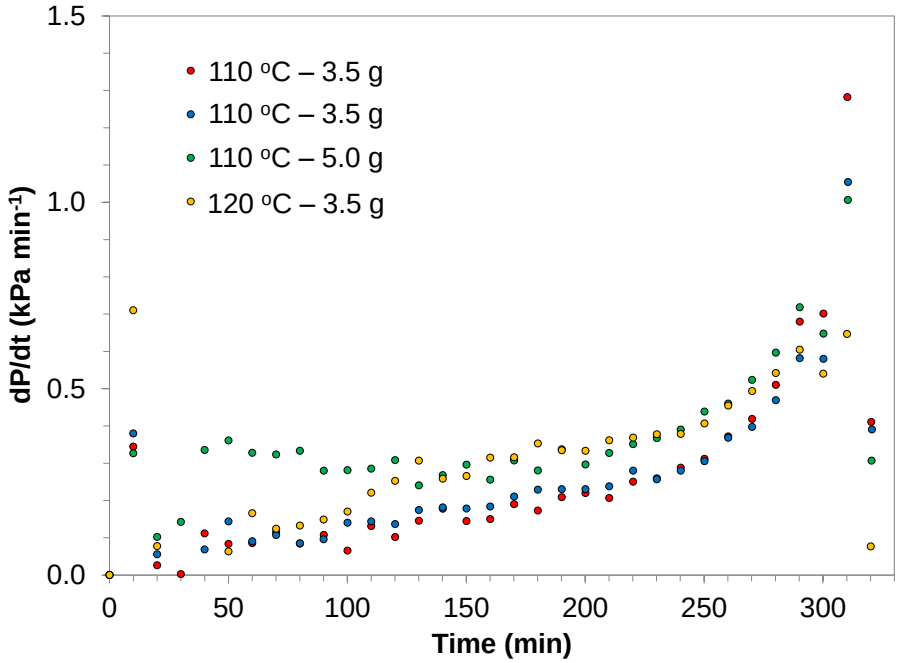

Figure 38. Pressure rate during the dosing (and stir-out) period for the *N*-oxidation of 2MP at different temperatures and amounts of catalyst

For the four isothermal tests previously shown in Table 11, the initial, P_1, and final, P_2, pressures obtained experimentally as well as the estimated dosing pressure P_{dos}, and the estimated oxygen pressure, P_{O_2} are shown in Table 12. The initial and final pressures were averaged over a 30-minute period before and after dosing. The calculated moles of oxygen and the 2MP conversion are also shown in Table 12. The number of moles of oxygen was estimated using the ideal gas law and it was employed to determine the amount of hydrogen peroxide decomposed in the respective measurement. Then, the amount of reacted 2MP was calculated assuming that all H_2O_2 which did not decompose reacted with 2MP. The conversion was estimated by dividing the reacted 2MP by the initial amount of 2MP.

Table 12. Pressure and conversion for the isothermal *N*-oxidation of 2MP at different temperatures and amounts of catalyst

T (^oC)	Catalyst mass (g)	P_1 (kPa)	P_2 (kPa)	* ΔP (kPa)	P_{dos} (kPa)	PO_2 (kPa)	NO_2 (mol)	2MP Conversion (%)
110	3.5	175.4	260.6	85.2	19.5	65.6	0.0118	99
110	3.5	177.1	262.4	85.3	19.5	65.8	0.0118	99
110	5.0	172.6	293.9	121.4	19.4	101.9	0.0183	98
120	3.5	229.4	325.1	95.7	17.6	78.1	0.0136	98

*$\Delta P = P_2 - P_1$ = Total pressure increase

Table 12 shows that, within the experimental error margin, a similar amount of oxygen was produced in all measurements, which agrees with the similar pressure rate profile obtained in Figure 38. For the conversion, values higher than 98 % were obtained demonstrating an increase in efficiency at temperatures above 100 ^oC, when comparing with measurements at temperatures between 90 ^oC and 100 ^oC where 50 % more H_2O_2 was required to achieve similar conversions [2]. Moreover, it can be seen that the number of moles of oxygen slightly increases with temperature and catalyst, which is the opposite of what has been found in previous works [36]. However, as mentioned earlier this disagreement is most likely apparent as it is well within the experimental error and as such it cannot be considered as a fact. Further investigation is needed with a more accurate measurement of the produced oxygen.

The reaction heat flow was estimated from the energy balance shown in Subsection 2.4, equation (6). All the terms in this equation have dimensions of energy per unit time.

$$\dot{Q}_{rxn} = \dot{Q}_j - \dot{Q}_h + \dot{Q}_{dos} + Baseline \tag{6}$$

where

$\dot{Q}_{rxn}$ is the overall power generated from the reaction

$\dot{Q}_j$ is the power exchanged with the jacket oil

$\dot{Q}_h$ is a small constant power provided by the heater during the measurement

$\dot{Q}_{dos}$ is the power transfer to the dosed material to bring the dosed material to the reactor temperature

Baseline is the power from the stirrer and all possible heat losses

The power exchanged with the jacket oil, $\dot{Q}_j$, is determined by equation (27):

$$\dot{Q}_j = UA \cdot \left(T_r - T_j\right) \tag{27}$$

where

U is the overall heat transfer coefficient

A is the area available for the exchange of heat between the reactor and the jacket. In subsequent calculations, the product UA is treated as a single variable.

T_r is the reactor temperature

T_j is the jacket temperature

The dosing power is given by equation (28), and represents the energy required to increase the temperature of the dosed material from the dosing temperature to the reactor temperature.

$$\dot{Q}_{dos} = (\dot{m}C_p)_{dos} \cdot (T_r - T_{dos}) \tag{28}$$

where

$\dot{m}$ is the mass flow rate of the dosed material

C_p is the heat capacity of the dosed material

T_{dos} is the temperature of the dosed material (equal to T_{amb} in Table 11)

As the dosed material was a solution of 35 % H_2O_2, the value of its heat capacity for equation (28) was calculated from the weight-average heat capacity of the solution, i.e. 3.635 J g^{-1} K^{-1}.

As UA and the baseline change with dosing, these quantities were evaluated from the calibration steps before and after the dosing period. During the calibration period, $\dot{Q}_{rxn}$ and $\dot{Q}_{dos}$ are equal to zero because no reaction or addition of mass are taking place. As such, the heat balance, equation (6), becomes:

$$\dot{Q}_h = UA \cdot \left(T_r - T_j\right) + Baseline \tag{29}$$

Two calibrations are employed for the calculation of the UA in each measurement: the calibration before dosing starts and the calibration after reaction completion. The procedure to determine UA and Baseline from Equation (29) is as follows:

- Two points are employed to estimate the unknown UA and baseline values: at thermal equilibrium when only the base power is applied ($\dot{Q}_h = \dot{Q}_{base}$, Table 11), and at thermal equilibrium when the calibration power is applied ($\dot{Q}_h = \dot{Q}_{cal}$, Table 11). For each value of $\dot{Q}_h$, the temperature difference, (T_r - T_j), is different.

- Using both points, UA can be determined from the slope of equation (29), while the intersection with the y-axis corresponds to the baseline.

- Subsequently it is assumed that U is practically the same as a great proportion of the reacting mixture is water, but A, changes due to reactant addition. Thus the baseline and UA are considered to change linearly with dosing. As dosing rate is

constant, UA and Baseline are taken to increase linearly with dosing time and proportionally to the dosing rate.

The reaction power is calculated using equation (6). The area under the reaction power profile determines the overall heat from the reaction, Q_{total}. Table 13 shows the calculated values for the heat transfer coefficient, UA, and the baseline as well as the total heat generated by each measurement.

Table 13. UA, baseline, and reaction heat estimated for the *N*-oxidation of 2MP at different temperatures and amounts of catalyst

T (^{o}C)	Catalyst (g)	UA_1 (W K^{-1})	UA_2 (W K^{-1})	$Baseline_1$ (W)	$Baseline_2$ (W)	Q_{total} (kJ)
110	3.5	2.31	2.80	63.71	39.49	282
110	3.5	2.21	2.79	60.65	37.96	282
110	5.0	2.18	2.80	56.98	34.67	262
120	3.5	2.22	2.87	73.26	44.19	304

Indices 1 and 2 stand for before dosing and after reaction completion, respectively

Figure 39 shows the reaction and dosing power for one of the isothermal measurements. The dots indicate the values obtained for each point in the measurement, and the black solid line represents their moving average. This figure shows that $\dot{Q}_{dos}$ remains almost constant during the dosing period and becomes zero when the dosing stops at around 300 min; while, the reaction power, $\dot{Q}_{rxn}$, reaches a value of approximately 18 W, and after 150 min, starts slowly decreasing to become zero approximately 20 min after the dosing stopped. A small increase in the reaction power can be observed at around 20 min which is caused by temperature instability because of the addition of the cold reactant which was immediately followed by the sudden energy release when dosing started.

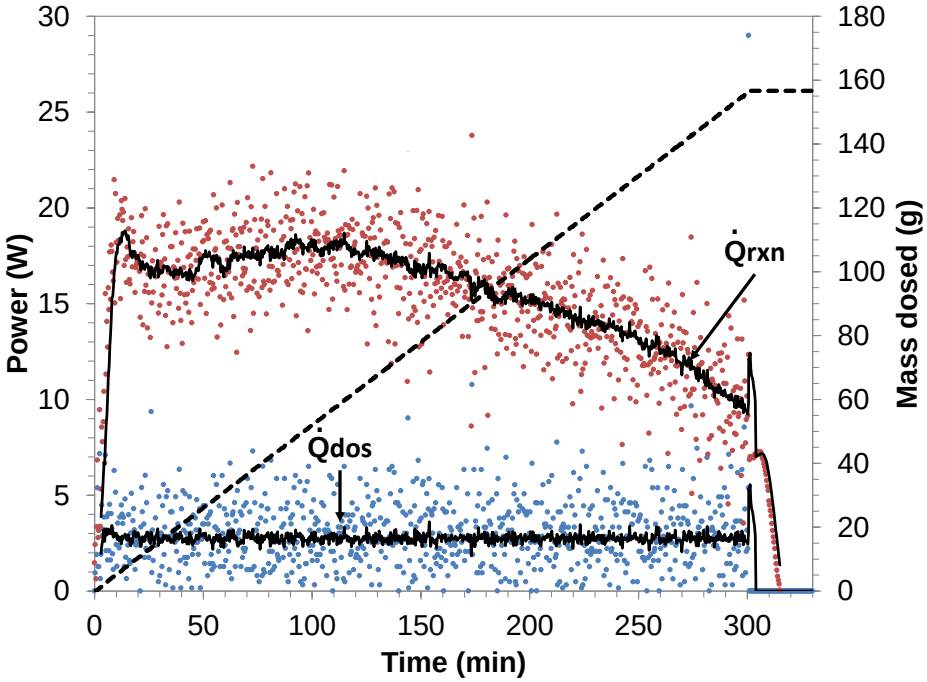

Figure 39. Reaction power and dosing power for the *N*-oxidation of 2MP at 110 ^{o}C and 3.5 g of catalyst

As mentioned earlier, the overall heat produced by both reactions, Q_{total}, is calculated from the area under the curve shown in Figure 28. The overall heat due to the decomposition, Q_{dec}, is calculated from equation (30) using twice the number of the calculated moles of oxygen (moles of H_2O_2 decomposed) and using a heat of decomposition, ΔH_{dec}, of -100 kJ mol $^{-1}$.

$$\dot{Q}_{dec} = -\Delta H_{dec} \cdot N_{H_2O_2} \qquad (30)$$

where

$N_{H_2O_2}$ is the moles of H_2O_2 which decomposed during the *N*-oxidation

From the overall heat generated during the reaction, Q_{total}, and the heat of decomposition, Q_{dec}, the heat generated from the *N*-oxidation, Q_{nox}, can be calculated from:

$$Q_{nox} = Q_{total} - Q_{dec} \quad (31)$$

The *N*-oxidation power and the decomposition power for one of the isothermal tests are shown in Figure 40. The average for the power is represented by the black solid line. The heat from the *N*-oxidation, Q_{nox}, and the heat from the decomposition, Q_{dec}, are estimated from the area under the curve in Figure 40 and are included in Table 14. The heat of reaction for the 2MP *N*-oxidation is calculated dividing Q_{nox} by the reacted moles of 2MP. The heat for the *N*-oxidation of 2MP was found to be between 160 and 190 kJ mol^{-1}. For all the measurements in Table 14, the heat generated by H_2O_2 decomposition (of the order of 2 kJ in each measurement) was negligible compared with the error of such measurements.

Table 14. *N*-oxidation heat, decomposition heat, and heat of reaction for the *N*-oxidation at different temperatures and amounts of catalyst

T (^oC)	Catalyst (g)	N_{O_2} (mol)	Q_{dec} (kJ)	Q_{nox} (kJ)	ΔH_{nox} (kJ mol^{-1})
110	3.5	0.0118	2.36	280.14	176
110	3.5	0.0118	2.36	279.39	176
110	5.0	0.0183	3.66	258.41	164
120	3.5	0.0136	2.72	301.00	190

Figure 41 shows the total power generated during the *N*-oxidation of 2MP at different amounts of catalyst and temperatures; while, Figure 42 shows the power generation exclusively due to H_2O_2 decomposition. As can be seen, the curves in Figure 42 are extremely noisy due to the noise present in the measurement of the pressure. Moreover, the values for Q_{dec} are two orders of magnitude smaller than those of the total heat generated by the *N*-oxidation reaction, Q_{nox}.

In Figure 41, the power for the two *N*-oxidations at 110 ^oC and 3.5 g shows practically an identical profile which emphasizes the good reproducibility of the tests. Moreover, those profiles are very similar to those of the remaining measurements, which proves that the *N*-oxidation is very fast, and therefore controlled by dosing, when it is

performed at higher temperatures than those employed in past research, e.g. [36, 38]. In regard with the effect of an increased catalyst concentration, no clear conclusions can be drawn because, within the error of such measurements, all power profiles shown in Figure 41 demonstrate practically a reaction of the same rate and further research work is required.

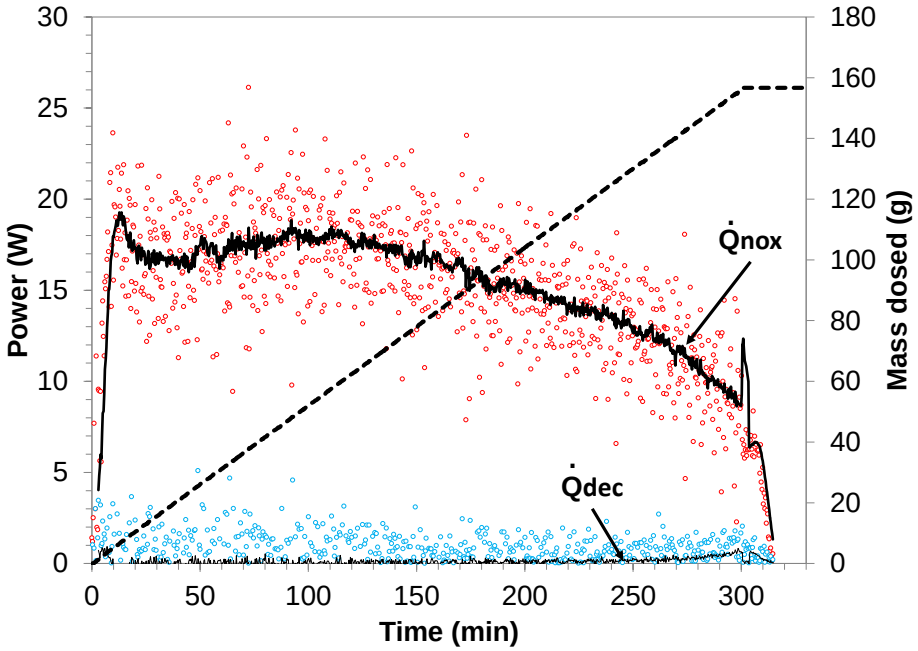

Figure 40. *N*-oxidation and decomposition power for the 2MP *N*-oxidation at 110 ^{o}C and 3.5 g of catalyst

Figure 42 shows the averaged power for the decomposition of hydrogen peroxide during the *N*-oxidation of 2MP. For all the cases, the power was below 1 W. Moreover, the power profiles were very comparable showing that a similar amount of H_2O_2 decomposed in all cases. In the first 200 min, Figure 42, the power was very low; while in the last 100 min, the power increased due to the drop of 2MP concentration, which subsequently gave way to an increased rate of decomposition of the small quantity of accumulated H_2O_2.

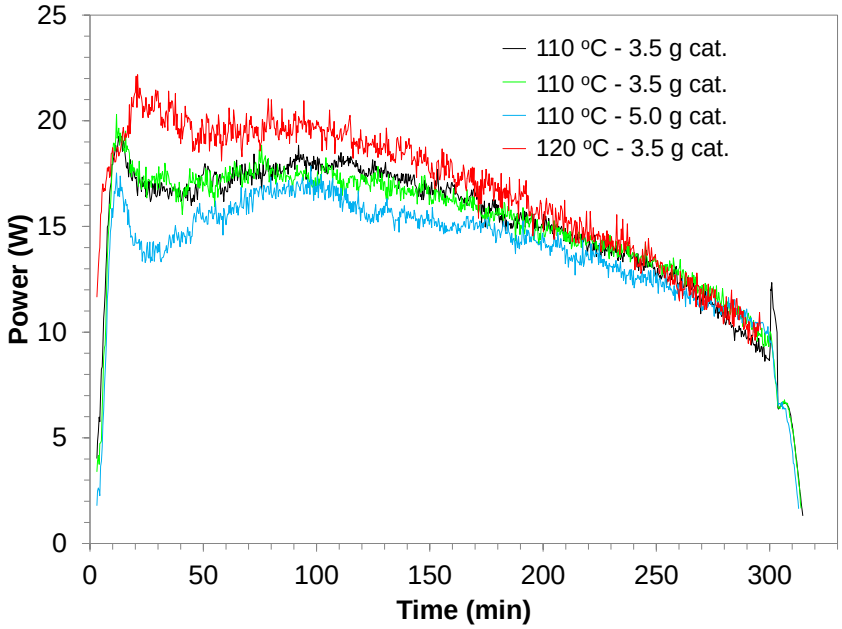

Figure 41. Averaged power for the *N*-oxidation of 2MP at different temperatures and amounts of catalyst

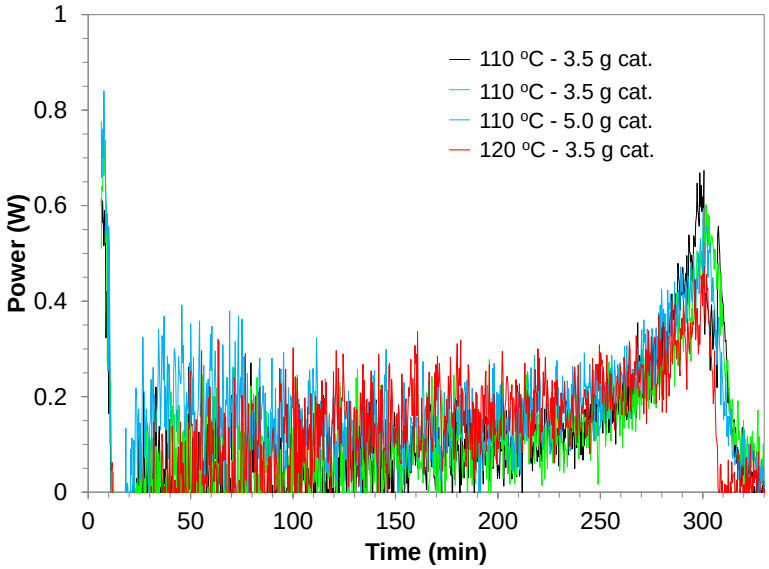

Figure 42. Averaged H_2O_2 decomposition power for the *N*-oxidation at different temperatures and amounts of catalyst

4.1.2 Study of H_2O_2 Accumulation and Dosing Rate Effects

In this section, the effect of H_2O_2 accumulation and the effect of different dosing rates have been studied in two different measurements. Additionally, the *N*-oxidation of 2MP at 125 ^oC is shown here, separately from the previous ones at 110 ^oC and 120 ^oC because the dosing in this measurement was done in steps and the calculation methodology was different than followed in the measurements presented in the previous section. In this particular measurement at 125 ^oC, in order to dose the stoichiometric amount of hydrogen peroxide without reaching the maximum safe operating pressure of 400 kPa, two dosing steps were performed with venting of the reactor in between. More specifically, the measurement was performed as follows: 150 g of 2MP, 100 g of water and 3.5 g of catalyst were put in the reactor and the system was heated to 80 ^oC where it was sealed. The mixture was then heated to 125 ^oC and after the appropriate calibrations; 60 g of 35 % H_2O_2 solution were dosed at a rate of 0.52 g min^{-1}. When the pressure of the system reached its maximum allowed value, dosing was interrupted and the reactor temperature was allowed to stabilize. The reactor was then vented and the measurement resumed by heating to 125 ^oC where dosing of 75 additional g of 35 % H_2O_2 solution was performed. After dosing, the mixture was left to react for an additional 60 min, after which the calibrations were performed, and finally followed by the cooling of the reactor. It is worth mentioning here that, for this measurement, instead of dosing the stoichiometric amount of H_2O_2, i.e. 1.61 moles, only 1.34 moles, were dosed.

To compare the different dosing steps when different amounts and rates were employed, a dimensionless time, t*, was defined as:

$$t^* = \frac{t - t_i}{t_f - t_i} \tag{32}$$

where

- t is any time in the dosing period
- t_i is the initial time of the dosing period
- t_f is the final time of the stir-out period considered in the calculation

Figure 43 shows the pressure increase for the two dosing steps during the *N*-oxidation of 2MP at 125 ^{o}C and the last 30 min (t* > 0.8) correspond to the stir-out period. For both cases, a similar pressure increase of approximately 110 kPa was obtained. The pressure increase was almost linear except for the first min of the dosing where the system was unstable. This linear change indicates that reaction rate is controlled by dosing. At the same time, this linear change of pressure can be predominantly caused by the increase of the mixture vapor pressure due to the change in its composition. However, in the absence of any reliable vapor pressure data, this is basically a speculation.

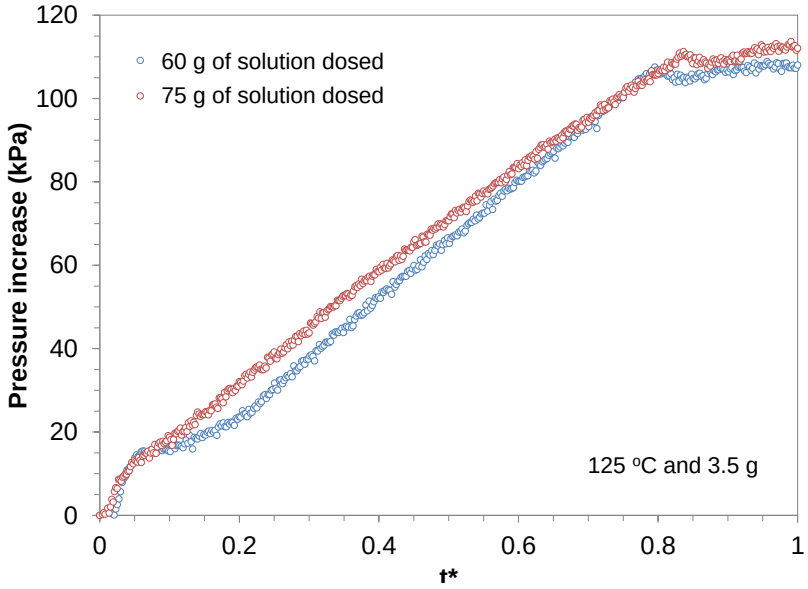

Figure 43. Pressure increase for the two stages of dosing (and stir-out) during the *N*-oxidation of 2MP at 125 ^{o}C and 3.5 g of catalyst

An additional measurement was planned to test the effect of H_2O_2 accumulation. The measurement was performed at 110 ^{o}C and employed 150 g of 2MP, 100 g of water, and 3.5 g of catalyst with dosing of 35 % H_2O_2 solution in two steps (62.4 g of solution in the first step and 93.4 g of solution in the second step) and a stabilization period of 60 min between dosing steps. The calibrations were performed before the first dosing step and after the second dosing step. Figure 44 shows the pressure increase during the two

dosing steps which corresponded to 12 kPa for the first dosing step and 72 kPa for the second dosing step. As Figure 44 shows, the pressure increase for the first step was slow and almost linear indicating, as in the previous measurement, that the reaction is control by dosing and that the change in pressure may be exclusively due to the change on the vapor pressure of the system. For the second step, the pressure increase was linear until t* = 0.6 where the increase became rapid and significant. This pressure difference between the two dosing steps demonstrates that the different pressure factors (among those, the production of oxygen) have a higher contribution at the end of dosing. Figure 44 makes evident that the accumulation of hydrogen peroxide, and therefore its decomposition, is much more significant at the end of dosing when the *N*-oxidation is not very competitive due to the reduction in the concentration of 2MP.

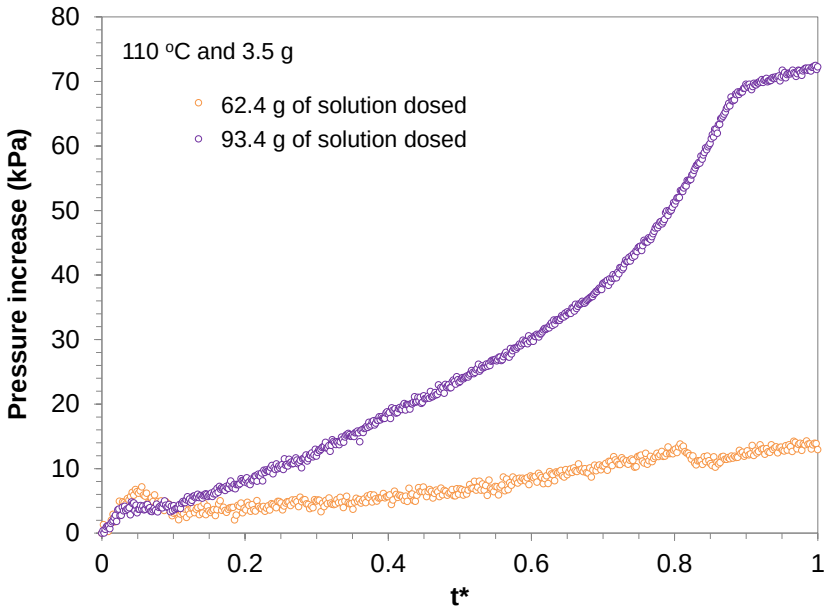

Figure 44. Pressure increase for the two stages of dosing (and stir-out) for the study of H_2O_2 accumulation during the *N*-oxidation of 2MP at 110 ^{o}C and 3.5 g of catalyst. The dosing rate was the same in both steps and equal to 0.52 g min^{-1}

To determine the effect of the dosing rate on the *N*-oxidation of 2MP, a measurement was performed at 110 ^{o}C and using 3.5 g of catalyst. The amounts of materials employed in the measurement are shown in Table 11. Calibrations were performed

before the first dosing step and after the sixth dosing step. The dosing steps started with 15.2 g of 35 % H_2O_2 solution at a rate of 0.26 g min^{-1}. After a 60-minute stabilization period, the second dosing stage started where 14.9 g of H_2O_2 solution were dosed at 0.52 g min^{-1}. The process continued with the dosing of 20.1 g of solution at 0.78 g min^{-1}, 24.9 g at 1.04 g min^{-1}, 40.0 g at 1.30 g min^{-1}, and 41.3 g at 0.78 g min^{-1} and with stabilization periods between the dosing steps. Figure 45 shows the pressure increase for the *N*-oxidation employing different dosing rates where the solid line represents the mass of H_2O_2 solution dosed and the dots represent the pressure increase for each dosing step. In order to compare the different pressure profiles, the dimensionless time, t*, was also used in this case.

Figure 45 shows that the pressure increase for the first four dosing steps, curves a) through d), is very noisy and lower than 10 kPa when employing dosing rates of 0.26, 0.52, 0.78, and 1.04 g min^{-1}. The level of noise is a clear indication that the pressure measurement cannot be accurately to a level of 10 kPa. For the last two dosing steps, the pressure increase reaches 20 and nearly 50 kPa and its values become more defined. This pressure increase, once again, shows higher decomposition at the end of the dosing period due to some accumulation of H_2O_2. For the last step, the dosing rate was the same as in the third dosing step (0.78 g min^{-1}), and even though the amount dosed was different, a higher pressure increase was obtained. Figure 45 also shows the dosing profiles in the solid line. For the curves a) through e), the pressure increase followed the dosing profile, within the noise of the measurement, which indicates that the pressure increase is mainly attributed to the reduction of the headspace from dosing. However, curve f), which corresponds to the last dosing step, shows a visible exponential increase for t* higher than 0.3 due to the decomposition of the accumulated H_2O_2.

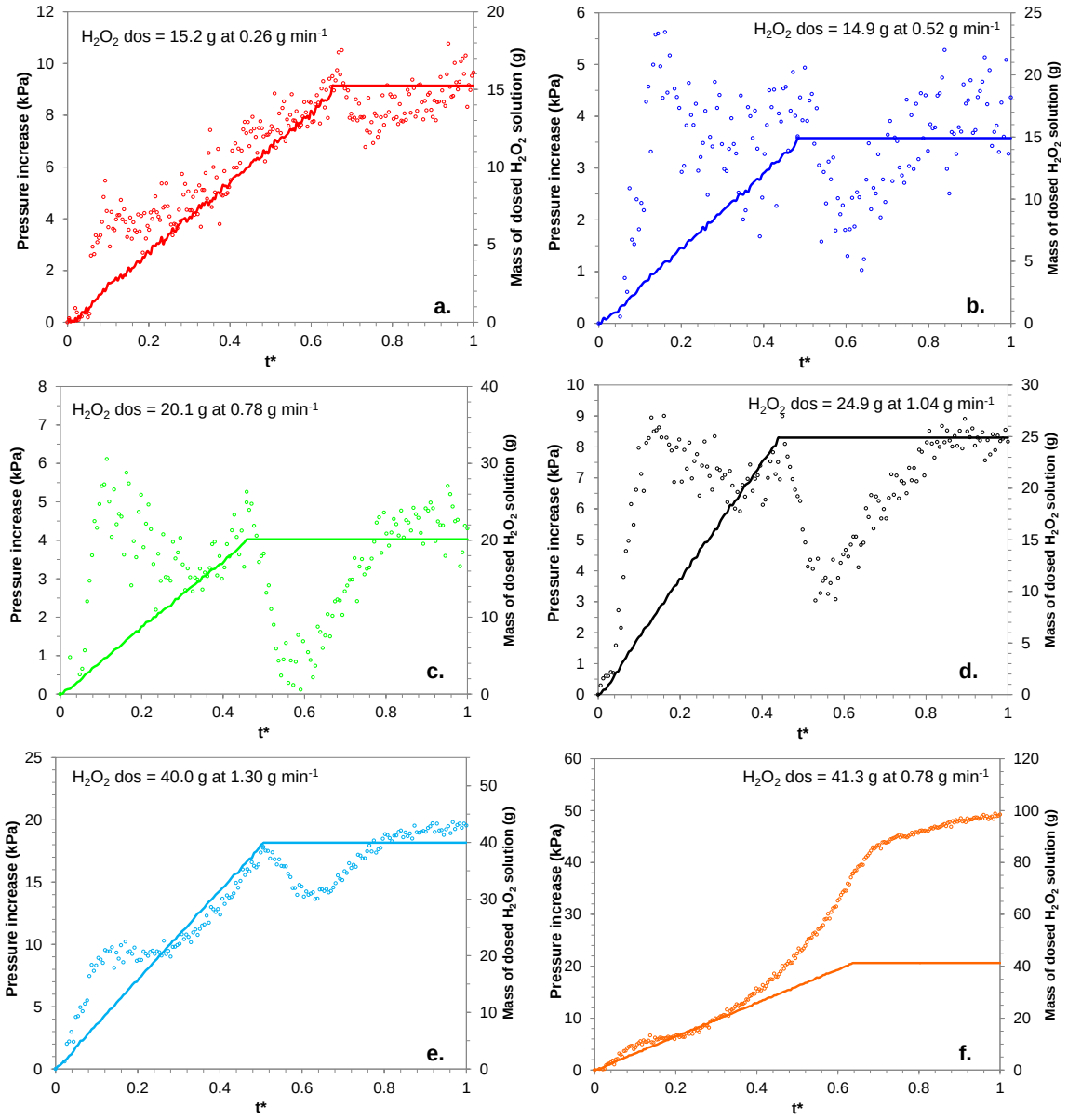

Figure 45. Pressure increase during the *N*-oxidation of 2MP at 110 ^{o}C and 3.5 g of catalyst using different dosing rates. **a)** dosing of 15.2 g at 0.26 g min^{-1}; **b)** dosing of 14.9 g at 0.52 g min^{-1}; **c)** dosing of 20.1 g at 0.78 g min^{-1}; **d)** dosing of 24.9 g at 1.04 g min^{-1}; **e)** dosing of 40.0 g at 1.30 g min^{-1}; and **f)** dosing of 41.3 g at 0.78 g min^{-1}. The dots represent the pressure increase, while the solid line represents the mass of H_2O_2 solution dosed in each step

The total amount of oxygen produced from the H_2O_2 decomposition for the three measurements described in this part is shown in Table 15. From these values, the conversion of 2MP was estimated and it is also shown in the table. For the first two measurements at 110 ^oC and 3.5 g of catalyst, the conversion was similar to the one shown in Table 12. For the test at 125 ^oC, the conversion was lower because in this case, the dosed hydrogen peroxide was lower than the stoichiometric amount.

Table 15. Dosing pressure, O_2 moles, and 2MP conversion for three isothermal tests studying different effects

T (^oC)	Catalyst (g)	Effect studied	[a]H_2O_2 (g)	P_{dos} (kPa)	N_{O_2} (mol)	2MP Conversion (%)
110	3.5	Accumulation	155.81	19.31	0.012	98.1
110	3.5	Dosing rate	156.42	19.46	0.013	98.3
125	3.5	Higher temperature	134.84	11.17	0.041	81.5

[a] H_2O_2 represents the solution of 35 % wt. H_2O_2

4.2 2,6-dimethylpyridine *N*-oxidation

The *N*-oxidation of 2,6-dimethylpyridine (26DMP) was studied using the isothermal calorimeter and the details of the measurements are shown in Table 16. The experimental procedure was similar to the one employed in 2MP where the reactor was loaded with the appropriate amounts of water, alkylpyridine and catalyst (shown in Table 16). The mixture was heated in a closed reactor up to 80 ^oC, the reactor was vented and then closed hermetically. The mixture was subsequently heated to the desired process temperature where, following the appropriate calibration, dosing of a 35 % aqueous solution of H_2O_2 started. When pressure reached the highest allowable limit, the dosing was stopped and the mixture was allowed to reach a steady state to then vent the reactor. The reactor was sealed and heated again to the desired temperature, where a new calibration was performed and dosing of hydrogen peroxide resumed again. The dosing-venting-calibration steps were repeated for all the dosing steps. When the dosing of the desired amount was completed, the mixture was left for a 60 min stir-out period and following the appropriate end-of-reaction calibration, the system

was cooled down and the measurement terminated. For all the measurements shown in this subsection, H_2O_2 was dosed in steps at a rate of 0.24 g min^{-1} in every step. Moreover, due to the vigorous H_2O_2 decomposition caused by the presence of two-liquid phases in the mixture, the quantity dosed in each measurement was smaller than the stoichiometrically required. Throughout the measurement a constant electric power of 14.8 W was supplied in the reactor by the calibration heater.

Table 16. Experimental details for the isothermal *N*-oxidation of 26DMP. The stirrer speed for the measurements was 250 rpm, the base power was 14.8 W, and the dosing rate was 0.24 g min^{-1}

T (^oC)	26DMP (g)	Water (g)	Catalyst (g)	H_2O_2* (g)	Calibration power (W)	T_{amb} (^oC)
110	180	30.24	7	139.7	37.8	23.1
120	180	30.24	7	113.9	30.1	23.5

*H_2O_2 represents the amount of H_2O_2 solution (35 wt. % in H_2O)

The mixture of 26DMP and water forms a two-liquid-phase mixture (See Section 5) in a wide range of conditions, and therefore, the *N*-oxidation advances differently. As mentioned earlier, in two phase alkylpyridine/water mixtures the reaction occurs in the interface of the organic/aqueous phase, while the catalyst remains in the aqueous phase, where H_2O_2 is also found, thus accelerating its decomposition. In order to achieve a good mixing of two phases, different measurements were conducted using different conditions, e.g. different agitator speeds. However, the decomposition of hydrogen peroxide was always so vigorous that the pressure of the closed system rapidly reached its maximum safe operating pressure, and the reaction had to be interrupted for venting. This was an extremely copious and time consuming process and as such, the *N*-oxidation was not completed.

Figure 46 shows the pressure increase during the four different and subsequent dosing steps for the *N*-oxidation of 26DMP at 110 ^oC using 7 g of catalyst. As mentioned, venting was performed in between the steps. Therefore, the oxygen moles were estimated for each individual step and are shown in Table 17.

In each step shown in Figure 46, 35 g of H_2O_2 solution were dosed. The maximum pressure increase was obtained for the first dosing step, and it is probably caused by the transition from the homogeneous mixture at the initial conditions (x_{26DMP}=0.5) to the two-liquid phases when the solution of H_2O_2 was dosed into the system. A similar pressure increase, which was a linear function of time, was obtained for the remaining three dosing steps indicating a decomposition controlled by dosing. The pressure increase of the forth dosing step appears to be higher than that of dosing steps 2 and 3, which is not unlikely to happen given that, at that stage, the concentration of the alkylpyridine has substantially dropped resulting in a similar reduction in the rate of the *N*-oxidation. However, the pressure increase is not considered significant due to the error in the measurement of pressure.

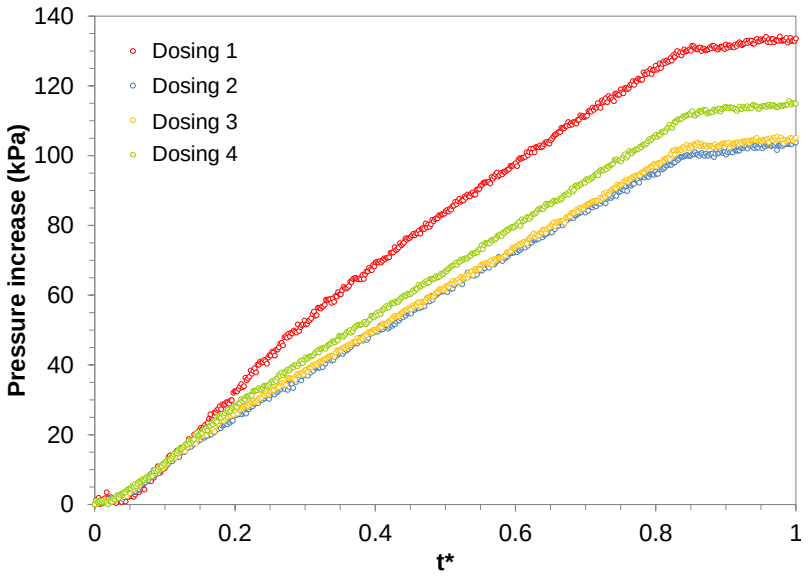

Figure 46. Pressure increase for the four different dosing steps during the 26DMP *N*-oxidation at 110 ^{o}C and 7 g of catalyst

Table 17 shows the pressure increase and the moles of oxygen produced in each dosing step. The production of oxygen was similar in each step but the first one. A total of 0.18 moles of H_2O_2 decomposed in this case, which left H_2O_2 available for a 2MP conversion of approximately 75 %. In addition to the H_2O_2 decomposition, this low

conversion was obtained because less than the stoichiometric amount of H_2O_2 was employed in the measurement. From the dosed H_2O_2, approximately 87 % was employed in the *N*-oxidation.

Table 17. Moles of oxygen produced in each dosing step during the *N*-oxidation of 26DMP at 110 ^{o}C and 7 g of catalyst

	H_2O_2* (g)	P_i (kPa)	P_f (kPa)	ΔP	No_2
Dosing 1	34.7	171.9	303.7	131.8	0.029
Dosing 2	35.1	187.9	292.0	104.1	0.021
Dosing 3	34.9	184.3	289.2	104.9	0.020
Dosing 4	35.1	180.7	297.6	116.9	0.021

The pressure increase for the *N*-oxidation of 26DMP at 120 ^{o}C and 7 g of catalyst is shown in Figure 47. In this case, five dosing steps were performed (the quantities added in each step are shown in Table 18). For the same reasons as in the case of the aforementioned measurement, only 70 % of the stoichiometrically required H_2O_2 was added in the reactor. As seen in Figure 47, a similar linear pressure increase was obtained for all the dosing steps. Moreover, as Table 18 shows, a similar amount of oxygen was produced in each step. As in the 26DMP *N*-oxidation at 110 ^{o}C, the total amount of H_2O_2 decomposed was around 0.18 moles. However, the conversion of 26DMP in this case was of 59 % because less H_2O_2 was dosed. From the dosed H_2O_2, approximately 85 % was used in the *N*-oxidation.

Figure 46 and Figure 47 show that the pressure increase in one dosing step during the 26DMP *N*-oxidation was almost the same as the pressure increase for the total dosing period during the 2MP *N*-oxidation, Figure 37. Similarly, the oxygen produced in one step during the 26DMP *N*-oxidation is equivalent to the amount of oxygen produced during the 2MP *N*-oxidation. The comparison between the 2MP *N*-oxidation performed in single phase with the 26DMP *N*-oxidation performed in two-liquid phases demonstrates that the presence of the phase separation plays, as expected, a preponderant role on the efficiency of the reaction reducing the selectivity of the *N*-oxidation reaction and favoring the decomposition of hydrogen peroxide.

Table 18. Pressure increase and moles of oxygen for each dosing step during the *N*-oxidation of 26DMP at 120 ^{o}C and 7 g of catalyst

	H_2O_2* (g)	P_i (kPa)	P_f (kPa)	ΔP	No_2
Dosing 1	26.1	224.2	308.5	84.4	0.0183
Dosing 2	20.4	226.4	309.6	83.2	0.0175
Dosing 3	23.1	223.3	312.7	89.4	0.0181
Dosing 4	21.9	223.6	316.1	92.5	0.0180
Dosing 5	22.1	220.8	315.9	95.1	0.0178

*H_2O_2 represents the solution of 35 wt. %H_2O_2

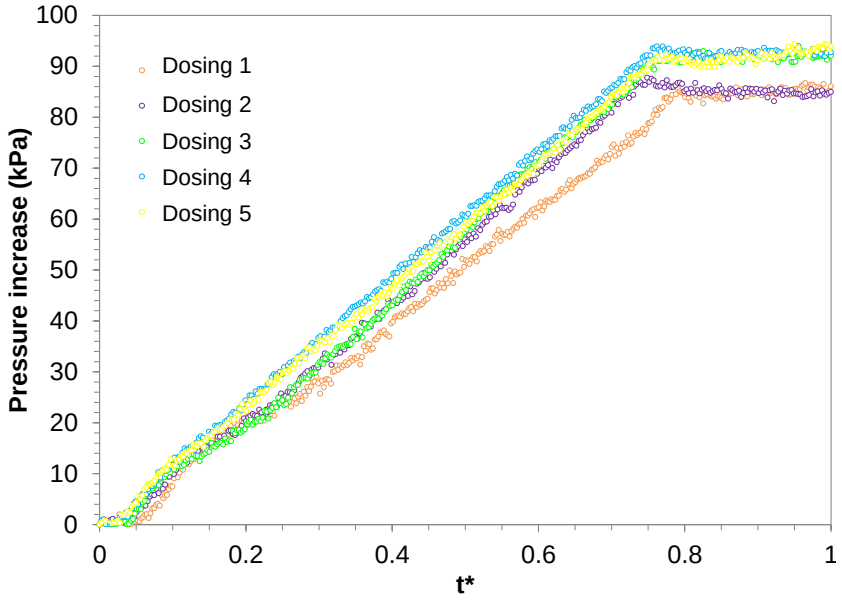

Figure 47. Pressure increase in the different dosing steps during the 26DMP *N*-oxidation at 120 ^{o}C and 7 g of catalyst

4.3 Summary

The *N*-oxidation of 2-methylpyridine and 2,6-dimethylpyridine were studied in a closed system at temperatures in the range of 110 ^{o}C - 125 ^{o}C to evaluate if an increase in temperature and amount of catalyst favors the *N*-oxidation reaction over the decomposition of hydrogen peroxide. The following points summarize the findings from Section 4:

- The conversion of 2-methylpyridine obtained during the *N*-oxidation at different temperatures and amounts of catalyst using a stoichiometric quantity of H_2O_2, was above 98 % which indicates that at the conditions considered in this study, the reaction was more efficient than when performed at temperatures below 100 ^{o}C where over 50 % of H_2O_2 excess was used to obtain similar conversions. At the conditions employed in the present research, the undesired decomposition of hydrogen peroxide was very low and occurred at the latest stages of the reaction.

- The efficiency of the process in the range of temperatures and catalyst studied here was very high. Similarly, very low production of oxygen was obtained in all measurements. The accuracy of the measurement of the pressure and the calculation of the produced oxygen is not as high as required in order to identify any clear trends.

- The presence of two-liquid phases during the *N*-oxidation of 2,6-dimethylpyridine affects the advance of the reaction. Likewise, the phase separation promotes the decomposition of hydrogen peroxide thus producing more than five times more oxygen than during the 2-methylpyridine *N*-oxidation.

5. PHASE EQUILIBRIUM IN THE *N*-OXIDATION OF ALKYLPYRIDINES

Subsection 4.2 showed that the liquid-liquid phase separation had a dramatic effect on the *N*-oxidation of 2,6-dimethylpyridine. The presence of two-liquid phases represents efficiency issues as well as safety concerns due to the promotion of the decomposition of hydrogen peroxide. Likewise, other alkylpyridines, e.g. 3,5-dimethylpyridine [65], form a two-liquid phase mixture with water, and it could present a similar concern during the *N*-oxidation.

This section considers the potential reduction of the phase separation by adding a third component in the mixture. The liquid-liquid equilibrium (LLE) was studied using the Gibbs minimization method to determine the phase split and the UNIQUAC method to estimate the activity coefficients. Both the Gibbs minimization method and the UNIQUAC method have been outlined in Section 2. For the prediction of the phase diagrams, ASPEN Plus® and ASPEN Properties® were employed.

5.1 Experimental Liquid-Liquid Equilibrium for 26DMP/Water

The liquid-liquid phase diagram for a mixture of 2,6-dimethylpyridine (26DMP) and water is shown in Figure 48. This phase diagram is recognized by a closed loop which represents the region of temperatures and concentrations where two-liquid phases are present. Outside the loop, a homogenous solution is obtained. The bottom and the top parts of the two-phase loop, where the diagram becomes almost flat, are known as the lower and upper critical points, respectively.

The liquid-liquid equilibrium for 26DMP-water has been studied experimentally by several authors, Figure 48. Flaschner [66] studied the system 26DMP-water in a wide range of temperature. This work determined a phase separation loop between 45 ^{o}C and 163 ^{o}C and weight percentages of 26DMP between 10 % and 70 %. Andon and Cox evaluated the solubility of 26DMP in water determining a wider phase loop with a lower critical point of 34 ^{o}C and an upper critical point of 230.7 ^{o}C [67]. The values shown in Figure 48 are approximate values read from the figure presented in their work

[67]; while Cox and Herington [68] provided data points in the range between the lower critical point and 60.0 ^{o}C. Stephenson [65] studied different pyridine and piperidine/water system between 0 and 90 ^{o}C. For the system 26DMP-water, a lower critical point of 34 ^{o}C was determined. The data obtained by both, Stephenson [65] and Cox and Herington [68], are in good agreement with each other and with those of Andon and Cox [67].

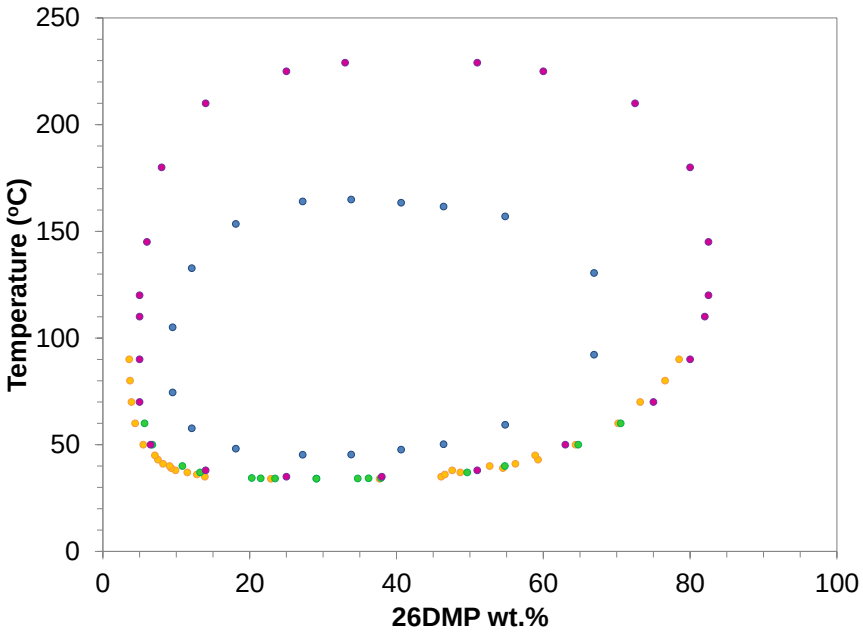

Figure 48. Experimental liquid-liquid phase diagram for 26DMP-water: Flaschner (blue)[66], Andon and Cox (purple) [67], Stephenson (Yellow)[65], Cox and Herington (Green)[68]

As seen in Figure 48, the phase diagram measured by Flaschner forms a smaller two-liquid phase loop, probably because of the lower accuracy of the measurements as Flaschner's work was published in 1909; while the data shown in Figure 48 are as recent as 1993. Flaschner also concluded that 3-methylpyridine forms a two-liquid phase mixture with water between 49 and 151 ^{o}C [66]. However, more recent works, including our group's unpublished research determined that 3-methylpyridine is miscible with water [65, 67].

Other thermodynamic properties for different pyridine derivatives-water systems such as vapor pressures, molar excess Gibbs energies, and heats of dilution have been previously evaluated at different conditions, e.g. temperatures [69-71]. Vapor–liquid equilibrium for 26DMP-water and water with other pyridine derivatives has been also considered in previous works [72]. Solid-liquid and liquid-liquid equilibrium for 26DMP-water as well as some thermodynamic properties are presented in [73]. Finally, Stephen and Stephen [74] and Sørensen and Arlt [75] present a collection of information for the miscibility of different pyridine derivatives systems.

5.2 Prediction of Liquid-Liquid Equilibrium

Because the information related to the liquid-liquid equilibrium (LLE) of different systems in the *N*-oxidation is scarce, while experimental testing is costly, time consuming, especially when different conditions are being investigated, and quite often, inconclusive or practically impossible to measure, it is imperative to be able to develop methodologies for the prediction of such properties so that the need for experimental measurements is minimalized. As such, the first step is to ensure that the predictive method can correctly represent experimental data, to then estimate the phase diagrams of systems where experimental data is not available.

The LLE for the different systems were estimated using the decanter model in ASPEN PLUS® V7.2. For the estimation of the phase split, the Gibbs minimization method was employed with UNIQUAC as the property method for the calculation of the activity coefficients (See Subsection 2.4).

5.2.1 System: 26DMP/Water

Because there is information available for the mixture 26DMP-water, this system has been used to determine the parameters that provide a good predictability of the LLE. The experimental data selected for comparison has been the one presented in the paper by Andon and Cox [67].

In Subsection 2.4, it was shown that the UNIQUAC method requires the parameters r and q which are parameters related to the structure of the molecules in the system and τ_{ij} which is a binary parameter that represents the interaction between two molecules. The binary parameters, τ_{ij}, are represented by the interaction energy as shown in equation (14), but typically, process simulator programs like ASPEN® represent the binary parameters by equation (33).

$$\tau_{ij} = exp\left(A_{ij} + \frac{B_{ij}}{T} + C_{ij} \cdot ln(T) + D_{ij} \cdot T + \frac{E_{ij}}{T^2}\right) \quad (33)$$

where

T is temperature

A_{ij}, B_{ij}, C_{ij}, D_{ij}, and E_{ij} are binary parameters

ASPEN Plus® contains the binary interaction parameters for the LLE of 26DMP-water using UNIQUAC method. However, these parameters contained in ASPEN were obtained from the data presented by Flaschner [66], see Subsection 5.1. As a result, new binary parameters for the UNIQUAC method, τ_{ij}, were estimated in this work using the data presented by Andon and Cox [67] and by Cox and Herington [68].

Table 19. Estimated UNIQUAC parameter for the LLE of 26DMP-water

UNIQUAC Parameters i = 26DMP j = Water	
	(K)
Aij	4.45
Aji	352.95
Bij	1801.29
Bji	-13533.83
Cij	-2.42
Cji	-57.74
Dij	0.0149
Dji	0.0646
RMSQ*= 89.94	

*RMSQ = Residual root mean square error

For the estimation of the binary parameters, the regression method incorporated in ASPEN Properties® V7.2 was employed. For the regression, the Maximum-likelihood objective function was used with a Britt-Luecke algorithm and the Deming method for the initialization. A convergence tolerance of 1.0 E-10 was specified and a LLE stability test was performed by the program after the regression was completed. The parameters determined by this method are included in Table 19.

The parameters in Table 19 were used in the prediction of the phase split using ASPEN Plus®. The predicted phase diagram and the comparison with the experimental data are shown in Figure 49.

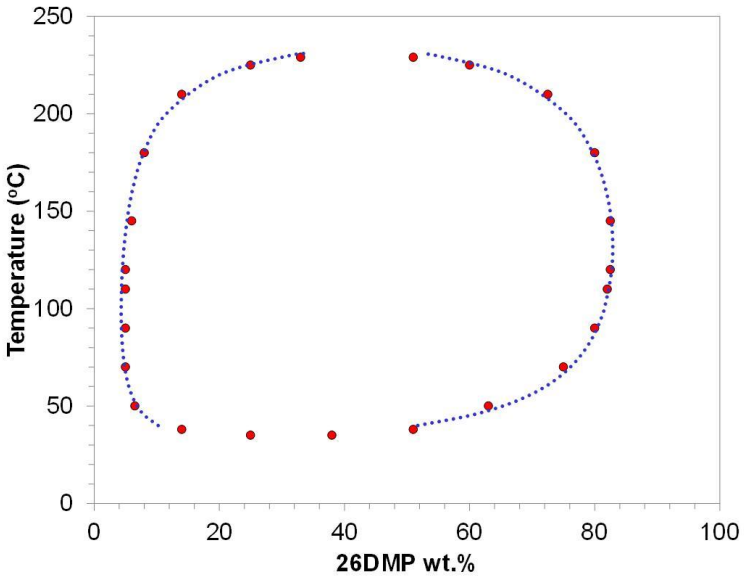

Figure 49. Comparison between the experimental (red dots) [67] and the estimated (blue dashed line) LLE for 26DMP-water using ASPEN®

As shown in Figure 49, the predicted data using ASPEN® (blue dashed line) is in good agreement with the experimental data (red dots). Therefore, the binary parameter included in Table 19 will be used for the LLE of the 26DMP-water system in the predictions presented in the next subsections.

5.2.2 System: 26DMP/Water/3MP

As an example of the LLE prediction for ternary systems, data for 26DMP-Water-3MP at 79 ^{o}C, also presented by Andon and Cox [67], was selected. In this case, the estimation of binary parameters for 26DMP-Water, 26DMP-3MP, and 3MP-water are required. For 3MP-Water, ASPEN® contains parameters obtained from Fleschner's work [66], but as mentioned before, more recent studies have determined complete miscibility of 3MP in water. As such, the parameters for 26DMP-3MP and 3MP-water were estimated using ASPEN Properties®. For the estimation, three different methods were employed to determine which provided the closet agreement with the experimental data: the UNIFAC method, the modified Dortmund UNIFAC method (UNIF-DMD), and the modified Lyngby UNIFAC method (UNIF-LBY) [76]. All the parameters were estimated in the range of temperature between 27 ^{o}C and 267 ^{o}C. After the binary parameters were obtained, the compositions at equilibrium were estimated using the decanter model in ASPEN Plus® with the Gibbs minimization method and the UNIQUAC property method. The results obtained for the different estimation methods are shown in Figure 50.

Figure 50 shows that the modified Dortmund UNIFAC method (UNIF-DMD) is in good agreement with the experimental data; while the other two methods, UNIFAC and UNIF-LBY, predict a much wider two-liquid phase region. The binary parameters, τ_{ij}, estimated by the UNIF-DMD method for the systems 3MP-Water and 26DMP-3MP are included in Table 20.

Table 20. Estimated binary parameters for the systems 3MP-Water and 26DMP-3MP

Component i	3MP	3MP
Component j	26DMP	Water
Temperature units	K	K
Aij	-0.79	-0.66
Aji	1.58	0.15
Bij	540.24	33.02
Bji	-935.82	-44.44
Tlower	300	300
Tupper	540	540

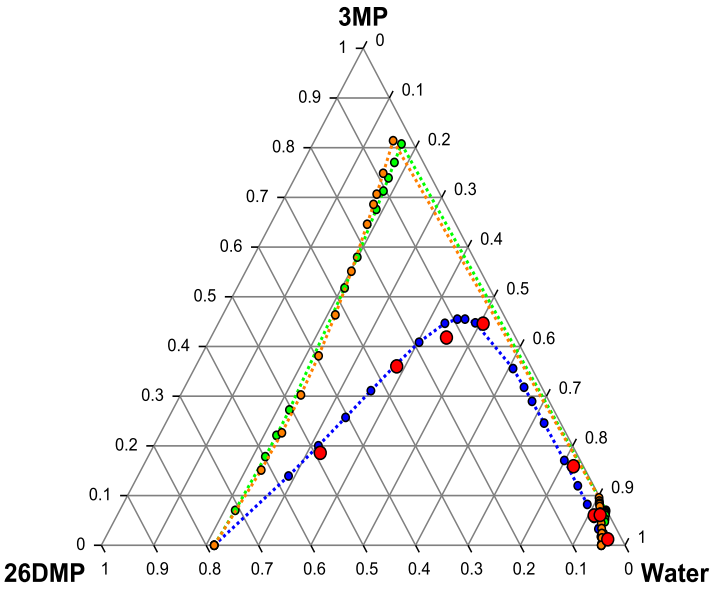

Figure 50. Comparison of experimental data (in red) with the prediction of the ternary diagram for 26DMP-3MP-Water at 79 ^{o}C using UNIFAC (in green), UNIF-DMD (in blue), and UNIF-LBY (in orange) methods. Diagram created using ProSim Ternary Diagram software. The concentrations are expressed in terms of mass fractions

5.2.3 System Containing Hydrogen Peroxide

Currently, no data is available in the open literature for the LLE of pyridine derivatives-hydrogen peroxide systems. Consequently, the effect of adding hydrogen peroxide on the phase separation of the 26DMP-water system was predicted using ASPEN® according to the procedure outlined above. For the generation of binary parameters for 26DMP-H_2O_2 and H_2O_2-water, two methods were employed: the UNIFAC method and the Lyngby modified UNIFAC method (UNIF-LBY). The binary parameters (τ_{ij}) determined for each method are included in Table 21 and the predicted liquid-liquid phase diagrams are shown in Figure 51.

Table 21. UNIQUAC Binary parameters for the system 26DMP-H_2O_2 and H_2O_2-H_2O using the UNIFAC and UNIF-LBY methods

	UNIFAC		UNIF-LBY	
Component i	**26DMP**	**H_2O**	**26DMP**	**H_2O**
Component j	**H_2O_2**	**H_2O_2**	**H_2O_2**	**H_2O_2**
Temperature units	K	K	K	K
Aij	-2.03	0.43	3.26	1.89
Aji	-0.21	0.18	4.13	1.82
Bij	-5.45	288.34	-1803.63	-691.56
Bji	-92.57	-878.39	-1634.35	-612.98
Tlower	300	300	300	300
Tupper	540	540	540	540

As shown in Figure 51, the two-phase region predicted by the UNIF-LBY method is wider than the one obtained with the UNIFAC method. For 26DMP mass fractions between 0.18 and 0.96, a homogeneous phase is reached when the mass fraction of hydrogen peroxide is larger than 0.25 for the data predicted by the UNIFAC method and 0.4 for the data predicted by the UNIF-LBY method.

To compare the effect of hydrogen peroxide with the effect of water, the liquid-liquid phase diagram for the system 26DMP-3MP-H_2O_2 was predicted at the same temperature as for the system 26DMP-3MP-water shown in Figure 50. The binary parameters for the pairs 26DMP-3MP and 3MP-H_2O_2 were estimated using the UNIFAC and UNIF-LBY methods in ASPEN Properties®, and are shown in Table 22. For the pair 26DMP-H_2O_2, the parameters can be found in Table 21. The predicted liquid-liquid phase diagrams are shown in Figure 52.

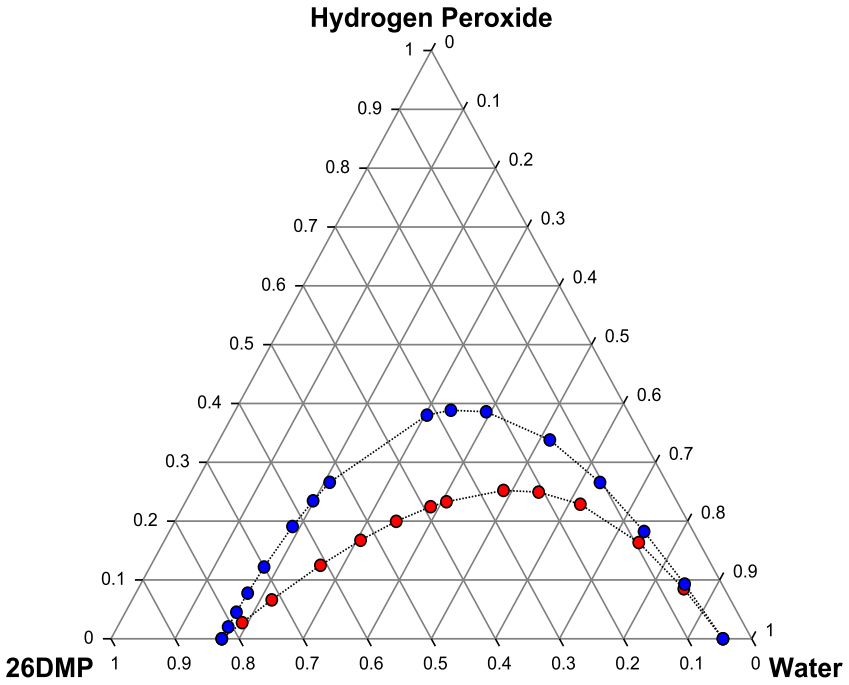

Figure 51. Predicted liquid-liquid phase diagram for the ternary system: 26DMP-Water-Hydrogen peroxide at 120 ^{o}C using the UNIFAC method (in red) and the UNIF-LBY method (in blue). Ternary diagram was created using ProSim Ternary Diagram Software. The concentrations are expressed in terms of mass fractions

Table 22. UNIQUAC Binary parameters for the system 26DMP-3MP and 3MP-H_2O_2 using the UNIFAC and UNIF-LBY methods

	UNIFAC		**UNIF-LBY**	
i	**26DMP**	**3MP**	**26DMP**	**3MP**
j	**3MP**	**H_2O_2**	**3MP**	**H_2O_2**
Units	K	K	K	K
Aij	0.36	-1.80	0.46	3.16
Aji	-0.40	-0.17	-0.52	2.97
Bij	-12.15	34.66	-60.92	-1621.41
Bji	15.44	-49.61	74.04	-1186.97
Tlower	300	300	300	300
Tupper	540	540	540	540

The two-liquid phase region predicted by both the UNIFAC and UNIF-LBY method is very similar. Figure 52 also shows that a homogeneous solution can be obtained at

limited conditions and mostly at high concentrations of 26DMP and high concentrations of 3MP. Additionally, when comparing with the LLE diagram for 26DMP-3MP-H_2O, it can be seen that a more extend two-phase region is obtained in this case, which can be also attributed to the accuracy of the methods employed for the prediction.

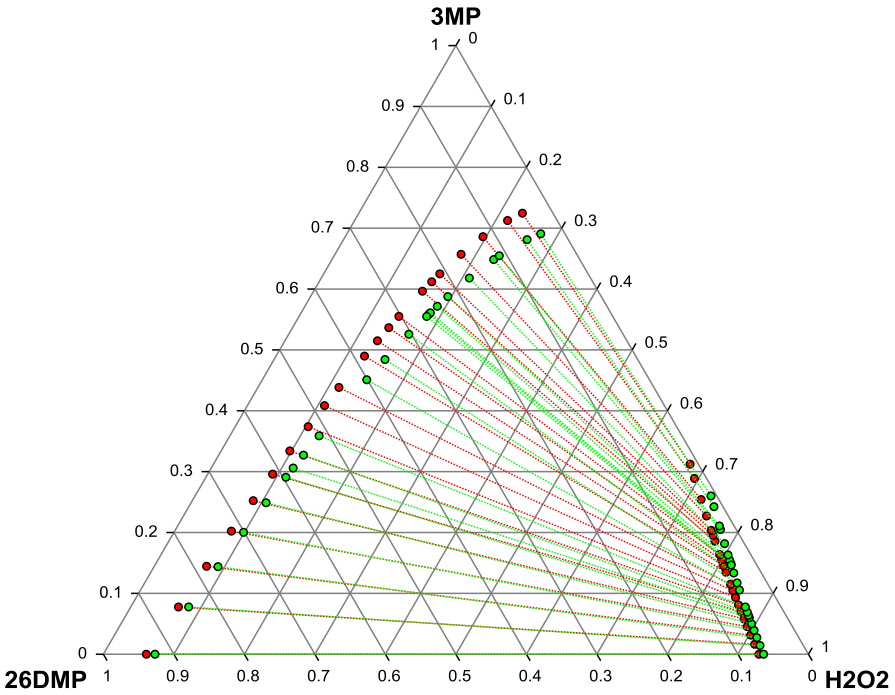

Figure 52. Predicted liquid-liquid phase diagram for the ternary system 26DMP-3MP-H_2O_2 at 79 ^{o}C using UNIFAC and UNIF-LBY methods. Ternary diagram was created using ProSim Ternary Diagram Software. The concentrations are expressed in terms of mass fractions

5.2.4 Systems Containing Acetic Acid

Andon and Cox presented the effect of different pyridine derivatives in the shape of the LLE of the 26DMP-water system [67]. Among their results, these authors demonstrated a reduction in the two-liquid region when adding 3MP in different proportions. Based on these findings, the addition of a third component in the system 26DMP-H_2O could increase the homogeneous region of the mixture, and as a consequence, the efficiency of the *N*-oxidation for alkylpyridines with limited miscibility in water can be addressed. A

limitation of adding a pyridine derivative to reduce the two phase loop is that this compound will react too and additional separation processes will have to follow the reaction.

In order to evaluate the effect that the addition of a third component has on the prediction of the equilibrium of the mixture of 26DMP with water, acetic acid was selected. This compound was chosen because acetic acid has been employed as a catalyst in alternative, less efficient methods for the *N*-oxidation of different alkylpyridines [4, 40]. In the absence of sufficient data for phosphotungstic acid, the effect that this homogeneous, less acidic catalyst had in the phase equilibrium of 2DMP-Water mixture has been studied. For the generation of the phase diagrams, the following two-step procedure, outlined in the previous sections, is employed:

Step 1 - Generation of binary parameters

The binary parameters for the UNIQUAC method were estimated using the Dortmund modified UNIFAC method in ASPEN Properties® and are included in Table 23. The binary parameters for 26DMP-water are included in Table 19.

Table 23. Estimated UNIQUAC binary parameters for the systems 26DMP-Acetic Acid and Acetic acid-water

Component i	26DMP	Acetic Acid
Component j	Acetic Acid	Water
Temperature units	K	K
Aij	2.68	2.94
Aji	-4.38	-4.27
Bij	-734.31	-965.97
Bji	1156.71	1357.24
Tlower	300	300
Tupper	540	540

Step 2 - Generation of phase diagrams

ASPEN Plus® was employed to generate the temperature-concentration diagrams of the system 26DMP-water-acetic acid of solutions of different initial concentration. The liquid-liquid phase diagrams are shown in Figure 53, and the initial concentrations of the solutions are included in Table 24. The phase diagram has been plotted in terms of a binary mixture where water was considered as one component and a mixture of 26DMP and acetic acid has been assumed to be the second component.

As seen in Figure 53, the two-liquid-phase region is reduced as the mass fraction of acetic acid is increased in the initial solution. For a mixture without acetic acid, solution *a*, the phase diagram extends from approximately 34 ^{o}C to 230 ^{o}C. For solution *f* containing an acetic acid mass fraction of 0.27, the temperature range is reduced, extending from approximately 60 ^{o}C to just above 120 ^{o}C.

Table 24. Initial concentrations for the generation of phase diagrams for a mixture of 26DMP, water, and acetic acid

	26DMP	**Acetic Acid**	**Water**
Solution a	0.50	0.00	0.50
Solution b	0.40	0.05	0.55
Solution c	0.40	0.10	0.50
Solution d	0.40	0.20	0.40
Solution e	0.25	0.25	0.50
Solution f	0.25	0.27	0.48

The region in yellow in Figure 54 represents the area where two liquid phases are present in a mixture of 26DMP-water-acetic acid at 120 ^{o}C. The dashed lines represent the tie-lines at 120 ^{o}C for the solutions *b* through *f* in Table 24. Solution *a* does not contain acetic acid, and therefore, falls over the line 26DMP-water. If the dashed lines are projected over the line 26DMP-water, the points for 120 ^{o}C in Figure 53 are obtained. Similarly, if a perpendicular plane is considered at 120 ^{o}C in Figure 53, Figure

54 can be obtained. Figure 54 also shows that a homogeneous solution can be found for acetic acid mass fractions above 0.3.

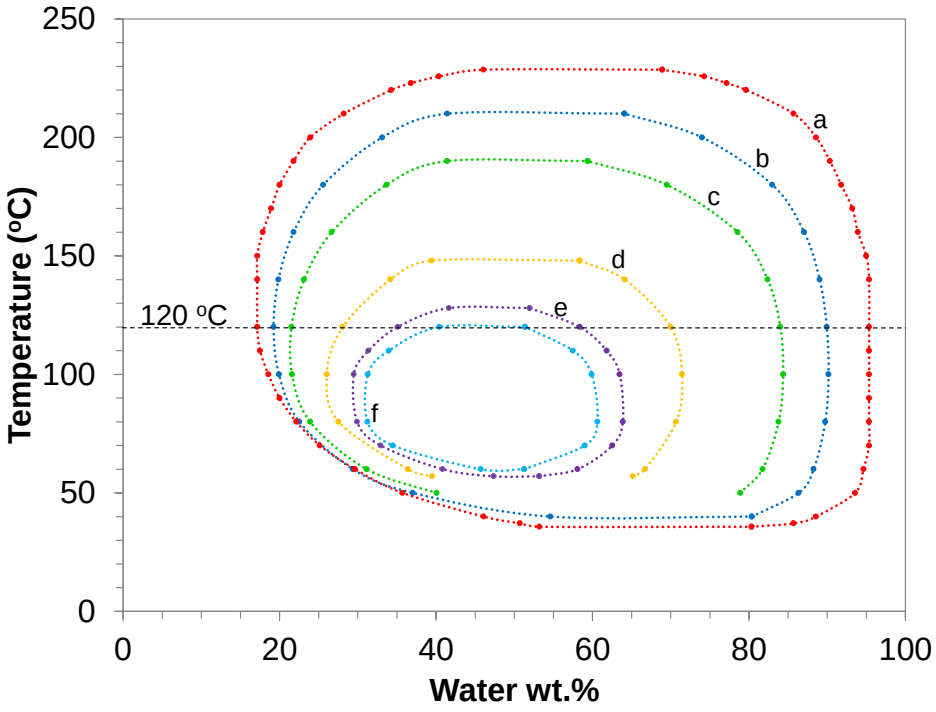

Figure 53. Liquid-liquid phase diagram in terms of water wt. % for a mixture of 26DMP, water, and acetic acid at different initial concentrations. *a* through *f* indicate solutions with different initial concentrations (See Table 24)

Figure 55 illustrates the effect of temperature on the liquid-liquid phase separation in a ternary diagram. The two-liquid phase region was plotted at temperatures between 60 °C and 140 °C using the same initial concentration. For 60 °C, this region was reduced, but in general, the two-liquid phase region did not change significantly within this temperature range.

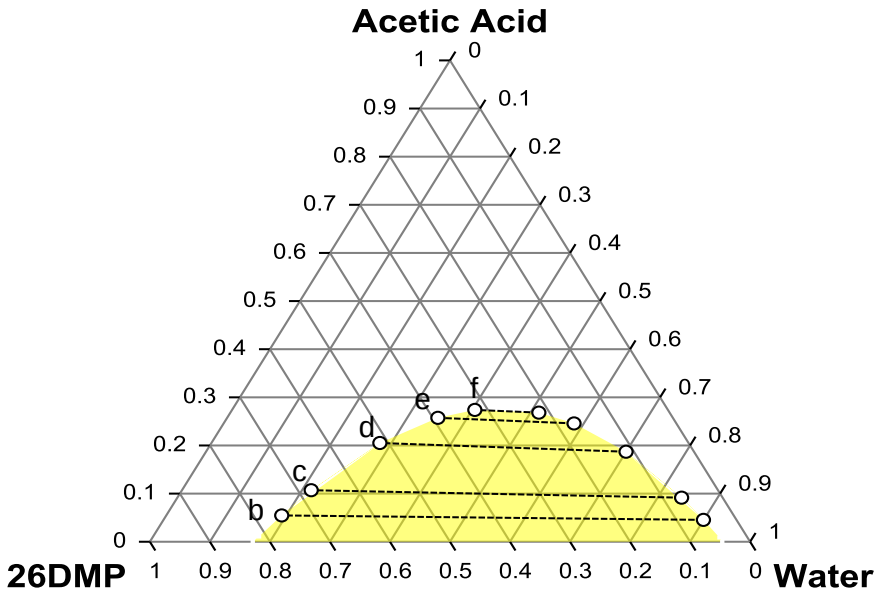

Figure 54. Predicted ternary liquid-liquid phase diagram for a mixture of 26DMP, water, and acetic acid at 120 ^{o}C. Ternary diagram was created using ProSim Ternary Diagram Software. The concentrations are expressed in terms of mass fractions

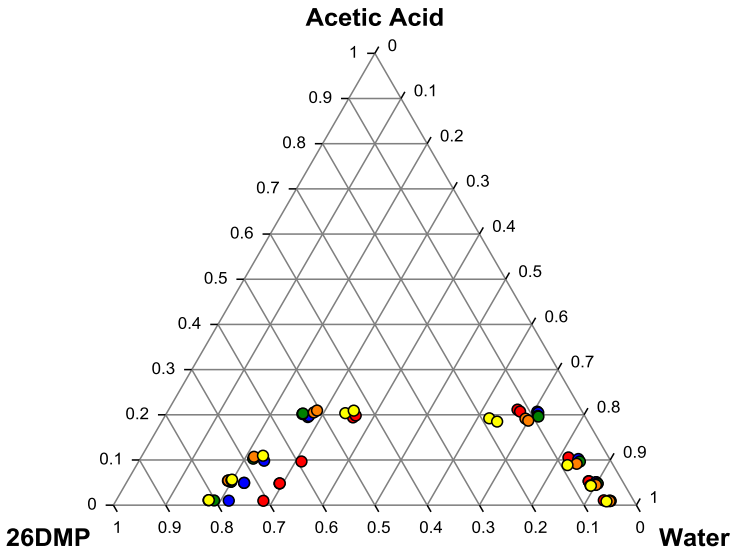

Figure 55. Predicted ternary phase diagram for 26DMP-water-acetic acid at different temperatures: 60 ^{o}C (red), 80 ^{o}C (blue), 100 ^{o}C (Green), 120 ^{o}C (Orange), and 140 ^{o}C (Yellow). Ternary diagram was created using ProSim Ternary Diagram Software. The concentrations are expressed in terms of mass fractions

5.3 Summary

This section presented the liquid-liquid equilibrium of the 2,6-dimethylpyridine-water system as well as the effect of adding a third component on the phase separation. The phase diagrams were predicted using ASPEN Properties® and ASPEN Plus® to explore the conditions that reduce the phase separation. A good agreement between the experimental data from other works and the estimated phase diagrams was determined. Other phase diagrams were no data is available in the literature were predicted. From the predicted ternary systems, a homogeneous phase was obtained for mass fractions above 0.3 of components such as hydrogen peroxide, acetic acid, and 3-methylpyridine. In general, the addition of a third component in the mixture is an alternative to reduce the presence of two phases; however, the third component should not form byproducts with the reactants. Moreover, the effect of such component on the runaway behavior and the cost of separation posterior to the reaction should be taken into account.

6. CONCLUSIONS AND FUTURE WORK

The present work was related to the study of alternatives to develop safer and more efficient processes in the industry. For illustration, the *N*-oxidation of alkylpyridines, reaction employed in the pharmaceutical industry, was used. Safety-wise, this reaction is of interest due to the combination of different hazards related to the flammability of alkylpyridines and the decomposition of hydrogen peroxide. Additionally, thermodynamics have a dramatic effect on the *N*-oxidation reaction for some of the alkylpyridine members with limited miscibility in water. The objective of this work was to study the *N*-oxidation of alkylpyridines to determine alternatives that can lead to a safer and more efficient reaction. A summary of the findings as well as a list of recommendations to continue this research in the future are included in the next two subsections.

6.1 Conclusions

The key finding of this research is that conditions were identified to perform the *N*-oxidation of alkylpyridines in an inherently safer way by reducing the decomposition of hydrogen peroxide (Subsection 6.1.1). Those conditions also coincide with an increase in the efficiency of the reaction where the consumption of hydrogen peroxide in the synthesis reaction is promoted without requiring an excess to obtain high conversions. The detailed analysis of the process to determine these conditions also allowed the identification of specific reactive hazards associated with a potential reaction runaway and the evaluation of the factors which can affect their evolution (Subsection 6.1.2).

6.1.1 Conditions for a Safer and More Efficient N-oxidation Reaction

Three alternatives for a safer and more efficiency *N*-oxidation of alkylpyridines were considered in this work and are summarized in Table 25. Along with these alternatives, additional safety issues that must be considered when implementing them were identified and are also shown in the table.

Table 25. Summary of the conditions considered in this work to increase efficiency and safety of the *N*-oxidation reaction and the safety considerations associated with each condition

Conditions to increase efficiency/safety		Safety considerations
Reduce H_2O_2 decomposition in 2-MP *N*-oxidation	Increase temperature	Excessive increase can induce the decomposition of the product. Reaction occurs in a closed system.
	Increase amount of catalyst	Excessive increase can induce the decomposition of the product. In runaway and if there is H_2O_2 accumulation: ▪ H_2O_2 decomposition onset decreases ▪ H_2O_2 decomposition can promote product decomposition
Identify homogeneous conditions in 26-DMP *N*-oxidation	Add a third component	Evaluate effect on *N*-oxidation and runway behavior

To reduce the decomposition of hydrogen peroxide during the *N*-oxidation of 2-methylpyridine (2MP), two conditions were considered: to increase temperature and to increase the amount of catalyst. The results from performing the *N*-oxidation in the range of 110-120 ^{o}C using an isothermal calorimeter to study both conditions showed that 2MP conversions above 98 % were obtained with stoichiometric quantities of H_2O_2, thus demonstrating an increase in the efficiency. Regarding the safety considerations, the findings included in Subsection 3.1 showed that increasing the temperature of the system above 180 ^{o}C can lead to the decomposition of 2-methylpyridine *N*-oxide, the product of the *N*-oxidation; while increased amounts of catalyst can promote the decomposition of the product, especially if H_2O_2 is present, and can lower the onset temperature for the decomposition of hydrogen peroxide (Subsection 3.2). Additionally, the operation at temperatures above the mixture normal bubble point (~100 ^{o}C) is possible, only if the reaction is performed in a closed system, which could represent an additional hazard if oxygen was produced from the decomposition of hydrogen peroxide in the flammable alkylpyridines environment. However, at temperatures between 110 ^{o}C

and 120 ^{o}C and using the normal quantity of catalyst, H_2O_2 decomposition is practically eliminated and no excess of H_2O_2 is required (Section 4).

For higher order alkylpyridines, phase equilibrium studies are required prior to any practical design. Such studies primarily aim at the identification of the conditions where homogeneous mixtures can exist. In the present study a very successful model was developed for mixtures of 2,6-dimethylpyridine/water which incorporated the addition of a third compound of known properties. More precisely, the addition of acetic acid in a 2,6-dimethylpyridine-water system was studied and it showed a reduction in the two-liquid phase loop. Calorimetric measurements were also successfully employed for the development of the phase equilibrium of 2,6-dimethylpyridine/water mixtures. However, further studies are necessary to precede any industrial design because, as the calorimetric studies have demonstrated, the *N*-oxidation of alkylpyridines in a two-phase mixture is extremely dangerous.

The applicability in the industry of the conditions listed in Table 25 is based upon the appropriate scale-up of the process as well as further evaluation of potential additional hazards no identified in the laboratory scale. The application needs to also consider the design variables to determine if the equipment can withstand the temperatures and pressures attainable during the worst case scenario and what additional utilities or instrumentation should be available.

In general, this research has provided a methodology to consider alternatives that develop a safer *N*-oxidation of alkylpyridines while considering the efficiency of the reaction too. The methodology combined different calorimetric techniques and highlighted the importance of considering the thermodynamics of the process because it can have a significant effect on process safety and efficiency. Moreover, while this research focused on the *N*-oxidation of alkylpyridines, a similar approach can be considered for other chemical reactions with similar safety concerns by evaluating the following points for the runaway behavior:

- Stability of reactants and products

- Effect of temperature and catalyst on the stability
- Decomposition products and their effects on the main reaction
- Synergistic effects between the decomposition reactions

Additionally, any alternative considered to increase the efficiency of certain process should be thoroughly evaluated because, as shown in Table 25, it can add or eliminate safety issues. Potential thermodynamic effects are also of importance. Industrial processes require the identification of properties of the chemicals that are used, especially those related to phase equilibrium because the presence of coexisting phases is a determining step in the design and performance of the equipment.

6.1.2 Additional Hazards in the N-oxidation of Alkylpyridines

The thorough study of the *N*-oxidation of alkylpyridines at different conditions to determine alternatives for a safer and more efficient reaction allowed the identification of some hazardous conditions that could present during the *N*-oxidation reaction. Following the findings in this research, Table 26 shows all the identified hazards. Three key points where included in the list presented in Section 1. One of the points is related to the alkylpyridine *N*-oxide, the product of the *N*-oxidation, which can decompose at temperatures above 200 ^{o}C producing non-condensable gases. This point is important to be examined, so as to ensure that a potential runaway of the synthesis reaction will not result in decomposition of the product, because the additional temperature and pressure rise caused by the product decomposition can worsen the runaway consequences. The other two points are related to the conditions of the system when the temperature and the amount of catalyst are increased. As mentioned in Section 3, both conditions can promote the decomposition of the product, but as mentioned in the previous subsection, when applied in moderation can be used as alternative to favor the *N*-oxidation reaction. Moreover, an excessive increase in the amount of catalyst can lower the "onset" temperature of the H_2O_2 decomposition; which means an earlier runaway; however, the application of alternatives that reduce the H_2O_2 decomposition would represent a reduction in the potential for a runaway. Thus, temperature and catalyst, in the proper dose, make the process safer and avert danger of a perilous

runaway, but in excess they can bring disaster. As reported in the last section, further research on this topic is proposed.

The last two factors in Table 26, temperature and catalyst, are very interesting as they are the factors which can guarantee the inherent safety of the process if the reactor is appropriately designed. In case of a reaction runaway due to a cooling malfunction, in a closed system, the temperature of the system will rise and the selectivity towards the *N*-oxidation will increase, thus while alkylpyridine is present it will be consuming practically all dosed H_2O_2. If reaction is performed at an adequately high temperature, no excess of H_2O_2 is necessary to be used, thus the danger originating from the decomposition of H_2O_2 is eliminated even in the case of the dosing pump malfunction. If on the other hand, a gas leak starts, the system temperature will drop to its bubble point and the heat generated by the system will be consumed in evaporation of the reacting mixture. The possibility of an agitator failure has not been assessed, but any potential H_2O_2 decomposition producing O_2 results in sufficient agitation due to O_2 bubbling, thus partially mitigating the effects of the stirrer failure.

Table 26. Updated list of hazards related to the *N*-oxidation of alkylpyridines

Hazards	
Alkylpyridines	▪ Flammable
Hydrogen peroxide	▪ Reactive and Unstable ▪ Decomposes at “low” temperature ▪ Produces heat upon decomposition ▪ Oxygen enrichment ▪ Over-pressurization
Alkylpyridine *N*-oxide	▪ Can decompose at temperatures around/above 200 ^{o}C ▪ Decomposition produces non-condensable gases
Hazardous conditions	
Phase separation	▪ Promotes H_2O_2 decomposition
Excessive temperature	▪ Product decomposition
Excessive increase in catalyst	▪ Promotes product decomposition ▪ Lowers H_2O_2 decomposition "onset"

6.2 Recommendations

Additional possibilities exist to continue this research. The following are recommendations for potential future work that can be developed in the study of the *N*-oxidation of alkylpyridines.

6.2.1 Calorimetric Studies

For the study of the *N*-oxidation runaway, different possibilities are present because of the instability and sensitivity of hydrogen peroxide. Studies can be conducted to determine the effect of contaminants. Moreover, additional work can be performed on the decomposition of 2-methylpyridine *N*-oxide using computational chemistry to define the decomposition pathways and intermediates. Furthermore, the study of the stability can be continued with other members of alkylpyridines and their *N*-oxides e.g. 2,6-dimethylpyridine.

During the isothermal studies of the *N*-oxidation of 2-methylpyridine, this research determined an increase in the conversion for the *N*-oxidation performed between 110 ^{o}C and 120 ^{o}C. However, a clear trend of the *N*-oxidation efficiency with temperature and catalyst could not be observed. Additionally, the study in a much wider range of conditions was limited by the operability limits of the equipment used. Therefore, additional experiments for the *N*-oxidation of other alkylpyridines can be conducted in a more significant interval of temperatures and amounts of catalyst to determine the effect of these parameters on the decomposition of hydrogen peroxide during the *N*-oxidation reaction. A more accurate determination of the oxygen produced during the H_2O_2 decomposition can be also implemented during the experiments to establish a clear effect of temperature and catalyst on this quantity. The isothermal study can be continued with other alkylpyridines such as 3-methylpyridine and 4- methylpyridine, dimethylpyridnes and collidines, but as mentioned before, to study the *N*-oxidation of alkylpyridines with limited solubility in water, the search of conditions of a homogeneous mixture is of key importance for the process efficiency and safety.

The potential of the development of a new calorimetric technique for the study of phase equilibrium is also worth investigating. The reasoning of such a proposal is justified by the following findings. One of the experiments conducted with 2,6-dimethylpyridine/ water involved the gradual addition of water into a solution with a 26DMP molar fraction of 0.26 to result in a solution with a 26DMP molar fraction equal to 0.1. Figure 56 shows the reactor and jacket temperatures just before and after dosing. At the temperature considered and at composition 0.26 of 26MP (two-liquid phases present), both temperatures shown in Figure 56 were unstable due to the heat evolved/absorbed by the solution as it was changing from homogeneous to heterogeneous while the reactor control system was trying to stabilize the mixture temperature (Section 5). After dosing, where the solution was close to the boundary between of the two-phase region but in the homogeneous region, the temperature changed smoothly and reached a constant value. Thus, temperature in an isothermal calorimeter could be used as a measurement of the liquid-liquid phase change. One more experiment was performed using PHITEC I, where a solution of 26DMP-water (26DMP molar fraction = 0.1) was heated from 25 ^{o}C to 40 ^{o}C at a heating rate of 1 ^{o}C min^{-1}. From the results of this test, a peak was observed at around 30 ^{o}C which is close to the temperature for the phase change (See Section 5), Figure 57. Previous works have mentioned the use of Calorimetry in the determination of phase equilibrium, mostly for solid materials employing using Differential Scanning Calorimetry and adiabatic Calorimetry [77, 78]. Additional studies can be performed to determine the conditions at which the liquid-liquid phase separation can be detected and to establish the accuracy of the method.

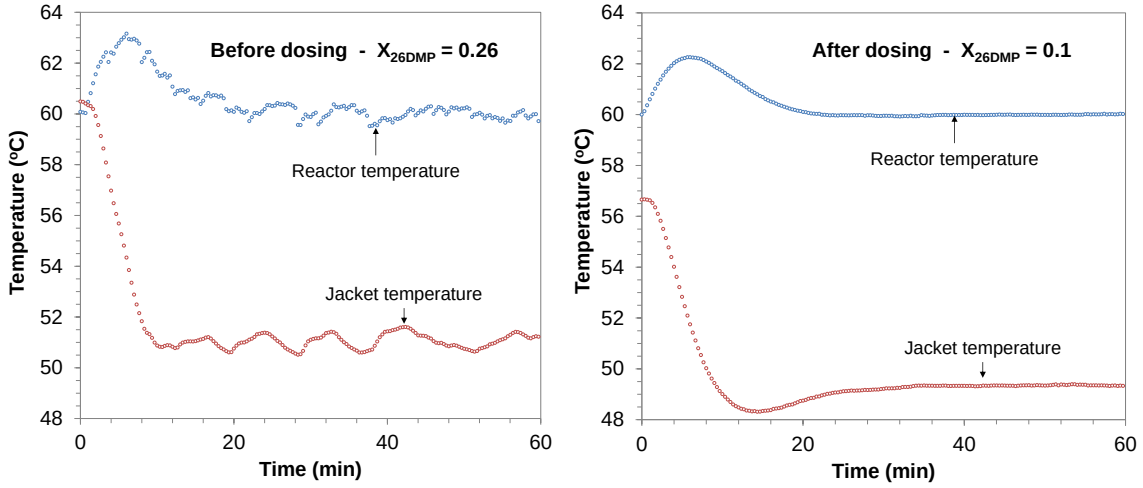

Figure 56. Reactor and jacket temperature before and after dosing for an experiment were water was dosed into a solution of 26DMP-water at 60 ^{o}C

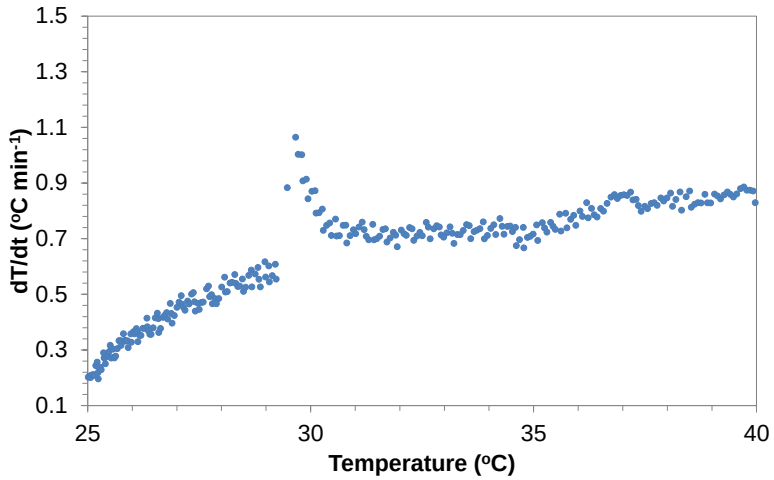

Figure 57. Detection of the phase change of a solution of 26DMP-water (x_{26DMP} = 0.1) during the heating at 1 ^{o}C min^{-1}

6.2.2 Thermodynamic Studies

Regarding the study of the liquid-liquid equilibrium of different binary and ternary systems in the *N*-oxidation, a commercial process simulator software was employed to predict the phase diagrams. This method provides an easy, rapid, and less costly study of the equilibrium under different conditions and it was suitable for the work presented

here since the change in the liquid-liquid loop when adding different compounds was being considered. However, experiments should be conducted to verify that the simulated conditions provide satisfactory results for both the thermodynamics of the system and the efficiency of the process. Reference [78] provides a complete compilation of different methods to measure the thermodynamics of the phase transition. Other methods to evaluate the liquid-liquid equilibrium can be found in the literature [79, 80].

For the *N*-oxidation of alkylpyridines where two-liquid phase can be distinguished, a change in the phase separation can be observed as the reaction advances until a homogeneous mixture is obtained by the end of a complete reaction. Thus, the production of alkylpyridine *N*-oxide reduces the presence of two-liquid phases. Studies on the change of the phase equilibrium of the reacting mixture can be performed experimentally or using the Gibbs minimization method. The Gibbs minimization method has incorporated, in recent years, chemical equilibrium into phase equilibrium to study the systems where both situations occur simultaneously [81-84]. A disadvantage of employing this method is the limited information available regarding alkylpyridine *N*-oxides.

Finally, as mentioned earlier, a challenge that this research encountered was the lack of data available in the literature related to the properties of alkylpyridine *N*-oxides. Therefore, there is an extensive opportunity for the study of these compounds. Regarding the study of the liquid-liquid equilibrium of the systems containing *N*-oxide, experimental work can be performed. Another alternative includes the generation of the binary parameters using computational chemistry [85-88].

REFERENCES

[1] A. Palomo-Coll, A process for the preparation of omeprazol, ES 2026761 (A6), in: European Patent Office, 1992.

[2] J. Sempere, R. Nomen, J.L. Rodriguez, M. Papadaki, Modelling of the reaction of N-oxidation of 2-methylpyridine using hydrogen peroxide and a complex metal catalyst, Chem. Eng. Process. 37 (1998) 33-46.

[3] Pyridine and pyridine derivatives. Kirk-Othmer Encyclopedia of Chemical Technology, 5th ed., John Wiley & Sons, Inc, New Jersey, 2007, Vol. 21, pp. 91-133.

[4] Pyridine and pyridine derivatives. Ullmann's Encyclopedia of Industrial Chemistry, 6th ed., Wiley-VCH Verlag GmbH & Co, Weinheim, Germany, 2005, Vol. 30, pp. 557-590.

[5] K. Weissermel, H.-J. Arpe, Industrial Organic Chemistry, 4th ed., Wiley-VCH GmbH & Co, Weinheim, Germany, 2003.

[6] Hydrogen Peroxide. Kirk-Othmer Encyclopedia of Chemical Technology, 5th ed., John Wiley & Sons, Inc., New Jersey, 2007, Vol. 14, pp. 35-78.

[7] Hydrogen Peroxide. Ullmann's Encyclopedia of Industrial Chemistry, 6th ed., Wiley-VCH Verlag GmbH & Co, Weinheim, Germany, 2007, Vol. 18, pp.393-428.

[8] O. Klais, Hydrogen Peroxide decomposition in the presence of organic material: a case study, Thermochim. Acta 225 (1993) 213-222.

[9] J. Mackenzie, Considerations for the safe design of processes using hydrogen peroxide and organics, Plant Oper. Prog. 10 (1991) 164-170.

[10] P.G. Urben (Ed.), Bretherick's Handbook of Reactive Chemical Hazards, Elsevier, Oxford, 2007, pp. 1692-1712.

[11] W.L. Wehrum, Case study of a hydrogen peroxide related deflagration in a wastewater treatment tank, Process Saf. Prog. 12 (1993) 199-202.

[12] J.P. Lacoursiere, An explosion caused by mixing incompatible liquids, Process Saf. Prog. 24 (2005) 115-119.

[13] M. Kumasaki, An explosion of a tank car carrying waste hydrogen peroxide, J. Loss Prev. Process Indust. 19 (2006) 307-311.

[14] I.V. Kozhevnikov, Advances in catalysis by heteropolyacids, Russ. Chem. Rev. 56 (1987) 1417-1443.

[15] L.C.W. Baker, D.C. Glick, Present general status of understanding of heteropoly electrolytes and a tracing of some major highlights in the history of their elucidation, Chem. Rev. 98 (1998) 3-49.

[16] M. Misono, I. Ono, G. Koyano, A. Aoshima, Heteropolyacids: versatile green catalyst usable in a variety of reaction media., Pure Appl. Chem. 72 (2000) 1305-1311.

[17] K.A. Campbell, M.J. Janik, R.J. Davis, M. Neurock, Ab Initio and microcalorimetric investigations of alkene adsorption on phosphotungstic acid, Langmuir. 21 (2005) 4738-4745.

[18] J.F. Keggin, The structure and formula of 12-phosphotungstic acid, Proc. Roy. Soc. Lond. 144 (1934) 75-100.

[19] I.V. Kozhevnikov, K.I. Matveev, Heteropolyacids in catalyst, Russ. Chem. Rev. 51 (1982) 1075-1088.

[20] A.K. Coker, Safety in chemical reaction engineering, in: Modeling of Chemical Kinetics and Reactor Design, Houston, 2001, pp. 910-1033.

[21] CSB, Hazard Investigation: Improving reactive hazard management, Report No. 2001-01-H, U.S. Chemical Safety and Hazard Investigation Board, October 2002.

[22] J.A. Barton, P.F. Nolan, Incidents in the chemical industry due to thermal-runaway chemical reactions, IChemE Symp.115 (1989) 3-18.

[23] B. Gielens, D. Bizzarri, C. Dobet, A. Germain, Manual for Identifying and Evaluating Thermal Runaway Reaction Hazards, Federal Ministry of Employment and Labour, Brussels, 2001.

[24] D.F. Leggett, Safe process development from reaction hazards testing, Thermochim. Acta, 367-368 (2001) 351-365.

[25] A.A. Aldeeb, W.J. Rogers, M.S. Mannan, Theoretical and experimental methods for the evaluation of reactive chemical hazards, Process Saf. Environ. Prot. 80 (2002) 141-149.

[26] T. Kletz, What you don't have, can't leak, Chem. Ind., 6 (1978) 287-292.

[27] R.W. Johnson, S.W. Rudy, S.D. Unwin, Essential Practices for Managing Chemical Reactivity Hazards, Center for Chemical Process Safety/AIChE, New York, 2003.

[28] R.E. Bollinger, D.G. Clark, A.M. Dowell, R.M. Ewbank, D.C. Hendershot, W.K. Lutz, S.I. Meszaros, D.E. Park, E.D. Wixom, Inherently Safer Chemical Processes: A Life Cycle Approach, 2nd ed., Center for Chemical Process Safety/AIChE, New Jersey, 2008.

[29] W.K. Lutz, Take chemistry and physics into consideration in all phases of chemical plant design, Process Saf. Prog. 14 (1995) 153-160.

[30] D.W. Mosley, A. Ness, D.C. Hendershot, Screen Reactive Chemical Hazards Early in Process Development, Chemical Engineering Progress, American Institute of Chemical Engineers (AIChE), November 2000, pp. 51-65.

[31] S.R. Saraf, W.J. Rogers, M.S. Mannan, Prediction of reactive hazards based on molecular structure, J. Hazard. Mater. A98 (2003) 15-29.

[32] M. Papadaki, R.J. Emery, E. Serra, R. Nomen, J. Sempere, Sensitivity analysis of the 2-methylpyridine N-oxidation kinetic model, Green Chem. 4 (2002) 199-205.

[33] M. Papadaki, V. Stoikou, D. Mantzavinos, J.L. Rodriguez Miranda, Towards improved reaction runaway studies: kinetics of the N-oxidation of 2-methylpyridine using heat-flow Calorimetry, Trans IChemE 80 (2002) 186-196.

[34] M. Papadaki, H.P. Nawada, Towards improved reaction runaway assesment methods I: simple calorimetric method of evaluation of heat transfer coefficient and reactor thermal mass, Int. J. Chem. React. Eng. 1 (2003) 1-12

[35] M. Papadaki, Use of reaction calorimetry in thermal risk assesment studies and safe design of batch reactions that can lead to a runaway: application on hydrogen peroxide, Top. Catal. 29 (2004) 207-213.

[36] M. Papadaki, J. Gao, Kinetic models of complex reaction systems, Comput. Chem. Eng. 29 (2005) 2449-2460.

[37] M. Papadaki, E. Marques-Domingo, J. Gao, T. Mahmud, Catalytic decomposition of hydrogen peroxide in the presence of alkylpyridines: runaway scenarios studies, J. Loss Prev. Process Indust. 18 (2005) 384-391.

[38] J. Gao, M. Papadaki, Global kinetic model: a case study on the N-oxidation of alkylpyridines, J. Hazard. Mater. 130 (2006) 141-147.

[39] M. Papadaki, H.P. Nawada, J. Gao, A. Fergusson-Rees, M. Smith, Isothermal calorimetry: impact of measurements error on heat of reaction and kinetic calculations, J. Hazard. Mater. 142 (2007) 705-712.

[40] E.N. Shaw, Pyridine N-oxides, in: E. Klingsberg (Ed.) Chemistry of Heterocyclic Compounds, Pyridine and its derivatives: Part II, Interscience Publishers Inc., New York, 1961, pp. 97-120.

[41] N.I. Ali-zade, Selective gas-phase oxidation of pyridine derivatives with hydrogen peroxide, Kinet. Catal. 47 (2006) 64-69.

[42] D.J. Robinson, P. McMorn, D. Bethell, P.C. Bulman-Page, C. Sly, F. King, F.E. Hancock, G.J. Hutchings, N-oxidation of pyridines by hydrogen peroxide in the presence of TS-1, Catal. Lett. 72 (2001) 233-234.

[43] K. Yamaguchi, T. Mizugaki, K. Ebitani, K. Kaneda, Heterogeneous N-oxidation of pyridines using a combined oxidant of hydrogen peroxide and nitriles catalysed by basic hydrotalcites, New J. Chem. 23 (1999) 799-801.

[44] NETZSCH, APTAC 264 Operating Manual, (2009).

[45] D.I. Townsend, J.C. Tou, Thermal hazard evaluation by an accelerating rate calorimeter, Thermochim. Acta 37 (1980) 1-30.

[46] N.P. Bansal, R.H. Doremus, Handbook of Glass Properties, Elsevier, London, 1986.

[47] Y. Sofyan, A.J. Ghajar, K.A.M. Gasem, Multiphase equilibrium calculations using Gibbs minimization techniques, Ind. Eng. Chem. Res. 42 (2003) 3786-3801.

[48] G.A. Iglesias-Silva, A. Bonilla-Petriciolet, P.T. Eubank, J.C. Holste, K.R. Hall, An algebraic method that includes Gibbs minimization for performing phase

equilibrium calculations for any number of components or phases, Fluid Phase Equilib. 210 (2003) 229-245.

[49] Y.S. Teh, G.P. Rangaiah, A study of equation-solving and Gibbs free energy minimization methods for phase equilibrium calculations, Trans IChemE 80 (2002) 745-759.

[50] J.M. Prausnitz, F.W. Tavares, Thermodynamic of fluid-phase equilibria for standard chemical engineering operations, AICHE J., 50 (2004) 739-761.

[51] Z.H.U. Yushan, X.U. Zhihong, A reliable method for liquid-liquid phase equilibrium calculation and global stability analysis, Chem. Eng. Commun. 176 (1999) 133-160.

[52] D.S. Abrams, J.M. Prausnitz, Statistical thermodynamics of liquid mixtures: a new expression for the excess Gibbs energy of partly or completely miscible systems, AICHE J. 21 (1975) 116-128.

[53] T.F. Anderson, J.M. Prausnitz, Application of the UNIQUAC equation to calculation of multicomponent phase equilibria: 1. Vapor-liquid equilibria, Ind. Eng. Chem. Process Des. Dev. 17 (1978) 552-561.

[54] T.F. Anderson, J.M. Prausnitz, Application of the UNIQUAC equation to calculation of multicomponent phase equilibria: 2. Liquid-liquid equilibria, Ind. Eng. Chem. Process Des. Dev. 17 (1978) 561-567.

[55] L. Saenz, V.H.C. Vazquez, L. Liu, W.J. Rogers, M.S. Mannan, M. Papadaki, 2-methylpyridine N-oxidation runaway studies, J. Loss Prev. Process Indust. 22 (2009) 839-843.

[56] L.R. Saenz, V.H. Carreto-Vazquez, W.J. Rogers, M. Papadaki, M.S. Mannan, Thermal decomposition of 2-methylpyridine N-oxide: effect of temperature and influence of phosphotungstic acid as the catalyst, Catal. Commun. 12 (2011) 1370-1373.

[57] J.H. Baxendale, Decomposition of hydrogen peroxide by catalyst in homogeneous aqueous solution, Adv. Catal. 4 (1952) 31-86.

[58] M. Eissen, A.Z.K. Hungerbuhler, The runaway scenario in the assessment of thermal safety: simple experimental access by means of the catalytic decomposition of hydrogen peroxide, J. Loss Prev. Process Indust. 16 (2003) 289-296.

[59] K.-T. Lu, C.-C. Yang, P.-C. Lin, The criteria of critical runaway and stable temperatures of catalytic decomposition of hydrogen peroxide in the presence of hydrochloric acid, J. Hazard. Mater. B135 (2006) 319-327.

[60] K.Y. Chen, C.M. Lin, C.M. Shu, C.S. Kao, An evaluation of thermokinetic parameters for hydrogen peroxide at various concentrations by DSC, J. Therm. Anal. Calorim. 85 (2006) 87-89.

[61] M.T. Phong, C.d.B. Aires, Experimental and theoretical analysis of a critical chemical reaction: decomposition of hydrogen peroxide, Sci. Technol. Dev. 11 (2008) 28-36.

[62] N. Frikha, E. Schaer, J.-L. Houzelot, Experimental study and modelling of thermal runaway: application to dichromate catalyzed hydrogen peroxide decomposition, Thermochim. Acta 449 (2006) 47-54.

[63] A. Hiroki, J.A. LaVerne, Decomposition of hydrogen peroxide at water: ceramic oxide interfaces, J. Phys. Chem. B 109 (2005) 3364-3370.

[64] Design Institute for Physical Properties, DIPPR Project 801: full version, Design Institute for Physical Property Research/AIChE, New York, 2010.

[65] R.M. Stephenson, Mutual solubility of water and pyridine derivatives, J. Chem. Eng. Data 38 (1993) 428-431.

[66] O. Flaschner, LXXXI.-The miscibility of the pyridine bases with water and the influence of a critical-solution point on the shape of the melting-point curve, J. Chem. Soc. Trans. 95 (1909) 668-685.

[67] R.J.L. Andon, J.D. Cox, Phase relationships in the pyridine series: Part I. The miscibility of some pyridine homologues with water, J. Chem. Soc. (1952) 4601-4606.

[68] J.D. Cox, E.F.G. Herington, The coexistence curve in liquid-liquid binary systems, Trans. Faraday Soc. 52 (1956) 926-930.

[69] J.-I. Abe, K. Nakanishi, H. Touhara, Thermodynamic properties of aqueous solutions of hydrophilic compounds 1: Pyridine and methylpyridines, J. Chem. Thermodyn. 10 (1978) 483-494.

[70] R.J.L. Andon, J.D. Cox, E.F.G. Herington, The thermodynamic properties of dilute solutions of pyridine bases in water, Discuss. Faraday Soc. 15 (1953) 168-174.

[71] V. Bassiloua, L. Ghaicha, M. Privat, R. Bennes, E. Tronel-Peyroz, Activities and thermodynamic excess properties of aqueous 2,5-dimethylpyridine mixtures near the critical demixing point: comparison with 2,6-dimethylpyridine-water mixtures, J. Solution Chem. 24 (1995) 935-952.

[72] R.J.L. Andon, J.D. Cox, E.F.G. Herington, Phase relationships in the pyridine series: Part 6. The thermodynamic properties of mixtures of pyridine, and of three of its homologues, with water, Trans. Faraday Soc. 53 (1957) 410-426.

[73] G. Perron, F. Quirion, D. Lambert, J. Ledoux, L. Ghaicha, R. Bennes, M. Privat, J.E. Desnoyers, Thermodynamic properties of aqueous organic mixtures near the critical demixing: cases of 2,6-dimethylpyridine and of 2-isobutoxyethanol, J. Solution Chem. 22 (1993) 107-124.

[74] H. Stephen, T. Stephen, Solubilities of Inorganic and Organic Compounds, Pergamon Press; Macmillan, New York, 1963.

[75] J.M. Sørensen, W. Arlt, Liquid-liquid equilibrium data collection, DECHEMA: Deutsche Gesellschaft für Chemisches Apparatewesen, New York, 1979.

[76] AspenPlus® v.7.2, Physical Property Methods and Models: Reference Manual, AspenTech.

[77] H.F. Ferguson, D.J. Frurip, A.J. Pastor, L.M. Peerey, L.F. Whiting, A review of analytical applications of calorimetry, Thermochim. Acta 363 (2000) 1-21.

[78] R.D. Weir, TH.W. De Loos (Eds.), Measurement of the thermodynamic properties of multiple phases, in: Experimental thermodynamics, Elsevier, Amsterdam, 2005.

[79] B. Kuzmanović, M.L. van Delden, N.J.M. Kuipers, A.B. de Haan, Fully automated workstation for liquid−liquid equilibrium measurements, J. Chem. Eng. Data 48 (2003) 1237-1244.

[80] H. Chen, J. Wagner, An apparatus and procedure for measuring mutual solubilities of hydrocarbons + water: benzene + water from 303 to 373 K, J. Chem. Eng. Data 39 (1994) 470-474.

[81] W.D. Seider, S. Widagdo, Multiphase equilibria of reactive systems, Fluid Phase Equilib. 123 (1996) 283-303.

[82] P. Koukkari, R. Pajarre, Introducing mechanistic kinetics to the Lagrangian Gibbs energy calculation, Comput. Chem. Eng. 30 (2006) 1189-1196.

[83] G.A. Iglesias-Silva, A. Bonilla-Petriciolet, K.R. Hall, An algebraic formulation for an equal area rule to determine phase compositions in simple reactive systems, Fluid Phase Equilib. 241 (2006) 25-30.

[84] A. Bonilla-Petriciolet, G.A. Iglesias-Silva, K.R. Hall, An effective calculation procedure for two-phase equilibria in multireaction systems, Fluid Phase Equilib. 269 (2008) 48-55.

[85] J.M. Prausnitz, F.W. Tavares, Thermodynamics of fluid-phase equilibria for standard chemical engineering operations, AICHE J. 50 (2004) 739-761.

[86] V. Gerbaud, X. Joulia, Molecular modeling for physical property prediction, in: L. Puigianer, G. Heyen (Eds.), Computer aided process and product engineering, Wiley-VCH Verlag GmbH & Co. KGaA, Weinheim, 2006.

[87] A.K. Sum, S.I. Sandler, Use of ab initio methods to make phase equilibria predictions using activity coefficient models, Fluid Phase Equilib. 158-160 (1999) 375-380.

[88] T. Banerjee, M.K. Singh, R.K. Sahoo, A. Khanna, Volume, surface and UNIQUAC interaction parameters for imidazolium based ionic liquids via polarizable continuum model, Fluid Phase Equilib. 234 (2005) 64-76.

APPENDIX A

ADDITIONAL STUDIES ON THE *N*-OXIDATION OF 2-METHYLPYRIDINE

Some preliminary measurements were performed during the runaway studies of the *N*-oxidation of 2-methylpyridine and are included in this Appendix.

A.1 pH Measurements

During the runaway studies of the 2-methylpyridine *N*-oxidation (See Section 3) performed in the Automatic Pressure Tracking Adiabatic Calorimeter (APTAC), the pH was measured at the end of the tests using pH-indicator strips. Unfortunately, the pH for the decomposition of 2-methylpyridine *N*-oxide (presented in Subsection 3.1) could not be measured due to the strong black color in the solution at the end of the tests. However, a measurement was performed at 230 ^{o}C without catalyst using a smaller amount of 2-methylpyridine *N*-oxide (2.3 g) and the pH changed from 4 at the beginning of the test to 7 at the end of the test. The pH for the tests employing hydrogen peroxide (shown in Subsection 3.2) was not measured; while, the pH for the solutions of the decompositions of hydrogen peroxide and 2-methylpyridine *N*-oxide (presented in Subsection 3.3) was between 5 and 6 for all the cases. The pH for the measurements of the stability of 2-methylpyridine (shown in Section 3) changed in the range 7-9 and are included in Table A1.

Table A1 pH measurements for the study of the stability of 2-methylpyridine

2MP (g)	Catalyst (g)	Water (g)	pH
6.6	0.00	0.0	9
1.6	0.09	14.4	7
1.6	0.30	14.2	7
3.2	0.09	12.8	8

A.2 2-methylpyridine *N*-oxidation Runaway

Two additional preliminary measurements were performed in the APTAC using Heat-Wait-Search mode. One of the measurements (Without 2NOX in Figure A1) employed 1.6 g of 2-methylpyridine, 0.09 g of catalyst, and 14.4 g of 17.5 % H_2O_2. The other measurement (with 1.6 g of 2NOX in Figure A1) employed the same quantities as in the previous measurement, but in this case 1.6 g of 2-methylpyridine *N*-oxide were added initially. Figure A1 shows the temperature and pressure profiles for these two measurements and two exotherms can be identified in the profiles. The first exotherm was measured at low temperatures and corresponds to the decomposition of hydrogen peroxide which is occurring simultaneously to the *N*-oxidation of 2-methylpyridine. As mentioned in Section 4, the rate of the *N*-oxidation is proportional to both the concentration of 2-methylpyridine and the concentration of hydrogen peroxide; while, the rate of H_2O_2 decomposition is proportional to the square of the concentration of hydrogen peroxide. As such, in these measurements, where all the hydrogen peroxide was added at the beginning of the test, more H_2O_2 decomposition was observed compared with the semi-batch reactions shown in Section 4 where H_2O_2 was gradually dosed and quickly consumed by the *N*-oxidation.

The first decomposition in the measurements shown in Figure A1 caused an increase in temperature and pressure of approximately 100 ^{o}C and 1500 kPa, respectively. After some additional steps in the Heat-Wait-Search procedure, a second exotherm was measured and corresponded to the decomposition of the product, 2-methylpyridine *N*-oxide, formed during the *N*-oxidation occurred at the beginning. The second exotherm was detected at approximately 230 ^{o}C when no 2-methylpyridine *N*-oxide was added to the initial solution; while the second exotherm was detected at approximately 200 ^{o}C when the initial solution contained 1.6 g of 2-methylpyridine *N*-oxide. Thus, these preliminary measurements showed that the addition of 2-methylpyridine *N*-oxide to the initial mixture lowers the "onset" for the decomposition of the product. However, additional measurements should be performed to understand in detail the effect of adding different amounts of *N*-oxide to solutions at different conditions, e.g. catalyst mass. The understanding of this effect is of importance because, as mentioned in

Section 6, adding *N*-oxide in the initial mixture can be considered as an alternative to reduce the two-liquid phase loop during the *N*-oxidation of alkylpyridines with limited miscibility in water. Further calorimetric and thermodynamic studies are needed.

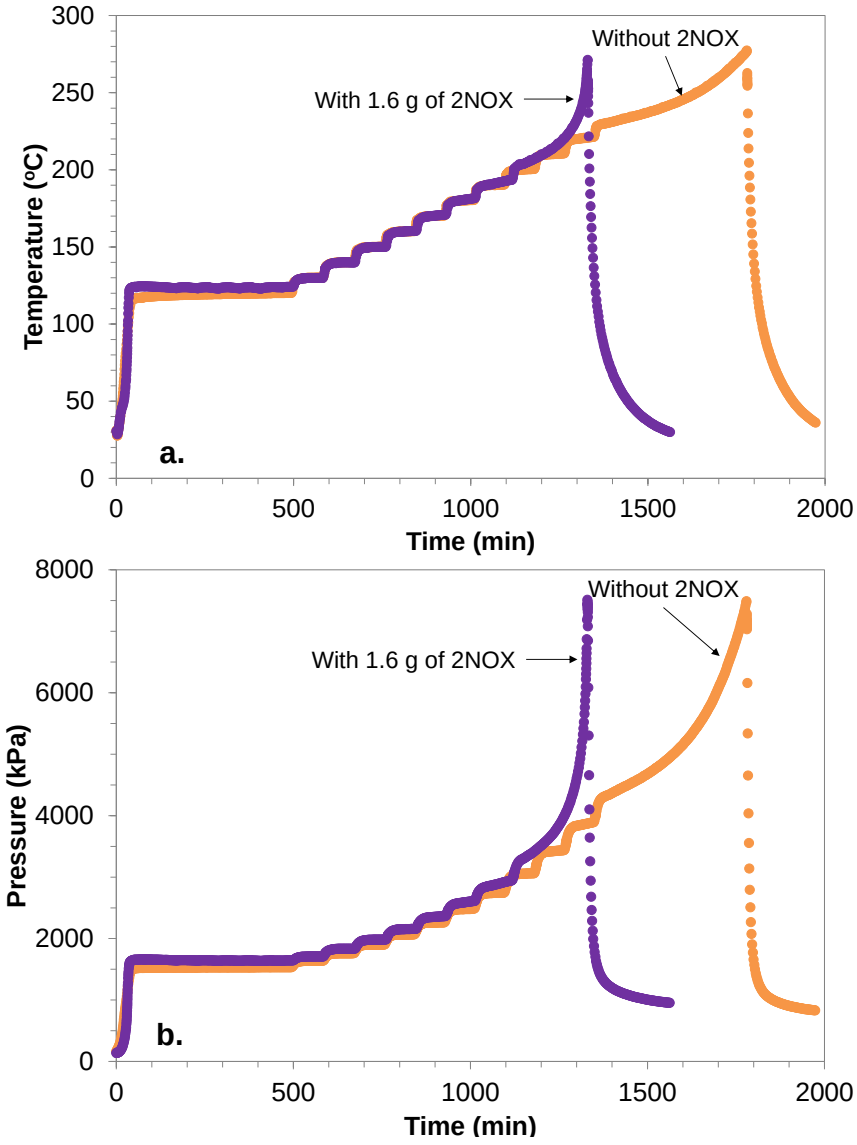

Figure A1 a) Temperature and **b)** pressure profiles for the decompositions during the *N*-oxidation of 2-methylpyridine without 2-methylpyridine *N*-oxide (2NOX) and with an initial amount of 2NOX

VITA

Name: Lina Rocio Saenz Noval

Address: Mary Kay O'Connor Process Safety Center
Artie McFerrin Department of Chemical Engineering
Texas A&M University
3122 TAMU
College Station, Tx 77843-3122

Education: B.S. Chemical Engineering, Universidad Industrial de Santander, Colombia, 2006
Ph.D. Chemical Engineering, Texas A&M University, 2011